Scuola Internazionale Superiore di Studi Avanzati - Trieste

SISSA  ISAS

SCUOLA INTERNAZIONALE SUPERIORE DI STUDI AVANZATI
INTERNATIONAL SCHOOL FOR ADVANCED STUDIES

Weak lensing and cosmic acceleration

Thesis submitted for the degree of
Doctor Philosophiæ

CANDIDATE:
Viviana Acquaviva

SUPERVISOR:
Prof. Carlo Baccigalupi

October 2006

SISSA - Via Beirut 2-4 - 34014 TRIESTE - ITALY

A mia madre e a mio padre,
che hanno sempre incoraggiato il mio amore per la ricerca,
e a mio fratello,
che forse seguirà questa strada... e forse no.

Table of Contents

Citations to Previously Published Works

Part of the contents of this Thesis has already appeared in the following papers:

Refereed Journals:

- *Weak lensing in generalized gravity theories.*
  Acquaviva V., Baccigalupi, C. and Perrotta, F., Phys. Rev. D **70**, 023515 (2004).
- *Structure formation constraints on the Jordan-Brans-Dicke theory.*
  Acquaviva V., Baccigalupi, C., Leach, S. M., Liddle, A. and Perrotta, F., Phys. Rev. D **71**, 104025 (2005).

Submitted:

- *Dark energy records in lensed Cosmic Microwave Background.*
  Acquaviva, V. and Baccigalupi, C., astro-ph/0507644, submitted to Phys. Rev. D.

Proceedings:

- *Weak lensing and gravity theories.*
  Acquaviva, V., Baccigalupi C., and Perrotta, F., proceedings of the IAU Symposium 225 "Impact of Gravitational Lensing on Cosmology", Mellier Y. & Meylan G. Eds., Lausanne, 2004, astro-ph/0409102.
- *The CMB as a dark energy probe.*
  Baccigalupi, C. and **Acquaviva, V.**, proceedings of the "International Conference on CMB and Physics of the Early Universe", Ischia, 2006, astro-ph/0606069.

Acknowledgments

This thesis is the result of the work of four years in Trieste, and these four years of life are going to be with me forever. It has been such an intense period, and I've grown up a lot as a scientist, as well as a person. I've been able to meet, talk to and interact with many people, and if not all, I would like at least to thank some of them.

The very first person I think of is Carlo Baccigalupi, who has been a supervisor, a colleague and a friend. He taught me more about Cosmology than everyone else, and he tried to transmit to me his genuine love for science and research. He had the patience of dealing with my ignorance, discouragement and disorganization in a way it always surprised me, and I never saw him angry or disappointed, even if he would have had many reasons, many times. This thank you comes with a mixture of affection, respect and admiration.

I have known for a few years now Sabino Matarrese. He is actually responsible for my being an astrophysicist. I could never say thanks to him enough, for this, for his continuous support, and for the countless scientific conversations I had with him during this time. The idea of research I got from him is of rigour, honesty and originality.

Another person who contributed to make me love this job is Andrew Liddle. I had the opportunity of working with him for a few months, and he has been a reference point for me afterwards. I thank him for sharing his precise and clever ideas, and for his many valuable advices.

The first people I met in Trieste were my astro-mates Lucia, Bruno, Daniele, Mao and Mattia. With them I shared the classes and the office during the first year, and much more all the time. We never experienced envy or competition, and I know I have been lucky to find such a good team. To them I'd like to add Franci, who has been a good friend, a precious smoker fellow, and recommended to me some of the best books I've ever read.

Fabbio was of great support for me in these years, both on the human side, when it came to science and when it came to computers. I probably wouldn't have been written this thesis without him, but for sure if we had still been sharing the office, for too much laughter, and gossip, and funny nicknames fluttering around.

With Simona and Federico I had the great joy of finding at the same time people with whom to talk about science and amazing friends. I think it's a rare, fortunate combination. I should thank them for many things but I'll choose their help and support with the "bibi-

tour", which provided me with a job and them with lots of headaches.
And then I want to thank Stefano, for having been the main reason why I came here, and for lots of good and bad times; Michele, Carlo ed Enrica, my first and gorgeous "gastronomical" friends, without whom I'd be much thinner, but also much sadder; the women-in-science who shared with me this male world, laFra, Chiara, Melita, Iryna, Manu, Laura and Claudia; and all the other people I spent my time with in these years, who are too many to count, so I'll mention only the ones I have at least once got drunk and/or talked about the sense of life with... Alessio, Beppe, Fabio, Marcos, and the historical travel companions from University Alberto and Fred.
Finally, I wish to thank Luca, who is making my life more intense, bright and complicated, a combination which I like a lot.

Introduction

Cosmology is commonly thought to have entered its "precision era", a threshold of every science. Some of the first - and essential in order to promote it to the rank of science - developments happened almost by chance, such as Hubble's discovery of expansion, or Penzias and Wilson's casual observation of the Cosmic Microwave Background, or CMB). Afterwards, the level of sophistication reached by the auxiliary pure sciences, like physics or mathematics, allowed room for fast and spectacular improvement. In the Sixties, after the couple of extraordinary events I mentioned, the new-born Cosmologists not only had a fantastic playground - the Universe itself - but were also supported by a well-established mathematical setting like Einstein's theory of General Relativity and by a good knowledge of most of the required physics of fluids; also, high-energy physicists were at the same time developing the standard model of particles. From the Hot Big Bang Cosmology to the formulation of the theory of inflation to the discovery of the CMB anisotropies, there were years that revolutioned the way people thought about the Universe. Then, after some tens of years, Cosmology has become a precision science, in the sense that the guidelines are written, and now we are cross-stitching on models, more often limited by the sensitivity of the instruments than by the cosmological community's capacity of having better ideas. We have quite a converging view (so converging, in fact, that we call it *Concordance model*) of the numbers that form the Universe matter-energy content, and still we profoundly lack a theoretical interpretation of these numbers. I think that the fact that we are conceiving more and more sophisticated experiments, while at the same time the nature of a good 96% of the Universe is obscure to us, renders the present era for Cosmology more thrilling than ever. This peculiar state-of-the-art sets as a crucial challenge the search for unusual point

of views, in the sense of new observables, able to resolve the present degeneracies among different parameters or give us new independent - in space or in time - constraints. We are in the intriguing era of "tricking the Universe" to force it to tell us something about itself... rather than the elegant Universe, I would call it the reluctant one.

The work I have been doing during my PhD tried to go in the direction that I outlined above - the choice of an observable which was capable to select one particular epoch in the history of the Universe, and the exploration of the information that we can infer from it. Our target is to shed some light on the mechanism giving rise to the observed cosmic acceleration, a relatively recent cosmological process, started a few billions years ago. The easiest theoretical interpretation is in terms of a non-zero energy density in the vacuum, the Cosmological Constant; however, its required value is extremely low with respect to any conceivable (in the sense of "natural") fundamental physical scale, and the corresponding riddle is motivating a huge theoretical and experimental effort for the understanding of this component. If we generally (although a bit inappropriately) call "dark energy" the component responsible for the acceleration, and constituting the 75% of the matter-energy content of the universe, one of the major present challenges, that motivated the present work, is to determine whether the dark energy has a constant behavior, or is instead characterized by some dynamics.

The instrument is the gravitational lensing by large-scale-structure on the CMB light; our starting point is the fact that the lensing "cross section", intended as the distribution in time of the lensing power, vanishes in proximity of both source and observer, picking up most of its strength at intermediate distances. Thus, given the peculiar collocation of us as observers at the present time and the CMB light at a redshift $z \simeq 1100$ as source, the gravitational lensing effect on the CMB is for its largest part generated in the redshift window around $z = 1$. On the other hand, the observational evidence in favour of an accelerated expansion suggests that this significantly overlaps with the epoch of the onset of acceleration itself. This latter statement means that whatever the mechanism giving rise to the acceleration, constraints set at this time will be crucial in order to discriminate among models, highlighting the peculiar dynamics of the expansion at times of the dark energy entering the cosmic picture. Moreover, since most of the constraints we get from photomet-

ric observations come from the local universe, we have by now set significant limits on the dark energy present abundance, and therefore the next challenge in the understanding of its nature is to trace its redshift behavior. The study of an observable which is independent of the present time evolution and was born at the same time of the acceleration is therefore most suitable for dark energy investigations.

The project was organized in different steps. The first theoretical objective to be achieved was to recast the formal theory of weak lensing for the case of generalized cosmologies. The latter classification included both dynamical dark energy in the form of a scalar field and modified gravity scenarios, which historically have been the main attempts of theoretical interpretation of the cosmic acceleration. We had to identify the relevant variables in the language of the cosmological perturbations for the different models, and translate them in that of the lensing observables. The pillars of the corresponding mathematical apparatus are the lensing equation, which describes the trajectory of photons in the space-time modified by the matter density field which produces the lensing effect, and the Poisson equation, which establishes the connection between the density perturbations power spectrum and that of the gravitational potential, and is crucially influenced by the underlying model-dependent dynamics of the expansion.

The second part of the work was numerical; the procedure for obtaining the lensed spectra had to be implemented in an integration code. The main difficulty of this part of the work relied in the necessity of keeping track of the modified cosmic expansion, and of the additional fluctuating components. Once this task was completed, we were able to study and fully understand the CMB lensing process in dark energy cosmologies. We demonstrated that the lensing distortion of the CMB keeps a record of the cosmological expansion rate at the time of the onset of acceleration, and we isolated the most promising tracer of the lensing effect in the reshuffling of the primordial polarization anisotropies due to lensing. We completed this part of the work quantifying the impact that the CMB lensing detection from forthcoming CMB experiments might have on our capability to determine whether the dark energy is indeed a Cosmological Constant.

We began a systematic investigation of the CMB lensing properties when the underlying gravity theory is modified. We considered the Jordan-Brans-Dicke model, building a rou-

tine for the integration of its equation of motion and conducting a likelihood analysis of the constraints that can be obtained from large-scale structure data together with CMB observations, but in absence of lensing. The inclusion of the latter in the game is the natural prosecution of this study, which moreover served to reveal some interesting open problems about this model in particular and the modified gravity theories in general.

Outline

The thesis is organized as follows.

In Chapter 1 I briefly sketch a picture of our current understanding of the Universe and describe the main steps both in the individuation of the cosmological parameters needed for an accurate description and in their determination. I retrace the path leading to the need for an explanation of the cosmic acceleration and depict the present concordance cosmological model.

Chapter 2 is dedicated to the physics of gravitational lensing which is relevant to cosmological purposes; here I also introduce the notation and the physics of the lensing-related observables. I concentrate on the effect of lensing from large-scale structure on the Cosmic Microwave Background, giving a qualitative overview of how the unlensed spectra are modified.

The formulation of the weak lensing theory in generalized cosmologies is the subject of Chapter 3. Although the general structure of cosmological perturbation theory is well-known, in this context new degrees of freedom arise, yielding to the necessity of recasting the corresponding sets of equations. I introduce the classes of models which have been object of my work, including the Cosmological Constant case, scalar field Quintessence models, scalar-tensor theories and Non-Minimally-Coupled scenarios, and provide a description of how the lensing-related variables are related to the cosmological parameters, pointing out where the effects of generalized cosmologies arise from and which are the most suitable variables to reveal them. Some examples of the new effects are also given.

Chapter 4 represents the first full application of the lensing theory which has been devel-

oped, and contains a thorough investigation of the CMB lensing process in models in which the dark energy is described by a scalar field. We study the various manifestations of the CMB lensing, and identify a particularly effective one in the way lensing redistributes the primordial polarization anisotropy power. We perform a Fisher matrix analysis in order to provide a quantitative estimate of how much these observables may help in constraining the dark energy dynamics.

In Chapter 5 I focus on a simple modified gravity theory, the Jordan-Brans-Dicke model. I present the results of an analysis which aimed to compute the constraint on the additional parameter of this theory, $\omega_{\rm JBD}$, from the combination of CMB and large-structure data; this was intended as preliminary study for the inclusion of the lensing signal in this model as well, and i discuss the outcome for the lensed spectra for this model, whose analysis however is still in due course.

A brief discussion of the work in progress and future directions is carried out in Chapter 6. Our main current lines of study are the impact of anisotropic stress in modified gravity theories and the inclusion of non-linear evolution in the calculation of the lensed CMB spectra.

The 7th and last Chapter contains the summary of the results we obtained and our conclusions.

Chapter 1

A puzzling inconsistency

Cosmology is the study of the large-scale structure of the Universe. In order to give a brief account of the developments leading to the formulation of the present concodance model, including a dark energy term, we therefore review the properties of the Universe (which come from a combination of assumptions and observations) on cosmological scales. The study of these characteristics will lead to the individuation of both

- the most suitable mathematical description of the Universe as a whole (*Cosmological model*),
- the "cosmological parameters", namely the minimal set of quantities which have to bet fixed in the cosmological model in order to provide an accurate description of the overall evolution of the Universe.

We will then review the basic steps of the determination of those cosmological parameters which have been fundamental for the formulation of the dark energy paradigm.

1.1 The mathematical description of the Universe

Our present understanding of the structure of the Universe on large (comparable to its own dimension) scales relies upon two basic assumptions:
- the Cosmological Principle, stating *homogeneity* and *isotropy* on large scales, holds; this amounts to say that there are no privileged positions nor geometrically preferred directions

of observations. This statement is indeed surprising if compared with the evidence on astrophysical scales, where matter is systematically distributed in clumps and voids. However, observations such as the Cosmic Microwave Background Radiation and the counts of Radio Galaxies suggest that the Universe as seen by our location on Earth is isotropic on scales ≥ 100 Mpc, and isotropy from any location is equivalent to homogeneity; if we believe the Copernican principle, stating that we are no special observers, we can infer the validity of the Cosmological Principle.

- the only relevant interaction on such scales is the gravitational force, described by Einstein's theory of General Relativity. This implies that the spacetime' structure is determined by its matter-energy content via the stress-energy tensor.

The properties of homogeneity and isotropy enforce some restrictions in the viable metric. The maximally symmetric resulting line element is of the *Friedmann-Robertson-Walker* (FRW) form (here in natural units):

$$ds^2 = -dt^2 + a^2(t)d\mathbf{x}^2 = -dt^2 + a^2(t)\left[\frac{dr^2}{1-kr^2} + r^2(d\theta^2 + \sin^2\theta d\phi^2)\right], \qquad (1.1)$$

where $a(t)$ is an arbitrary function of time which describes the expansion of the spacetime, k may assume the values $\pm 1, 0$ according to the curvature of the 3-space, and we have assumed spatial coordinates *comoving* with the expansion.

The evolution of the system can be obtained with the specification of the stress-energy tensor T_{ab}. For a variety of non-interacting matter and energy components, the total stress-energy tensor is simply the sum of the ones relative to single species; under the assumption of local isotropy, each one is bound to assume the form of a perfect fluid, *i.e.* to be diagonal with

$$(T^0_0)_i = -\rho_i; \qquad (T^k_k)_i = 3\,p_i, \qquad (1.2)$$

where $k = 1, 2, 3$ identifies the spatial components and i labels the different species.

The Einstein equations thus read:

$$\frac{\ddot{a}}{a} = -\frac{4\pi G}{3}\sum_i (\rho_i + 3p_i)\,; \qquad (1.3)$$

(Rayachaudhuri equation), and

$$\left(\frac{\dot{a}}{a}\right)^2 = \frac{8\pi G}{3}\sum_i \rho_i - \frac{k}{a^2}, \qquad (1.4)$$

(Friedmann equation), which is nothing but the previous one's first integral. The quantity $\dot{a}/a$ is crucial in the determination of the expansion rate and is denoted as Hubble parameter H. If we define, as it is often done, a *critical density* $\rho_{\rm cr}$ as the one needed for the universe to be exactly flat: $\rho_{\rm cr} = (3\,H^2/(8\pi G\rho_{\rm tot})$ and a dimensionless density parameter $\Omega_i = \rho_i/\rho_{cr}$, the above equation can be rewritten as

$$1 = \sum_i \Omega_i - \frac{k}{a^2 H^2}, \tag{1.5}$$

where sometimes the last term is considered as well as a relative curvature density $\Omega_K = -k/(a^2H^2)$. Conservation of energy-momentum $T^{ab}_{;b}$ gives the further relation, needed for consistency:

$$\dot{\rho}_i + 3(\rho_i + p_i)\dot{a}/a = 0 \quad \forall \text{i}. \tag{1.6}$$

In order for the system to be solved, it is still necessary to specify the equation of state, the relation between the energy density and the pressure, for each cosmological component. From the above equations we can infer the parameters we need to specify in order to determine completely the system of Einstein equations, which are nothing but the initial conditions for the evolution. We will have (with reference to the present time t_0):

- The Hubble parameter H_0, often rewritten in terms of h defined by the relation $H_0 = 100\,h$ km/sec/Mpc for notational convenience;
- The density parameter Ω_{i0} for each species of matter (or energy) density present, for which we also need $p_i = f(\rho_i, T_i)$, since in general the pressure can depend not only on the density ρ, but also on the temperature T;
- The spatial curvature $K = k/a_0^2$;
- The *deceleration parameter* $q_0 = -(\ddot{a}/a)_0\, H_0^{-2}$.

For the two equations (1.3) and (1.4) the set of relevant initial conditions is made up respectively of the first three data, and the second and the fourth (which however includes the Hubble constant). In each case one of them is redundant in the sense that it can be determined if the others are known: this can be used a an internal consistency check or to obtain one of the cosmological parameters for difference.

In the following, we will try to describe the processes of independent determination of the listed quantities, with the purpose to show the underlying inconsistency. It is important to stress that there are a number of probes which can provide an accurate measurement of some *combinations* of cosmological parameters (those above and others), but that only the determination of the set of three of them at the same time can be regarded as an accurate representation of the Universe' global picture.

1.1.1 The measurement of the Hubble parameter

The Hubble parameter acts as a friction term for the expansion of spacetime, therefore directly influencing comoving trajectories of objects: it can be regarded as the most important distance indicator in Cosmology. The history of its determination is strictly related to this property.

It is often convenient to use a different variable in order to describe observables related to the cosmic expansion, the *redshift* z, defined as

$$z = \frac{1-a}{a}, \tag{1.7}$$

so that at the present epoch $a_0 = 1$ corresponds a redshift 0.

For photons emitted by comoving sources, such as astrophysical objects in nearby galaxies, the comoving line-of-sight distance (or any other distance ruler used in cosmology, since they converge at this level) can be approximated *at first order in redshift* as

$$d = c \int_0^z \frac{dz'}{H(z')} \simeq \frac{c \cdot z}{H_0} \tag{1.8}$$

This relation can be reinterpreted in terms of a Doppler shift, reading the change in the wavelength of light from emission to observation as an effect of peculiar recession velocity of the object itself. It follows that low-redshift objects are seen as moving away from us at a rate

$$v = c \cdot z = H_0 \, d, \tag{1.9}$$

which is the well-known Hubble's law, discovered back in 1929 [1]. Therefore, if we can measure at the same time the distance and the velocity of objects which are far enough for not having a significant peculiar motion and close enough for the $\simeq$ sign in eq. (1.8) to hold

(from the above equation this corresponds to recession velocities small with respect to c), the Hubble parameter follows straight as the slope of the velocity-distance relation.

Despite the simplicity of the mathematical setting of the problem, from an experimental point of view the determination of the Hubble parameter has been, and still is at some level, extremely controversial. Accurate measurements require calibration of distances to far galaxies (in order to minimize the impact of peculiar velocity fields) [2]; this is in general achieved by means of the inverse square radiation law, and requires the use of "standard candles", objects whose luminosity is either constant or related to another distance-independent property (*i.e.* the period of oscillation or rotation rate); moreover, in order to be a good distance indicator the underlying physics should be well understood, the systematic effects known to be kept under control, and the objects should be abundant enough for the sample to be statistically significant; these requirements are, as predictably, not easily met. A turning point in the experimental panel was the development of the Hubble Space Telescope (HST) Key Project [3]; here we give a brief account of their method and results.

The most widely used astrophysical rulers are the Cepheid variables, pulsating stars whose period is both independent of the distance and very well correlated with the intrinsic luminosity, leading to an uncertainty in the distance to the host galaxy of $\simeq 10\%$ for a single object. Since Cepheids are abundant in nearby spiral and irregular galaxies, a final precision a few times better can be achieved through this method.

Another important distance indicator is represented by the supernovæ type Ia. These objects, believed to be the result of the explosion of C-O white dwarfs, have very high intrinsic luminosity and therefore allow the use of distances well in the cosmological Hubble flow, possibly uncorrelated with peculiar streaming effects, giving an uncertainty in the distance as small as 6% for the single event. On the other hand, these objects are much rarer than Cepheid stars and their physics is less clearly understood. Type II supernovæ, altough not proper standard candles and fainter than the former, can be used as distance ladder as well by following the time-evolution of their spectra in combination with their photometric angular size.

Other ways of distance determination are by means of the Tully-Fisher relation, correlating the luminosity of a spiral galaxies with its maximum rotation velocity; an analogous rela-

Table 1.1: SUMMARY OF KEY PROJECT RESULTS ON H_0 (from [3]).

Method	H_0 ($\pm$ random $\pm$ systematic error)
Local Cepheid galaxies	$73 \pm 7 \pm 9$
SBF	$70 \pm 5 \pm 6$
Tully-Fisher clusters	$71 \pm 3 \pm 7$
FP / $D_N - \sigma$ clusters	$82 \pm 6 \pm 9$
Type Ia supernovæ	$71 \pm 2 \pm 6$
SNII	$72 \pm 9 \pm 7$
Combined	$72 \pm 3 \pm 7$

tion, known as the "fundamental plane" law, holds for elliptical galaxies; another method relies on the correlation, for different kind of galaxies, between their distance and their surface brightness fluctuation (SBF).

The combination of all these observations, summarized in Table 1.1 being Cepheids used as the leading distance indicator and the others as secondary probes has lead, in the last few years, to a (partial or substantial, according to different groups) solution of the H_0 controversy; the discrepancy among different groups was still of a factor two up to 1980 (the top and bottom values being 100 and 50 km/sec/Mpc), mildly improved to a dichotomy between 50 and 80 in the early nineties, up to the present value [3] $H_0 = 72 \pm 3$[random] $\pm$ 7[systematic]. However, the level of agreement on this number is still being questioned, and some groups claim a significant deviation towards a smaller value arising from Supernovæ diagrams [4].

1.1.2 The matter budget

The matter content of the Universe includes contributions from different species, each of which must be determined in order to get the right total amount in equation (1.4). However, it has been now known for long that besides the "ordinary" matter which constitutes people, planets and stars there are forms of matter which evade direct detection (do not emit light, basically) and can only be investigated through their gravitational interaction. The former kind of matter is usually referred to as *baryonic*, even if this characterization is

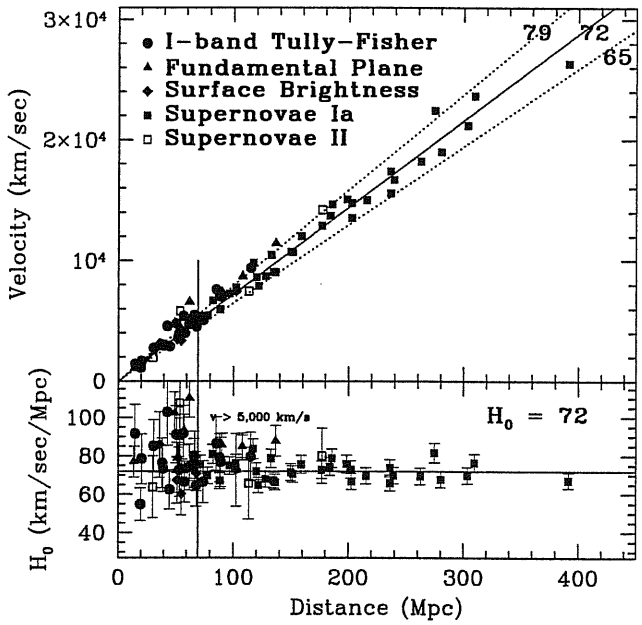

Figure 1.1: The distance-velocity diagram for different secondary indicators. From [3].

not strictly true: electrons, for examples, do not carry a baryonic number and still are part of this classification. However, being them so light, their support to the total "baryonic" budget is extremely limited and therefore we can assess that neutrons and protons - the proper baryons indeed - bear good resemblance of the significant baryonic matter. The latter type of matter is, correspondingly, known as *dark*, and its nature is one of the big puzzles of modern Cosmology. Moreover, there is some indication of superposition of these two species: some of the dark matter may be baryonic, or on the other hand some of the baryonic matter may be dark. We will try to give an essential review of the determination of the amount of both kinds in the following.

Finally, in equation (1.4) there are other species of energy densities to be taken into account: at least the radiation component, photons of cosmological origin such as the CMB signal, and the neutrinos (which are described as massless in the Standard Model of Particles, but have by now been shown to carry a - small but potentially significant - amount of mass). However, for these relativistic particles the energy density rapidly decreases with time, so

that in the late Universe, which is the context we are presently interested in, they can be safely neglected.

Constraints on the baryonic matter content. Baryonic matter is thought to have been produced in the primordial Universe at $t \simeq 1$ s and $T \simeq 1$ MeV, from nucleosynthesis of primordial light elements: Deuterium is first produced from protons and neutrons, then ^{3}He, ^{4}He, which is the most stable and therefore accounts for most of the baryon production, and some ^{7}Li. What influences the ratio of the corresponding reactions is the initial ratio of baryons (nucleons) to photons, often denoted as η. Metallicity measurements are carried out in metal-poor regions in white dwarfs (mainly for the ^{4}He), as well as in high-redshift quasar absorption system (for Deuterium) and in our own Galaxy (for Lithium and ^{3}He). A substantial agreement among all the observations require $\Omega_B h^2$ to be in the range $0.017 - 0.024$; this seems to be consistent with the cosmological results from the CMB data of the Wilkison Microwave Anisotropy Probe (WMAP) satellite [16], giving a similar result and uncertainty window if no strong prior on other parameters is assumed.

A final remark is worth to be spent on the fact that the optical matter density appears to be significantly lower than the above value [17], $\Omega_{\rm lum} \simeq 0.0024$, so that a significant fraction of baryonic matter, whose precise amount depends on h, is seemingly transparent to optical observations.

Dark matter: evidence and measurements. Hints for the presence of dark matter in the Universe come from observations on different scales.

Maybe the first indication was found on the scale of galaxy clusters in 1933 [5], when the study of velocity dispersion of galaxies in the Coma cluster led to a measurement of a mass-to-light ratio two orders of magnitude larger than the one observed in the solar System neighborhood; this value still basically holds from most recent analysis [6]. Another important indication on the cluster scale can be obtained applying of the virial theorem in order the temperature as a function of the total mass, and comparing it with direct temperature observation; again, there is a relevant inconsistency if the total mass is assumed to be the baryonic one.

On the galactic scale the most direct and convincing evidence for dark matter relies on the *rotation curves* of galaxies, where photometric observations suggest the presence of a

luminous disk with a characteristic radius. This would give a Newtonian circular velocity:

$$v(r) = \sqrt{\frac{G\,M(r)}{r}} \tag{1.10}$$

falling $\propto 1/\sqrt{r}$, while observations exhibit a *flat* behavior of the velocity well beyond the optical disk. This appears to be the consequence of an extended halo of dark matter with a mass density profile $M(r) \propto r$.

Other probes from cosmological scales, *i.e.* the ones coming from CMB observations, basically confirm this picture.

There are of course various methods to measure the dark matter cosmological abundance. We will try to concentrate on constraints independent of the underlying model of structure formation; however, some of the estimates we get are in combination with the measurement of the reduced Hubble parameter $h = H_0/(100$ Mpc/km/sec) since the latter is crucial to the growth of structure.

A well-exploited method to estimate Ω_M is to compute the mass-luminosity ratio of galaxy clusters, and assume that they can be representative of the universe as a whole, rescaling its observed luminosity (e.g. [7]); this leads to estimates of $\Omega_M = 0.2 \pm 0.1$. In alternative, one may consider as a known constant the baryon-to-total-mass factor, which may be an estimator less biased by locality. Assuming that the baryon content in clusters is faithfully traced by the hot intracluster gas, whose amount can be measured via X-ray observations [8], and under the hypothesis (from BBN constraints) of $\Omega_B \simeq 0.04$, this gives $\Omega_M = 0.3 \pm 0.1$. On cosmological scales, the power spectrum of density fluctuations provides an estimate of the *shape parameter* $\Gamma = \Omega_m h$ in the range $0.2 - 0.3$ (*i.e.* [9]), indicating an Ω_M of $0.2 - 0.5$ even assuming very conservative errorbars in h.

1.1.3 The overall geometry of the Universe

The last piece to complete equation (1.4) is the assessment of the global spatial curvature of the Universe, K. The most direct and reliable proof of its value come from CMB observations, which show a peak-and-troughs structure having its origin in the acoustic oscillations of the baryon-photon plasma at the time of recombination. The imprint of the oscillations at this time has a phase depending on their relative wavelength with respect

to the sound horizon: those which are caught at a perfect compression give rise to peaks, while valleys come from rarefactions. Therefore, the angular scale at which we presently detect the acoustic oscillations is influenced by the ratio of the sound horizon and the angular-diameter distance to the last scattering surface, with the convenient feature of being independent of absolute distance measurements. This ratio in turns depends on the overall spatial geometry: for flat universes, namely those whose mass density coincides with the critical one, the angular scale θ of the first peak roughly corresponds to a multipole

$$l \simeq \frac{\pi}{\theta}; \tag{1.11}$$

it scales along with the matter content (if we assume $\Omega_T = \Omega_m + \Omega_K = 1$) like $\Omega_m^{-1/2}$ to smaller values (larger angular scales) if the Universe is closed ($\Omega_T > 1$) and larger values if it is open ($\Omega_T < 1$), according to the differently curved geodesics.

It is however to be noticed that CMB data are to be treated with great care because they usually provide measurements of a large number of cosmological parameters at once, six or more in most of the currently acknowledged models. Therefore, it is possible in some extent that some combination of parameters mimics the effect of a spatial curvature; moreover, the CMB data interpretation relies on the statement, not necessarily exact, that structure growth happens via gravitational instability from a primordial, usually adiabatic and Gaussian, spectrum of perturbations [14].

As a result, without any previous assumptions on the cosmological parameters we are not able to put strong constraints on the curvature even through the most accurate CMB available data, the three-year WMAP release [16]: closed models only filled by matter can still be consistent with the data. Nevertheless, these models requires values of the cosmological parameters which are in open conflict with a host of astronomical data: the Hubble constant is predicted to be as small as $H_0 = 30\,\mathrm{Kms}^{-1}\mathrm{Mpc}^{-1}$ and the matter content as large as $\Omega_M = 1.3$.

This strong relative dependence implies that a very weak prior on the Hubble parameter $h > 50\,\mathrm{Km/s/Mpc}$ is enough to state a 10% limit

$$0.98 < \Omega_T < 1.08 \quad (\text{or equivalently} - 0.02 < \Omega_K < 0.08\ ) \tag{1.12}$$

[18].

However, CMB data are able to provide much stronger constraints if combined with other datasets. In fact, the degeneracies arising in the determination of the total matter density are mainly related to uncertainties in the evaluation of the distance ratio $r_s/D(z_{ls})$; if we can determine a standard ruler (*i.e.* an absolute distance measurement) through some other cosmological observations, the space of allowed parameters will be significantly shrunk.

Such rulers can be obtained, for instance, from the measurement of the power spectrum of matter perturbations, which exhibit a peak at the wavelength of the horizon at the matter-radiation equivalence, due to the different growth factor of anisotropies in these two epochs [20, 19]; or from the scale of the baryon acoustic oscillation (BAO) peak, which measures the distance to a redshift $z = 0.35$ [21]. The combination of the three-year WMAP data with these probes improves the above constraint to an impressive [16]:

$$\Omega_K = -0.01 \pm 0.02. \tag{1.13}$$

Observations are thus seemingly converging towards a flat Universe - one with a density very close to the critical one.

In addition to it, the curvature density Ω_K has the very special property of having - unlike most of the other cosmological parameters - a strong theoretical motivation in support of a given value, in this case zero or a very small number. This support come from the inflationary hypothesis - a theory claiming a phase of accelerated expansion in the very early Universe. The inflationary paradigm has been formulated in the early eighties [22, 23] and is at present widely accepted by the cosmological community because of its ability to solve the *horizon* and the *primordial flatness* problems, explaining on one hand the homogeneity and isotropy of the Universe on scales larger than those expected in the standard Big Bang theory, and on the other hand avoiding the necessity of a tremendous fine-tuning in the value of the primordial curvature.

However, the relevant property of inflation in this context is the fact that it drives the curvature to small values also at late times: although the signal of a flat, or quasi-flat Universe can of course be read as a confirmation of the inflation theory rather than the result of a reliable prediction, we may safely regard the indication of a small curvature as a

satisfying indication of consistency between theory and observations.

1.1.4 The deceleration parameter

The determination of the present value of q_0 is necessarily related to the one of the Hubble parameter. In fact, its very definition comes from the higher-order expansion of the luminosity distance relation in powers of the redshift, whose first term is the Hubble law, as observed before. At second order in z we find:

$$D_l H_0 = z + z^2 \left(\frac{1 - q_0}{2}\right) + \mathcal{O}(z^3), \tag{1.14}$$

rendering this parameter convenient to be measured as a deviation from the Hubble law. As for the linear term case, sensible constraints can be obtained only as long as objects of precise magnitude-distance relation are used: type-Ia Supernovæ are therefore the best candidates. It was estimated [24] that for a single supernova event of magnitude $m \pm \Delta m$ at redshift z the resulting uncertainty in the deceleration parameter would be $\Delta q_0 = 0.9 \Delta m / z$, giving good results even for a few events if the observed supernova are well determined spectroscopically and are at sufficiently high distances.

Different groups have been dealing with the evaluation of the q_0 parameter in the last ten years [25, 26]. The results are not easy to quantify mainly because of the approximation due to the Taylor expansion in eq. (1.14), which affects maximally the supernovæ at higher redshift, which would otherwise have the smallest intrinsic error, and because of other sources of systematics error, such as extinction by intergalactic dust [27]. In fact, in latest works [28] the deceleration parameter is often rephrased as the function of z encoding the deviation from the Hubble law, thus assuming a further parametrization. However, for the simplest description adopted here the data strongly favor a negative value for q_0:

$$q_0 = -0.75 \pm 0.32 \tag{1.15}$$

at the 95% confidence level [29], a result indicating that the expansion of the universe is most certainly *accelerating* at late times.

1.2 Pulling numbers together

The numerical values of cosmological parameters quoted in the previous sections concur to give us a picture of the Universe which is far from being satisfactory.
Let's examine first the consequences of the Friedmann equation, which should read

$$1 = \sum_i \Omega_i + \Omega_K \tag{1.16}$$

if divided by the critical density $3H^2/8\pi G$.
The observed small value of the spatial curvature denotes an average density close to the critical one, which is determined by the Hubble parameter to be $\rho_{\rm cr} \simeq 10^{-29}$ g/cm^3; the fluids entering the summation in the above equation, basically non relativistic matter (both luminous and dark), because of the rapid decrease of the relativistic particles density with time, cannot account for this density at all, being in fact at least three times smaller than required. What we have to deal with is an equation whose left hand side amounts to 1 while the right hand side, even taking into account large errorbars, is certainly smaller than 0.5.
The Rayachaudhuri equation can shed some more light on this inconsistency. In fact, it relates the second derivative of the expansion rate with respect to the redshift to the Hubble constant and the equation of state of the matter content of the Universe; with the notation $w_i = p_i/\rho_i$ it can be rewritten as a function of the deceleration parameter:

$$q = \frac{1}{2}\sum_i \Omega_i + \frac{3}{2}\sum_i \Omega_i w_i. \tag{1.17}$$

The exact value of the deceleration parameter depends of course on the relative abundances of different species of matter and on the assumptions we make on the total density (*i.e.* shall we believe the left or right hand side of the Friedmann equation)? However, a very general consideration is in order: since the equation of state of *any* type of known matter, both relativistic or Newtonian, is positive or null, and being the relative densities Ω_i positive as well, the parameter q cannot in this context assume a negative value... the one which is nevertheless observed.
What does this mean? This is one of the questions that cosmologists have been most often called to answer in the recent years, and for which there is still no concordance.

What we may try to assess without losing generality is that the Einstein equations for a matter-dominated Universe show a sharp contradiction with the present data, revealing something wrong in this way of describing the spacetime where we live. But what are the possible explanations?

Our derivation of eqs. (1.3) and (1.4) starts from the action:

$$S = \frac{1}{16\pi G}\int R\sqrt{-g}\,d^4x + \int \mathcal{L}_{\rm matter}(q,\dot{q})\sqrt{-g}\,d^4x \tag{1.18}$$

where R is the Ricci scalar, g is the metric determinant, q and $\dot{q}$ are the canonical variables of the Lagrangian of the matter fields, $\mathcal{L}$.

Therefore, we may either be missing some relevant fluid-type component in $\mathcal{L}_{\rm matter}$, or need to modify the gravitational part of the above action. The requirement of consistency for the Einstein equations is predictive only if we choose *a priori* which of these two roads we want to follow.

For instance, if we assume that the gravitational coupling to matter is correctly described by the Einstein-Hilbert Lagrangian, the form of the Friedmann and Rayachaudhuri equations is preserved and we have to conclude that there is some unknown source of energy density which contributes for some 70% to the matter-energy budget of the Universe (from (1.4)) and has a strongly negative equation of state, in order to enforce the observed negative sign in the right hand side of eq. (1.17).

On the other hand, the evidence for cosmic acceleration has a natural interpretation as the tendency of neighboring geodesics to get further from each other: in other words, it seems to suggest the presence of a repulsive form of gravity. We cannot exclude this possibility (gravity modification on large scales, for instance) by means of any of the constraints mentioned in the previous sections, because all of them are based on the use of standard General Relativity in order to infer the equations of motions.

For the moment we just want to depict the simplest of these scenarios, that is often regarded as the *Concordance model* being the one the requires less additional parameters with respect to the picture drawn above. In this case General Relativity holds, and the Universe is partially filled by a constant, positive energy (often thought of as the vacuum energy of some fundamental field theory and denoted as Λ) whose exact amount is determined by the

fulfillment of consistency in the Friedmann equation. The introduction of this *Cosmological Constant* alters the corresponding energy-tensor (we will regard it as a new fluid component in the matter Lagrangian rather than a modification of the gravity coupling to matter, although of course the latter interpretation is conceptually equally valid) in the following manner:

$$T^a_b\,(\text{new}) = 8\pi G(T^a_b\,(\text{old}) + Q^a_b); \qquad Q^a_b = -\frac{\Lambda}{8\pi G}\delta^a_b. \tag{1.19}$$

This is nothing else than the stress-energy tensor of a perfect fluid with

$$\rho_\Lambda = -Q^0_0 = \frac{\Lambda}{8\pi G}; \qquad p_\Lambda = Q^i_i/3 = -\rho_\Lambda, \tag{1.20}$$

which is the required sign of equation of state for eq. (1.17). In fact, if we assume that the Cosmological Constant contributes for the 70% to the total matter-energy density, the ordinary matter for the 30%, and the geometry is flat, we have

$$q = \frac{1}{2}\Omega_T + \frac{3}{2}\sum_i \Omega_i w_i \simeq \frac{1}{2}\Omega_M - \Omega_\Lambda \simeq -0.55, \tag{1.21}$$

thus a value not only negative, but also in agreement with the observations reported before. The one traced above is the cosmological setting that we will refer to as the ΛCDM (Cold Dark Matter) one, and we will consider it as our reference model for the next Chapter.
We postpone to Chap. 3 a more detailed analysis of the problems of this scenario, of some of the most popular alternative models that have been proposed in the literature and a more detailed description of the differences in their relative phenomenology which may be useful for discriminating among them.

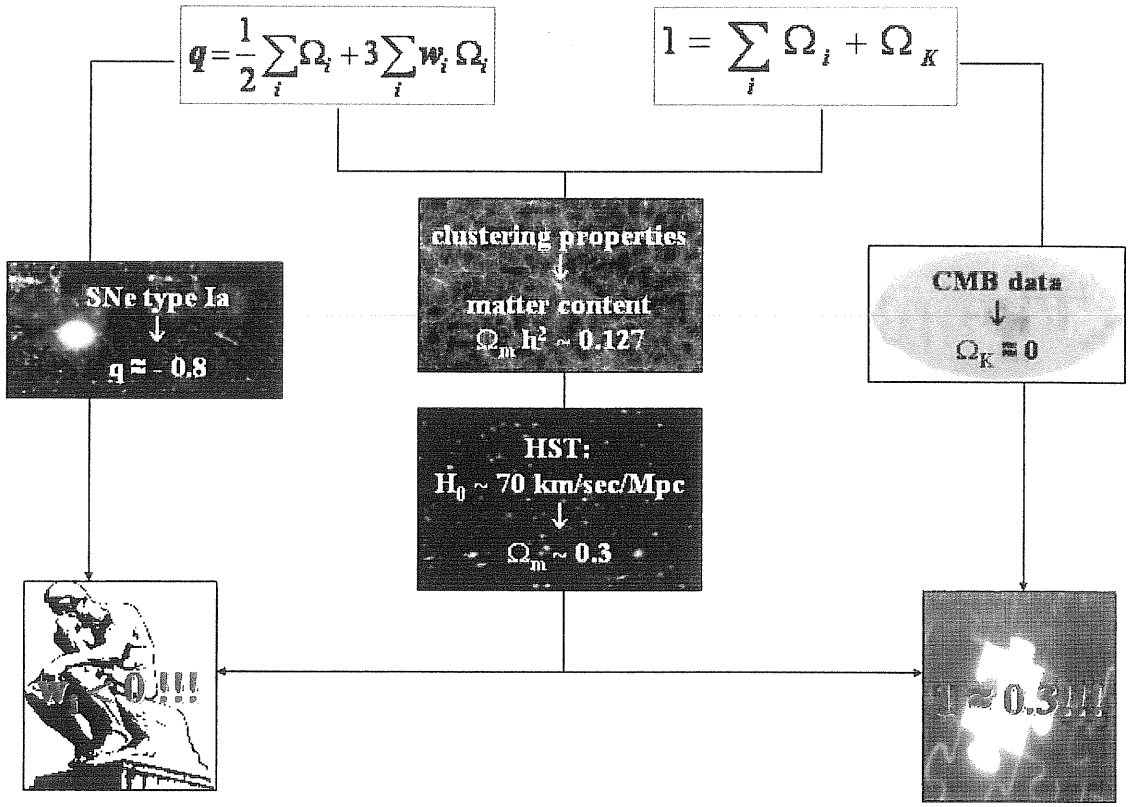

Figure 1.2: A graphical representation of the inconsistencies arising from the Friedmann and Rayachaudhuri equations if no vacuum energy is assumed.

Chapter 2

The physics of gravitational lensing

In this chapter we review the basic principles of gravitational lensing in astrophysical contexts. Lensing has a plethora of applications in Cosmology and Astronomy and of course we cannot mention all of them; we will therefore focus on the aspects that are more relevant for the present work, namely the *weak* lensing and its effect on the Cosmic Microwave Background, and we will try to explain why we regard it as a particularly suitable tool for dark energy studies. Most of the content of this Chapter is based on refs. [30, 31, 32, 33].

2.1 Notation

Our framework for this discussion will be the concordance cosmological model discussed in the previous Chapter; however, for the time being we will drop the hypothesis of spatial flatness.

The growth of structure in the ΛCDM scenario is assumed to be seeded by quantum oscillations of a inflationary scalar field in the very early Universe, during a transient phase characterized by a finite vacuum energy driving accelerated expansion; those oscillations are reinterpreted in a quantum-to-classical transition as small primordial perturbations in the matter fields (the Cosmological Constant does not experience perturbations by definition), which evolve under the gravitational interactions. The dark matter is assumed to be "cold", *i.e.* non-relativistic at the epoch of its decoupling, and thus gives rise to hierarchical

structures (first the smallest objects, like stars, are formed, then galaxies and clusters as a result of progressive mergings).

We will assume the simplest inflation model to hold, with a single scalar field being the source of matter inhomogeneities, and will assume that the cosmological perturbations theory at the linear level is a good approximation. The corresponding FRW metric element is modified in the following way:

$$ds^2 = -(1+2\,\Psi)dt^2 + a^2(t)((1+2\,\Phi)\gamma_{ij})dx^i dx^j \tag{2.1}$$

where γ_{ij}, $i,j = 1,2,3$ is the metric of the 3-space, so that the line element dl^2 is

$$dl^2 = \gamma_{ij}dx^i dx^j = d\chi^2 + f_K^2(\chi)(d\theta^2 + sin^2\theta d\phi^2), \tag{2.2}$$

and $f_K(\chi)$ is the radial function

$$f_K(\chi) = \begin{cases} K^{-1/2}\sin(K^{1/2}\chi) & K > 0, \\ \chi & K = 0, \\ |K|^{-1/2}\sinh(|K|^{1/2}\chi) & K < 0. \end{cases} \tag{2.3}$$

notice that this form of the metric is equivalent to eq. (1.1) of the previous Chapter, being the result of a redefinition of the radial coordinate χ as $\chi(r) = 1/\sqrt{K}\arcsin\sqrt{K}r$.

We are using the conformal Newtonian gauge, and we are only taking into account lensing by density perturbations rather than from gravitational waves (for a complete treatment of the cosmological perturbation theory, including justifications of the assumptions listed here, see the following Chapter).

The equation (2.1) is often rewritten in terms of the *conformal time* η, defined as the time measured by the clock of an observer comoving with the expansion, and related to the proper time as

$$dt = a(t)\,d\eta. \tag{2.4}$$

Throughout the discussion we will in general use the conformal time, however labeling respectively with dots and primes the derivatives with respect to the proper and conformal time in order to avoid confusion.

Finally, we want to introduce here another distance indicator which we will use often in

the following, the *angular diameter distance* $D(z)$, defined as the ratio between the physical cross section δS of an object at redshift z and the solid angle $\delta\Omega$ it subtends for an observer at the present time: $\delta\Omega\, D^2(z) = \delta S$. Computing the latter explicitly it follows easily that it is related to the radial coordinate $f_K(\chi)$ by

$$D(z) = a(z)\, f_K(\chi(z))\,. \tag{2.5}$$

2.2 Lensing systems

The basic idea of gravitational lensing is extremely simple: any mass distribution modifies the structure of the spacetime, and therefore the trajectories that free falling objects follow in this spacetime. If the free falling objects are photons along their null geodesics, this amounts to say that observed light rays which have encountered a density distribution in their path towards us have suffered a deviation.
Gravitational lensing system are made up by three essential ingredients:

- a physical objects that emits light, identifiable with the **source**; it can be a star, a galaxy, or a quasar, for instance;
- a matter concentration acting as the deflector (or **lens**), which does not need to be luminous but only to feel gravitational interactions, and thus can be a star, a galaxy, but also a dark matter halo or a black hole;
- an **observer**, namely someone collecting the emitted light at known distance from source and lens by means of a telescope or a detector.

In addition to these elements, in order to be determined we need knowledge of the properties of the **spacetime**, which may be regarded as the fourth element of the picture, in which the gravitational lensing system is embedded.
The relative position of the set source-lens-observer will play its role as well: although in principle *any* mass distribution in the Universe bends the spacetime thus acting as lens for *any* source, a (rough) alignment among the three elements is needed in order for the effect to be appreciable.

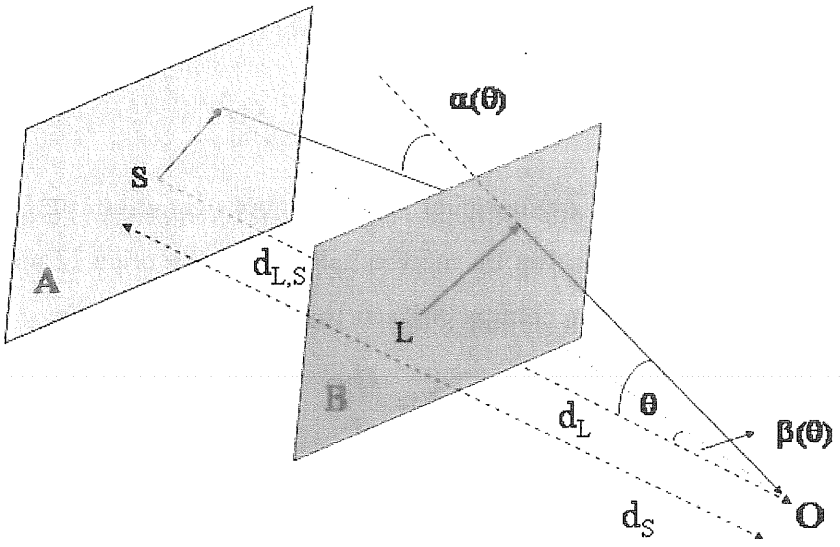

Figure 2.1: Sketch of a typical lensing system: A e B denote respectively the source and lens planes, O is the location of an observer at the origin of coordinates.

In almost all the astrophysical lensing situations the light behavior is well described through the *geometrical optics approximation*, basically requiring that the wavelength of the light is much smaller both than its typical travel distance and the Universe' radius of curvature, which is proportional to H_0^{-1}. If this is the case:

- light can be treated as particle-like, forgetting about its wave nature, and the laws of gravitational lensing coincide with those of geometrical optics;

- since the radial extension of the involved astrophysical entities is much smaller than their relative distances (which are of "cosmological" - comparable with the Universe's one - size), source, lens and observer can be thought of as lying on planes. In particular, the spatial coordinates can be separated into a "radial" coordinate along the line of sight and two angular ones lying on a plane perpendicular to it, and characterizing the angular displacement from the polar axis. This latter is often referred to as the "flat-sky" approximation. The geometry of the problem is depicted in Fig. 2.1.

From the Figure we read that a source whose angular position is β will be seen by an observer at the origin as arriving from an apparent angular position $\vec{\theta}$, *i.e.* differing from

the true one by an amount $\vec{\alpha}$ called *deflection angle*. In a few words, solving the lensing system is equivalent to find the function remapping the observed light path into the emitted, unlensed ones:

$$\mathcal{A}(\vec{\theta}) = \frac{\partial \vec{\beta}}{\partial \vec{\theta}}. \tag{2.6}$$

If we are in presence of weak gravitational fields the above equation can be linearized. The validity of such approximation can be checked calculating the order of magnitude of fields generated by the most massive clumpy objects, the clusters of galaxies:

$$\Phi \simeq \frac{M\,G}{r}; \tag{2.7}$$

substituting typical values $M \simeq 10^{15} M_{\odot}$ and $r \simeq$ few Mpc we get an order of magnitude for $\Phi \leq 10^{-5}$, ensuring the reliability of this method at least for this type of lenses. Therefore

$$\mathcal{A}(\vec{\theta}) \simeq \delta_{ij} - \Psi_{ij}(\vec{\theta}) \tag{2.8}$$

where Ψ_{ij} is called *distortion tensor*.

From now on we will focus on the situation that we want to study, the lensing from large-scale structures, and we will discuss the properties of convergence and shear in this context.

2.3 Weak lensing by large-scale structures

Gravitational lensing effects are relevant in many different astrophysical situations. One important classification is related to "how much the lensing change the image of the source". In particular, the geometry of the source-lens-observer system allows to define a quantity called *critical surface mass density* (again we are assuming units $c = 1$):

$$\Sigma_{\rm cr} = \frac{1}{4\pi G} \frac{D_S}{D_L D_{L,S}} \tag{2.9}$$

where D_S, D_L and $D_{L,S}$ are the angular diameter distances to source, lens and from source to lens as in Fig. 2.1. This quantity can be compared with the *surface mass density* Σ of the lens, which is the integral of its density distribution along the line of sight. It can be shown (*i.e.* [34]) that if

$$\Sigma > \Sigma_{\rm cr} \tag{2.10}$$

Figure 2.2: The double image of the quasar Q0957+561, the first observed multi-lensed object.

at some point, the mapping given by eq. (2.6) is not unique,and the lens is able to produce multiple images of a single source.

This type of lensing effects are often referred to as *strong*, and are indeed fairly spectacular. Such phenomenon was first observed in 1979 with the discovery of the multiple-imaged quasar Q0957+561 [35] at redshift $z = 1.41$, together with its galaxy at $z = 0.36$. However, if the surface mass density of the lens is small with respect to the critical one, the lensing will show up as a weak distortion of the background source. If this is case a single observation cannot provide cosmological information, but the use of statistical approach is needed. In order to do so, the source has either to be diffuse, so that observations can be made in different directions in the sky, or to be made up by a very large number of objects. This requirement confine the choice to basically two candidates: the background galaxies and the Cosmic Microwave Background. The latter, and the weak lensing effects on it, are the subject of the present work.

2.4 Lensing theory

In order to reconstruct the lensing effect on the background CMB image it is necessary to work out the form of the lensing equation for the photons in the perturbed

FRW spacetime, which is nothing but the geodesic equation in the General Relativity context with the condition $ds^2 = 0$.

We follow the approach by [36], deriving the photon trajectories as solutions with $ds^2 = 0$ of the geodesic equation for the metric (2.1); the lensing deflection around a given direction in the sky is described introducing new angular coordinates θ_x and θ_y, defined as

$$\theta_x = \theta \cos\varphi; \quad \theta_y = \theta \sin\varphi\,, \tag{2.11}$$

where $\theta = \sqrt{\theta_x^2 + \theta_y^2}$ and φ are the polar coordinates in the (θ_x, θ_y) plane.

We use the convention, already mentioned,

$$\chi(r) = \frac{1}{\sqrt{K}} \arcsin\sqrt{K} r \tag{2.12}$$

so that the spatial background metric takes the more readable form:

$$dl^2 = d\chi^2 + \frac{\sin^2\sqrt{K}\chi}{K}(d\theta_x^2 + d\theta_y^2) \tag{2.13}$$

notice that the above substitution is valid also for open Universes ($K < 0$) and leads to an equivalent expression with $arcsin \to arcsinh$. Therefore, this notation is equivalent to

$$dl^2 = d\chi^2 + f_K^2(\chi)(d\theta_x^2 + d\theta_y^2)\,; \tag{2.14}$$

which makes use of the radial function $f_K(\chi)$ introduced at the beginning of this Chapter, and we may indifferently use both of them.

Finally, the chosen notation for the angular part is convenient because the weak lensing hypothesis immediately reflects in the condition

$$\theta \ll 1\,, \tag{2.15}$$

which allows to write the geodesic equation at first order in the deflection angle, in addition to the usual linear approximation for metric perturbations. The geodesic equation is indeed

$$\frac{d^2 r^\alpha}{d\lambda^2} = -g^{\alpha\beta}\left(g_{\beta\nu,\mu} - \frac{1}{2} g_{\mu\nu,\beta}\right)\frac{dr^\mu}{d\lambda}\frac{dr^\nu}{d\lambda}\,, \tag{2.16}$$

The above equation is valid order by order; at order zero (both in the cosmological perturbations and in θ) it is simply a null identity for the angular part, but solving for $\alpha = 0$ and $\alpha = 1$ gives the relations:

$$d\eta = 1/a^2 d\lambda, \quad dr = 1/a^2 d\lambda; \tag{2.17}$$

these expressions can be substituted into the perturbed first order equation for the angular part in order to get

$$\frac{d^2\theta_x}{d\eta^2} = 2\frac{K}{\sin^2\sqrt{K}\chi}\partial_{\theta_x}\Phi - 2\sqrt{K}\frac{\cos\sqrt{K}\chi}{\sin\sqrt{K}\chi}\frac{d\theta_x}{d\eta} \tag{2.18}$$

for the angular coordinate θ_x, and another formally equivalent one for θ_y, with $x \longrightarrow y$.
In terms of the comoving displacement from the polar axis, being at first order $x_i = \theta_i f_K(\chi)$, equation (2.18) simply reads

$$x_i'' = -K\,x_i + 2\frac{\partial\Phi}{\partial x_i} \tag{2.19}$$

where the first term on the right hand side describes the tendency of two nearby rays to converge, diverge or remain parallel according to the geometry of the universe, while the second accounts for the lensing effect due to the metric perturbations. The general solution of this equation is

$$x_i + A_i\,f_K(\chi) + B_i\frac{d\,f_K(\chi)}{d\chi} = 2\int_0^\chi d\chi' f_K(\chi-\chi')\nabla_i(\Phi(\mathbf{x},\chi')) \tag{2.20}$$

where A_i and B_i are integration constants, and the potential has to be generally evaluated along the real (perturbed) trajectories.
For the situation we have in mind we need to determine the comoving separation between two lensed rays, starting from the same point, one in the direction of the polar axis and the other one in a direction $\hat{\mathbf{n}}$, on a source plane at distance χ_s; these initial conditions fix $A_i = \theta_i$ and $B_i = 0$ above. However, the truly meaningful quantity is not the absolute difference in the trajectories of the two rays, simply because there is no "straight" fiducial ray (or a uniquely defined polar axis) in a perturbed cosmological background; we will want to evaluate the *difference* in the relative deviations of two arbitrary neighboring rays, which will thus follow the equation

$$(\ddot{\Delta x_i}) = -K\Delta x_i + 2\Delta x_j\nabla_j\nabla_i\Phi \tag{2.21}$$

whose solution, assuming continuity of the gravitational potential, is

$$\Delta x_i = \Delta\theta_i f_K(\chi) + 2\Delta\theta_j\int_0^{\chi_H} d\chi' f_K(\chi')f_K(\chi-\chi')\nabla_i\nabla_j\Phi(\mathbf{x},\chi')\,. \tag{2.22}$$

For the sake of simplicity we can redefine x_i, rather than Δx_i, to represent the separation between the two rays, and rewrite the solution in vector form:

$$\mathbf{x}(\mathbf{n},\chi) = f_K(\chi)\mathbf{n} + 2\int_0^\chi d\chi' f_K(\chi')\, f_K(\chi-\chi')\Delta(\nabla_P\Phi(\mathbf{x},\chi')), \tag{2.23}$$

where the notation ∇_P reminds that the gradient is two-dimensional and evaluated along a plane perpendicular to the line of sight.

The solution of the above equation would be very complicated in lack of the weak lensing hypothesis, stating that the relative deviation of two nearby rays is small in comparison to their unperturbed comoving separation:

$$\frac{|\mathbf{x}(\mathbf{n},\chi') - f_K(\chi')\mathbf{n}|}{|f_K(\chi')\mathbf{n}|} \ll 1. \tag{2.24}$$

As a result, the potential Φ in the above integral can be computed at first order along the unperturbed path $\mathbf{x} = f_K(\chi')\mathbf{n}$; this is the so-called *Born approximation*, and the difference in the gradients amounts to a term only depending on χ, which can be safely ignored.

It is quite intuitive to define the deflection angle as the first correction to the trajectories of the two neighboring rays divided by their comoving angular diameter distance:

$$\alpha(\mathbf{n},\chi) = \frac{f_K(\chi)\mathbf{n} - \mathbf{x}(\mathbf{n},\chi)}{f_K(\chi)} = -2\int_0^\chi d\chi' \frac{f_K(\chi-\chi')}{f_K(\chi)}\nabla_P\Phi(f_K(\chi')\mathbf{n},\chi'). \tag{2.25}$$

Finally, remembering that in terms of the angular separation θ_i in the direction i one has

$$x_j(\chi) = (\delta_{ij} - \psi_{ij})\, f_K(\chi)\theta_i\,, \tag{2.26}$$

the relevant distortion tensor ψ_{ij} is identified to be

$$\psi_{ij}(\mathbf{n},\chi) = -2\int_0^\chi d\chi' \frac{f_K(\chi')f_K(\chi-\chi')}{f_K(\chi)}\nabla_i\nabla_j\Phi(f_K(\chi')\mathbf{n},\chi'). \tag{2.27}$$

The components of ψ_{ij} are usually interpreted in terms of a 2-dimensional tensor called *shear* $\gamma = \gamma_1 + i\gamma_2$ and a scalar quantity named *effective convergence* κ, respectively identified as

$$\begin{aligned} \gamma_1 &= \frac{1}{2}(\psi_{11} - \psi_{22})\,; \quad \gamma_2 = \psi_{12}\,; \\ \kappa &= \frac{1}{2}(\psi_{11} + \psi_{22})\,. \end{aligned} \tag{2.28}$$

The equation above can be inverted with the purpose of finding the component of the distortion tensor as

$$\psi_{ij} = \begin{pmatrix} -\kappa - \gamma_1 & -\gamma_2 \\ -\gamma_2 & -\kappa + \gamma_1 \end{pmatrix}, \tag{2.29}$$

which allow to give an intuitive physical meaning to the above quantities.

It is clear that the lensed images are modified both in shape and size. Although gravitational lensing cannot create or destroy photons, it redistributes them so that some sources in the sky appear larger and some other shrunk, conserving the surface brightness and thus changing the observed flux. A useful measure of this effect is the *magnification*, given by the determinant of the Jacobian matrix $\mathcal{A}(\vec{\theta}) \simeq \delta_{ij} - \Psi_{ij}(\vec{\theta})$. In terms of convergence and shear it is given by

$$\mu(\vec{\theta}) = \frac{1}{det[\mathcal{A}(\vec{\theta})]} = \frac{1}{(1-\kappa)^2 - |\gamma|^2}. \tag{2.30}$$

From Eq. (2.27), γ_1, γ_2 and κ are read to be small because of their proportionality to the gravitational potential Ψ; therefore the magnification primarily depends on κ:

$$\mu(\vec{\theta}) \simeq \frac{1}{(1-2\,\kappa)} \simeq 1 + 2\,\kappa, \tag{2.31}$$

so that the convergence can be interpreted as the responsible for the *isotropic* distortion of the images.

In a similar fashion, the off-diagonal terms of this matrix, *i.e.* the components of the shear, accounts for anisotropic effects; in particular, its first (second) component describes the elongation of an initially circular image along the x,y (x = y, x = -y) axes, as represented in Fig. 2.3.

Finally, it is worth noticing that with the definitions above a simple relation between convergence and deflection angle holds:

$$\kappa = \frac{1}{2}(\psi_{11} + \psi_{22}) = \frac{1}{2}\nabla_n \alpha(\mathbf{n}, \chi), \tag{2.32}$$

in analogy with the optics' thin-lens approximation.

The lensing equation can be as well rewritten in terms of the *projected potential* ϕ, defined through the relation

$$\psi_{ij} = \frac{1}{f_K(\chi)^2}\,\nabla_i\,\nabla_j\,\phi\,, \tag{2.33}$$

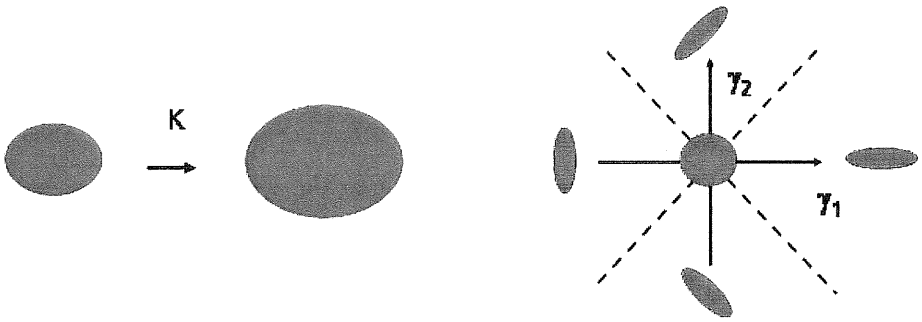

Figure 2.3: The effect of magnification and shear. LEFT: Convergence does not change the shape of the object but only its size. RIGHT: A positive (negative) first component of the shear stretches an initially circular figure along the x (y) direction; the same happens for the second component, with a 45° rotation.

so that

$$\phi(\mathbf{n},\chi) = -2\int_0^{\chi} d\chi f_K(\chi)\,\Phi(f_K(\chi)\mathbf{n},\chi)\int_{\chi}^{\chi_\infty} d\chi' \frac{f_K(\chi'-\chi)}{f_K(\chi')}, \tag{2.34}$$

where χ_∞ stands for the comoving distance at infinite redshift.

Finally, since we usually deal with lensing phenomena from a multiplicity of sources, the distortion tensor, and thus the projected potential, are usually meant to be integrated over the possible source distances:

$$\psi_{ij}(\mathbf{n}) = \int d\chi\, g(\chi_s)\,\psi_{ij}(f_K(\chi_s)\mathbf{n},\chi_s)\,, \tag{2.35}$$

where $g(\chi)$ is a normalized function describing the distribution of the relevant sources. By defining the integral involving the source distribution as

$$g'(\chi) = f_K(\chi)\int_{\chi}^{\chi_\infty} d\chi' \frac{f_K(\chi'-\chi)}{f_K(\chi')} g(\chi')\,, \tag{2.36}$$

the lensing potential (2.34) takes the compact form

$$\phi(\mathbf{n}) = -2\int_0^{\chi_\infty} d\chi\, g'(\chi)\Phi(f_K(\chi)\mathbf{n},\chi)\,. \tag{2.37}$$

Noticeably, when one considers the effect of lensing on the CMB, the source distribution may be replaced by a delta function at the last scattering surface.

2.5 From lensing to Cosmology

We have already emphasized that since we are working in the weak lensing hypothesis, we will need to use the statistical properties of the lensing deviation rather than observables related to the single trajectories. Therefore, we will be basically interested in the above quantities correlation functions, or for algebraic convenience in their Fourier transforms, beginning with the first momentum of the distribution, the power spectrum. Given the Fourier coefficients $\delta(\mathbf{k})$of a homogeneous and isotropic random field, the power spectrum is defined by the relation

$$\langle \delta(\mathbf{k})\delta^*(\mathbf{k}')\rangle = (2\pi)^n \delta(\mathbf{k}-\mathbf{k}')P_\delta(k)\,, \tag{2.38}$$

where n is the dimension of the space (n = 2 in this case) and the average is meant as the average over all the possible statistical realizations.

Since power spectra are defined in Fourier space, derivation with respect to the angular components θ_i corresponds to multiplication by the wave vector l. For the convergence one will need the ensemble average of

$$P_\kappa \propto \langle \left(\sum_i \nabla_i \nabla_i \phi(\mathbf{n}) \right)^2 \rangle \propto (l_1^2 + l_2^2)^2 P_\phi = |\mathbf{l}|^4 P_\phi, \tag{2.39}$$

while for the shear

$$P_\gamma \propto \langle \left(\nabla_1^2 - \nabla_2^2 + 4\,\nabla_1^2\nabla_2^2\phi(\mathbf{n})\right)^2 \rangle \propto |\mathbf{l}|^4 P_\phi, \tag{2.40}$$

so that thanks to the symmetry of the Jacobian matrix (2.29), the power spectra of convergence and shear are equivalent for cosmological purposes; our notation choice will be to work out the expression for the former.

The link between the gravitational lensing-related variables defined above and the cosmological ones is provided by the Poisson equation, which in the fiducial ΛCDM model reads

$$\triangle\Phi = \frac{3H_0^2\Omega_0}{2\,a}\delta, \tag{2.41}$$

where δ is the density contrast $\delta\rho/\rho$ of the cold dark matter, which, together with the baryons, is the only fluctuating component in this scenario. The left hand side if this equation contains the full 3-dimensional Laplacian of the gravitational potential rather

than the perpendicular one appearing in the definition of the convergence; however, the derivative with respect to the line of sight direction averages to zero in the integral along the comoving distance, allowing to replace $\triangle_P\phi$ with $\triangle\Phi$ in our case (the validity of this approximation has been verified numerically to high accuracy in [37]). Therefore,

$$\kappa(\mathbf{n}) = \frac{3H_0^2\Omega_0}{2}\int_H^\chi d\chi g'(\chi) f_K(\chi)\frac{\delta(f_K(\chi)\mathbf{n},\chi)}{a(\chi)}. \tag{2.42}$$

The final step leading to the expression for the power spectrum of the convergence in terms of that of the density contrast relies on the *Limber approximation*, which we won't report here, based on the assumption that δ does not vary significantly over the typical correlation length scale (*i.e.* [32]). This last piece of information allows to simplify the product of integrals in χ arising from the definition of the power spectrum of κ which is quadratic in the Fourier coefficients, finally leading to

$$P_\kappa(l) = \frac{9H_0^4\Omega_0^2}{4}\int_0^{\chi_H} d\chi\frac{g'(\chi)}{a^2(\chi)}P_\delta\left(\frac{l}{f_K(\chi),\chi}\right) \tag{2.43}$$

Our first aim is to generalize the treatment of both the gravitational lensing and perturbations formalism in order to get its equivalent for the generalized gravity and dark energy models which are our target; only once this has been done we will be in the conditions of computing the lensing effect for these scenarios making use of a Boltzmann integrator in order to get the right-hand side, and getting in turn the value of the convergence power spectrum (or, as often used, that of the lensing potential, which follows straightforwardly from Eq. (2.34).

Having worked out the instruments we need and defined the notation and the language for our analysis, we now turn to a brief account of the effect of lensing on the CMB, which is the specific subject of the present PhD research.

2.6 Lensing of the Cosmic Microwave Background

The Cosmic Microwave Background signal is a prediction of the hot Big Bang theory (*i.e.* [50]), thought to have been generated in the early stages of the Universe' life by the decoupling of photons from baryons. At that epoch, corresponding to a cosmic age

of roughly 380000 years, or to a redshift $z \simeq 1100$, the energy of free electrons progressively decreases below the hydrogen ionization threshold, so that the occurrence of Thomson scattering between electrons and photons diminishes. Eventually, the mean free path of those photons becomes so large that they can be treated as freely travelling towards the present epoch: the Universe has become transparent to this radiation, and the Cosmic (not yet Microwave) Background is born.

While the number density of these non-interacting photons stays constant, they suffer nonetheless a loss of energy due to the cosmological expansion: their physical wavelength scales like $1/a$, so that their energy density is proportional to $1/a^4$. If we assume - as a rough approximation - that their distribution function is well described by a black-body radiation (for a more precise treatment see e.g. [41]) with $\rho \propto T^4$, we can infer the scaling of the temperature to be $T \propto a^{-1}$. Therefore, we expect to see the echo of that signal in the form of diffuse radiation roughly one thousand times colder than it was at its birth, corresponding to a temperature of a few Kelvin degrees. This radiation was indeed first observed in 1965 [43]. Many afterwards observations confirmed that it is indeed extremely uniform [42, 16], with relative variations as small as 10^{-5}. However, the tiny anisotropies of the CMB are of invaluable importance for cosmologists, mainly because their presence and amplitude confirm the theory of cosmological perturbations as the mechanism for structure formation, and from their specific features a large number of the cosmological parameters can be computed.

The CMB signal is lensed in its journey towards us because it crosses the gravitational fields of the forming structures. However, since lensing conserves the surface brightness (which amounts to say that it cannot generate photons but only redistribute them), if the CMB was completely uniform we wouldn't be able to appreciate any lensing effect. It is thanks to the anisotropies that cold and hot spots, which are magnified in different measure, that the lensing can give rise to an observable effect.

2.6.1 The unlensed CMB radiation

We introduce here the notation for the CMB spectra which will be the basis for the description of the lensing effect; we use the conventions of CMBfast for the perturbations equations, [108] in order to make easier the comparison between theory and numerical work. The anisotropies in the background radiation are usually described by a random Gaussian field. This assumption is sustained on the theoretical side by the predictions of the simplest inflationary models in the context of the linear perturbation theory, and is supported up to a reasonable extent by observations. However, there are numerous possible sources of non-Gaussianity which may weaken the validity of such approximation. Some primordial non-Gaussianity (however strongly model-dependent) is always present due to the higher orders in perturbations theory (*i.e.* [44, 45, 46] and references therein); a larger amount of non-Gaussianity is introduced at later times, primarily by the lensing itself.

However, since we are considering here the spectra at last scattering, we will assume that the signal is Gaussian and therefore the correlation functions (or the power spectra) are the only relevant statistical quantities.

The anisotropies in the temperature are naturally represented by the direction-dependent relative temperature anisotropy, $\Theta(\hat{\mathbf{n}}) = \delta T(\hat{\mathbf{n}})/T$, where T is the average CMB temperature. In addition to it, the distribution of temperature anisotropies also shows a quadrupole moment in its angular pattern. The electromagnetic interactions at T $\simeq$ 3000 K (that of decoupling) are dominated by electron scattering in the Thomson regime, and it is known (*i.e.* [47]) that the scattering of an anisotropic radiation with a quadrupole moment scattering produces some linear polarization, whose amount will be a fraction of the total intensity of the anisotropies, in the outcoming radiation. Polarization is a rank-two tensor; assuming that circular polarization is absent (which is indeed true for most of the early Universe models) it is further constrained to have only two independent degrees of freedom, and its components are well described by the so called *Stokes parameters* Q and U, which are the analogous of the shear components γ_1 and γ_2 for the shear tensor.

Formally, the procedure by which the power spectra of the CMB anisotropies are defined is the following [39]. The relevant components of the anisotropies can be expanded in a com-

plete set of functions in the sky, the *spherical harmonics* ${}_sY_l^m(\mathbf{n})$, where $\mathbf{n}$ is the propagation direction and s is the spin index, which is zero for a scalar field such as the temperature and two for a spin-2 field like the polarization. Therefore,

$$\Theta(\hat{\mathbf{n}}) = \sum_{lm} \Theta_{lm} Y_m^l(\hat{\mathbf{n}}) \tag{2.44}$$

for the temperature case, while the polarization on the sky may assume the tensor form

$$\mathbf{P}(\hat{\mathbf{n}}) \;=\; {}_+X(\hat{\mathbf{n}})\,(\mathbf{m}_+ \otimes \mathbf{m}_+) + {}_-X(\hat{\mathbf{n}})\,(\mathbf{m}_- \otimes \mathbf{m}_-)\,, \tag{2.45}$$

where

$$\begin{aligned} {}_\pm X(\hat{\mathbf{n}}) &= Q(\hat{\mathbf{n}}) \pm iU(\hat{\mathbf{n}})\,, \\ \mathbf{m}_\pm &= \frac{1}{\sqrt{2}}(\hat{\mathbf{e}}_\theta \mp i\hat{\mathbf{e}}_\phi)\,. \end{aligned} \tag{2.46}$$

The complex Stokes parameter ${}_\pm X$ is a spin-2 object which can be decomposed in the spin-spherical harmonics

$${}_\pm X(\mathbf{n}) = \sum_{lm} {}_\pm X_{lm}\, {}_{\pm 2}Y_l^m(\hat{\mathbf{n}})\,. \tag{2.47}$$

The parity properties of the spin-spherical harmonics

$${}_sY_l^m \to (-1)^l\, {}_{-s}Y_l^m\,, \tag{2.48}$$

allows to introduce the parity eigenstates [48, 49]

$${}_\pm X_{lm} = E_{lm} \pm iB_{lm}\,, \tag{2.49}$$

such that E_{lm} just like Θ_{lm} has parity $(-1)^l$ ("electric" parity) whereas B_{lm} has parity $(-1)^{l+1}$ ("magnetic" parity). This combination is convenient because it was noticed (*i.e.* [48, 49]) that though E-modes of polarization are sourced by all types of perturbations, the B-modes are generated from vectors and tensors only. Since in linear theory different types of perturbations evolve independently, and under our condition of absence of the vector modes, this representation allows an immediate interpretation of the mechanism responsible for the single components.

Due to the assumption of Gaussianity, the power spectra and cross correlation of these quantities can be defined as

$$\left\langle X^*_{lm} X'_{l'm'} \right\rangle = \delta_{l,l'} \delta_{m,m'} C_l^{XX'}, \tag{2.50}$$

where X and X' can take on the values Θ,E,B. The cross power spectrum between B and Θ or E vanishes because of their opposite parity classification.

The physics of the CMB anisotropies is well understood and has been reviewed in many papers (*i.e.* [151]); here we only want to assess some basic features which are essential for the description of the lensing effect, and will consider only scalar perturbations in what follows.

On a very general basis, in the very early Universe the baryons and the photons form a tightly coupled fluid, glued by the electrons which interact with photons via Thomson scattering, and with protons via Coulomb interactions. With the decrease of the temperature following the expansion, the rate of photon-electron scattering decreases in favour of that of the combination of electrons with protons to form neutral hydrogen (recombination). Once the cross section of the latter process becomes larger than that of Thomson scattering, as a first approximation photons propagate freely towards us, somehow bringing a snapshot of the anisotropy distribution at such epoch. The evolution equation for the Fourier modes of the temperature were following an evolution equation which is that of a harmonic oscillator with elastic constant given by the sound velocity c_s [151]:

$$\ddot{\Theta} + c_s^2 k^2 \Theta = 0. \tag{2.51}$$

With the ansatz of negligible initial velocity (which has been confirmed by observations), the above equation has the oscillatory solution:

$$\Theta(\tau_{\rm rec}) = \Theta(0) \cos(k\, s_{\rm rec}), \tag{2.52}$$

where $s_{\rm rec}$ is the sound horizon, which is thus recognized to be the crucial scale of reference. Perturbations with a larger wavelength had not time to interact yet, and should be seen as "frozen" at their initial conditions in the TT spectrum. On smaller scales, the way modes which were inside the horizon appear now depend on the phase with which they have been

caught. Modes at the maxima or minima of their oscillation will set the largest temperature anisotropy, and therefore will correspond to "acoustic peaks" of the distribution; in particular, the largest-scale peak is set by the mode for which the sound horizon corresponds to half of its wavelength, so that it reaches its first maximum just at the recombination. On the other hand, modes for which recombination occurs half the way between a maximum and minimum are will generate the minima of the distribution; notice that in this simple representation the latter should be zero, and the maxima should all have the same height. The real physical situation is complicated by the gravitational force and the presence of baryons, which appears as non-null right hand side of Eq. (2.51), so that the relative height of the peaks changes and the equilibrium point is shifted toward a non-null value. Moving now on even smaller scales, where the peaks are much lower, another phenomenon enters the picture: the fact that the mean free path of photons overcomes the wavelength of the perturbations. In other words, residual scattering for these modes can destroy the memory of the anisotropies distribution: this feature is known as dumping [40] and cause the TT power spectrum to be rapidly decreasing for $l \geq 1000$.

While the mechanisms described up to now were due to physics at the last scattering, the CMB spectra can be modified in their journey from $z \simeq 1100$ to $z = 0$ by other effects, known as *secondary* anisotropies (compared to the *primary* ones, which are those imprinted at last scattering). Apart from the lensing itself, which naturally belongs to this category but will be treated separately in the next Sections, we only want to mention here the Integrated Sachs-Wolfe (ISW) effect, which acts on the otherwise featureless large scales, and is particularly important for dark energy models. Its physical origin lies in the possible time variation of the gravitational potential in the time interval by which a photons falls and climbs out a potential well. While in matter domination the potential Φ is constant, it effectively decays once the dark energy component becomes significant; therefore we can expect a rise in the large-scale power of the TT spectrum proportional to $\dot{\Phi}$, which in turn will be determined by the dark energy abundance.

We don't want to propose an analogous discussion for the polarization modes here. We just remark that the acoustic peaks are a clear feature of the EE modes as well; their equation of motion, however, is sourced by $\dot{\Theta}$ and therefore the oscillatory behavior is proportional

to $\sin(k\, s_{\rm rec})$, and shifted of $\pi/2$ with respect the temperature case. This feature is reflected in the TT and EE spectra as a switch of the positions of peaks and troughs. Primordial BB modes, on the contrary, are not sourced by scalar perturbations. The only primary anisotropies of the latter are the gravitational waves, coming from tensor-type perturbations and appearing at $l \simeq 100$: modes on larger scales have not entered the horizon yet, and on smaller scales rapidly decay, since the gravitational waves are massless. A significant secondary mechanism is the reionization: CMB photons are re-scattered on electrons freed again by the light of first luminous objects, and this generates some power of the same order of that of the gravitational waves but on very large scales $l \simeq 10$, which is the typical coherence length for such electrons.
We show the (still unlensed) TT, EE, BB and the correlation TE power spectra here for a ΛCDM model in Fig. 2.4.

In the following we give a qualitative account of the main effect of lensing on the CMB signal, while the mathematical treatment of the lensed spectra is postponed to the next Chapter.

2.6.2 Qualitative overview

The first questions that we want to answer are which is the order of magnitude of the lensing with respect to the primordial power spectra and where in the multipole space we may expect to observe the effect.
It is clear that lensing will be a small, second-order correction, because it is generated by the anisotropies in the matter distribution onto the CMB spectra, whose amplitude is already proportional to that of the gravitational potentials. How small, though? General Relativity tells us that the order of magnitude of the deflection angle for a light ray passing through a potential well of amplitude few $\times 10^{-5}$, which is the typical value for large clustered objects as already discussed, will be $\delta\alpha \simeq 4\,\Phi \simeq 10^{-4}$ (in radians). A reasonable estimate of the size of the potential well is given by that of the peak in the matter power spectrum, which is $\simeq 300$ Mpc in comoving units, we may expect a single bundle to encounter $\simeq 50$ of those wells in its $\simeq 14000$ comoving Mpc of its journey from the last scattering surface to us. Assuming that the potential wells are uncorrelated, this gives a global effect of $\sqrt{50} \times 10^{-4}$,

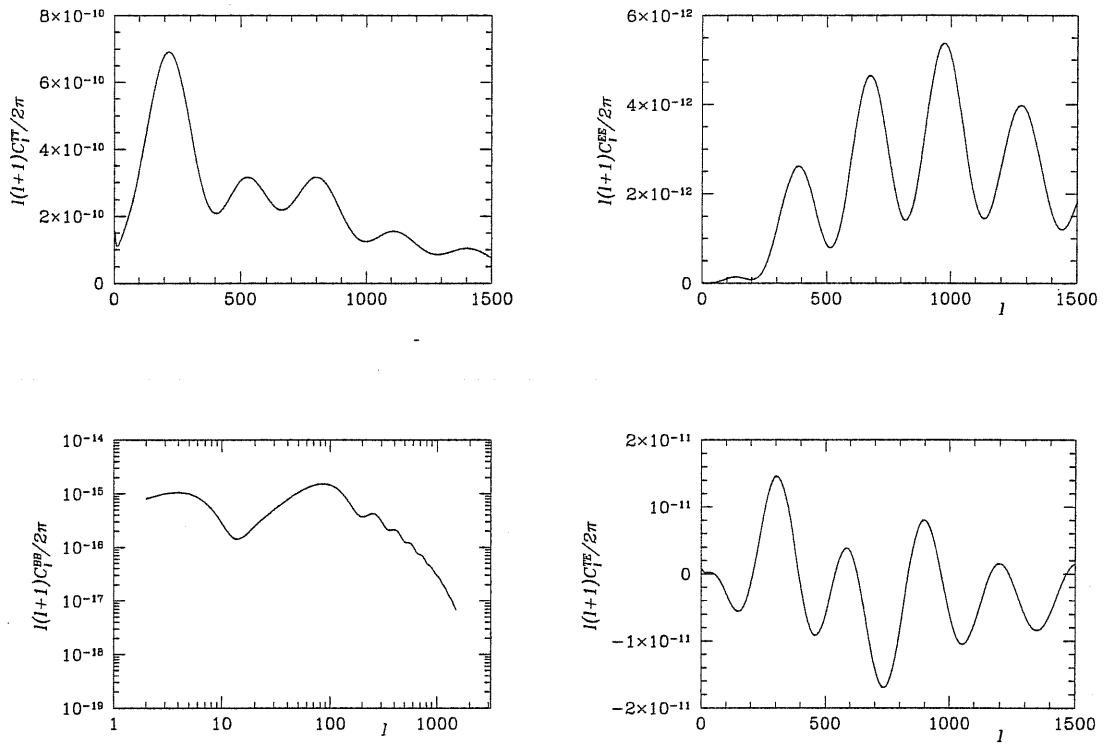

Figure 2.4: Unlensed power spectra for the ΛCDM concordance model: from left to right and top to bottom, temperature, E and B modes of polarization, and T-E correlation spectra. The plot relative to the B modes is in logarithmic scale.

corresponding to an angle of $\simeq 7 \times 10^{-4} \times 180/\pi \simeq 2$ arcminutes [33].

This is the angular size of the lensing corrections, which however has to be compared with its coherence scale. A rough estimate of the latter can be obtained assuming a potential well of the above size located midway to the distance to the last scattering, which subtends an angle $\simeq$ 300 Mpc /7000 Mpc $\simeq 2°$ (a more rigorous calculation corrects this estimate by a factor $\simeq 3$, leading to a corresponding decrease of this number [32]). Therefore, lensing corrections appear already at the acoustic scales where coherent light deflection sets in, despite the fact that the physical range of the effect is much smaller: on the degree scale it corresponds to a correction of a few %, while on very small scales ($l \geq 3000$) lensing can be regarded as a order unity contribution to the global CMB signal, since the primordial amplitude is so small in the damping tail. In summary, lensing redistributes the power

coming from larger and smaller scales, mixing different wavelength contributions; the effect is visible starting from the degree scale and the amplitude of the mixing is of the order of a few arcminutes.

The order-of-magnitude discussion above holds both for the temperature and the polarization power spectra, but the lensing features appear very different in the two cases.

In the temperature case, the main effect of lensing is to smooth the peaks-and-troughs distribution: the low-power regions in vicinity of a peak are slightly enhanced, while the amplitude of the peak itself diminishes. On smaller scales, those of the damping tail, there is a systematic increase of the power due to mixing with larger scales [38]. In the case of the polarization, lensing warps the polarization vector and alters its symmetries, causing a reshuffle of the power coming from the different-parity EE and BB modes. The effect on the former is rather similar to the temperature case, but more pronounced because the features of the primordial spectrum are sharper, and thus the smoothing process in more evident.

The mathematical explanation for the discussed effects relies in the facts that the lensed C^{TT}, C^{TE} and C^{EE} are obtained by a convolution of the unlensed spectra with that of the lensing potential: the latter peaks at $l \simeq 60$, setting the broadness of the power mixing, as shown in Fig. 2.5.

However, the situation is significantly different for the BB modes of polarization. In the concordance model (coming from the simplest but effective inflationary scenarios) the only primordial magnetic modes are the gravitational waves, which appear at lower multipoles (with a maximum at $l \simeq 100$, as already discussed). In this case lensing is the only responsible for the power in the BB modes at smaller scales.

The effect of gravitational lensing is shown in Figs. 2.6,2.7,2.8 for the temperature, polarization and their cross correlation power spectra in the fiducial ΛCDM model. In the temperature case, as well as for the EE modes of polarization, the large scale are substantially unaffected, while the acoustic peaks structure is broadened and smoothed. In particular, Fig. 2.6 shows an enlargement of the lensed and unlensed temperature power spectra in the multipole region $l = 700 - 1200$, where the effect is largest. Lensing appear as a small correction in these cases, where the primary anisotropies are dominant; on the other hand, it is the only source for the BB modes of polarization at $l \geq 200$, due to the

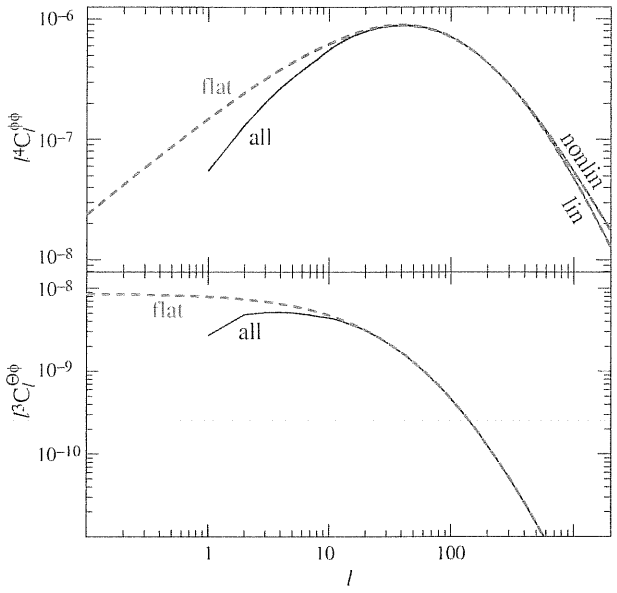

Figure 2.5: The lensing potential power spectrum, showing its characteristic peak at $l \simeq 40$ which gives a measure of the broadness of mixing between different modes. From [39].

lack of primordial signal on these scales. The amplitude of the lensing contribution in the latter case is one order of magnitude larger than those of the reionization bump and the gravitational waves, as evident from the linear plot in Fig. 2.8.

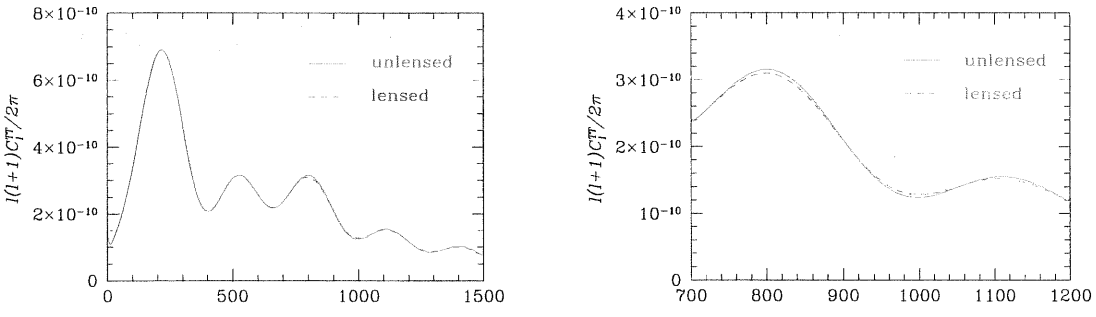

Figure 2.6: Lensed and unlensed temperature power spectrum (left panel) and its enlargement in the multipole region l = 700-1200 (right panel).

We conclude here our qualitative discussion on the physics of CMB lensing: a more formal derivation will be given in the Chap. 4.

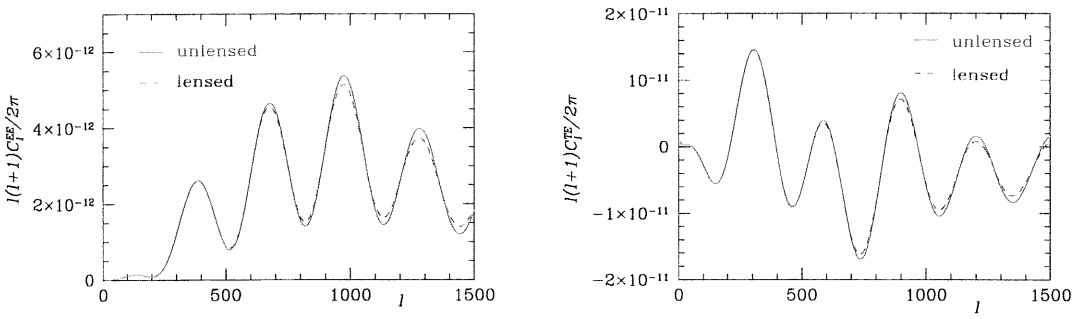

Figure 2.7: Lensed and unlensed EE polarization modes (left panel) and its cross-correlation with the temperature (right panel).

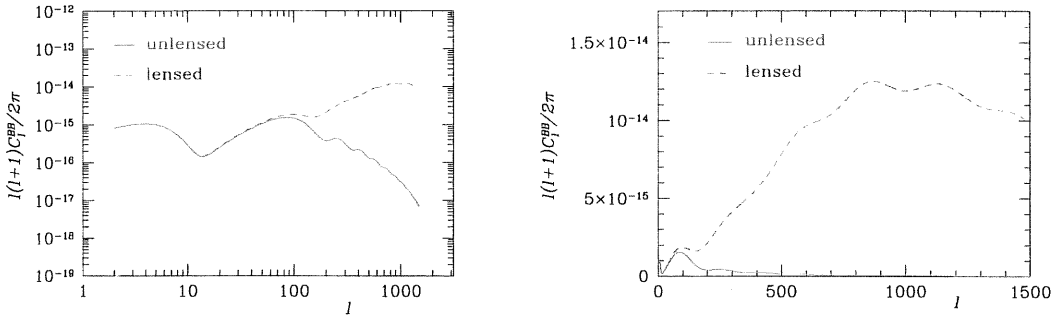

Figure 2.8: Logarithmic (left panel) and linear (right panel) lensed and unlensed BB polarization power spectrum.

2.7 Why CMB lensing for dark energy?

In the light of what discussed up to now we are in the condition to answer this question, which represents the motivation for this PhD research.

A basic feature which makes lensing particularly suitable for Cosmology as a whole is the fact that lensing correlates with the total matter distribution, regardless of its interactions or state. We have already shown, in Chap. 1, some of the difficulties in the determination of the cosmological parameters arising from the necessity of using model-dependent assumptions; a straightforward example is the case of observations of luminous matter, where an empirical mass-to-light ratio (and consequently a bias) must be introduced in order to re-

construct the "true" mass profile. On the other hand, lensing allows to detect and study everything that is subject an object of a gravitational field, which is maybe the most unbiased definition of "matter" one can think about.

However, in the case of dark energy studies there is another major reason that makes lensing a good cosmological estimator. In fact, it is well known (and it will be shown precisely in the following Chapters) that the lensing cross section is not uniform between source and observer, given the position of the lens, but peaks somewhere in the middle, exactly in the same fashion as in the geometrical optics case: if we observe an object through a magnifying glass we won't expect a large magnification if the lens is too close to the observer or too close to the source, but midway between them. In the special case of the CMB as a source, this half-distance corresponds to redshift $z \simeq 1$, which is the most relevant in order to discriminating among different models: it is the one at which the vacuum energy contribution to the global stress-energy tensor starts to be comparable to the matter's one, and it is strongly correlated with the process of structure formation, making the lensing sensitive not only to the expansion' dynamics, but also to the growth of structures. Furthermore, while we have quite tight constraints on the equation of state of dark energy (or in the case of modified gravity, on the deviation from General Relativity's laws) at present (*i.e.* [16]), limits are still rather loose at that epoch, which means that the models are allowed to larger deviations from each other at those redshifts, and thus detection of different behavior is favoured.

Not less important is the fact that the lensing cross section, beyond having its maximum at intermediate redshifts, drops rapidly both in vicinity of observer and source: the effect will therefore be rather insensitive to early times, as well as to the present ones. This last features is particularly interesting since many of the constraints obtained spectroscopically are limited to lower redshift, and thus these two type of probes are independent, which makes the combination of the methods especially powerful. A cartoon representation of how lensing picks up its power in the dark energy rise region is shown in Fig. 2.9.

The very last piece of the puzzle is the reason why we chose the CMB as a source. Again, some of the arguments have general validity: the CMB physics is well understood, there are many different ongoing and future experiments aiming at measuring its temperature and

polarization with increasing precision, and in particular in the case of the lensing having a single source at known redshift is a great simplification of the mathematics one one hand, and of interpretation of the results on the other.

However, the challenge of isolating the lensing effect on the CMB spectra should not be underestimated. The TT and EE modes are dominated by the contribution of primary anisotropies, and one would have to evaluate with the necessary precision the small smoothing effect caused by lensing, and to extract from there an estimate of the dark energy equation of state. On the other hand, in the prospect of isolating the BB modes of polarization, they have the remarkable feature of being almost entirely generated by lensing at late ($z \simeq 1$) redshift, so that they are faithful tracers of the dark energy density (or gravity coupling constant) at that epoch.

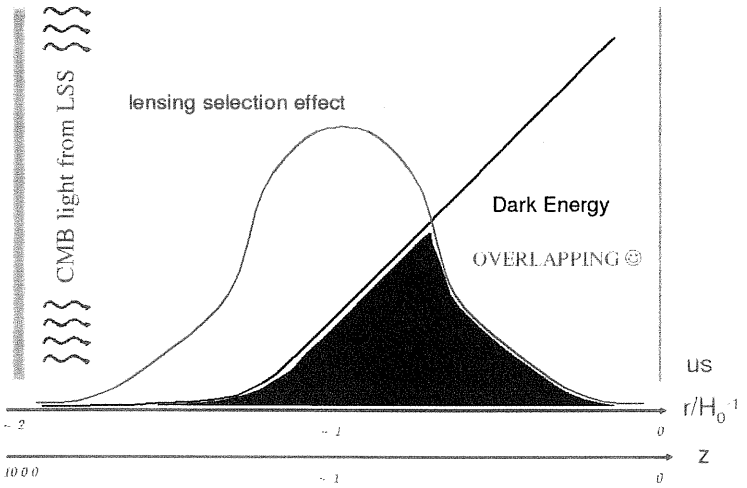

Figure 2.9: A cartoon representation of the CMB lensing cross section and the dark energy behavior.

2.8 Lensing and dark energy: not only CMB

The final section of this Chapter is devoted to a very brief account of another, complementary from the observational point of view, aspect of how the lensing can be useful in order to recover dark energy properties, the lensing on the background galaxies, or

cosmic shear.

The basic idea is that galaxies, considered as a statistical ensemble, have an average ellipticity that the lensing process modifies. Assuming that the shear profile can be reconstructed via ray tracing from N-body cosmological simulations, this method provides a map of the dark matter distribution in the Universe (for a review, see [51]). It has been shown that the weak lensing can directly measure different cosmological parameters, such as σ_8, $\Omega_m$and the shift parameter Γ, or help in removing degeneracies among them [36, 53, 54, 55]. However, in analogy with the lensing of the CMB, this technique is sensitive to the expansion history as well, and it has been proposed as a method for investigating the dark energy dynamics, also in correlation with other measurements such as Supernovæ [52].

The cosmic shear signal was detected for the first time in the year 2000 by several independent groups using different surveys, and all the result showed an impressive agreement. The specific observable is the variance of the shear in randomly placed cells of aperture θ, which obviously depends on Ω_m and σ_8, with the important addition of the mean redshift of the survey. This observable is directly related to the power spectrum of the shear C_l^γ since

$$\sigma_\gamma^2 = \frac{1}{2}\int_0^\infty dl\, C_l^\gamma \mid W_l \mid^2, \tag{2.53}$$

where W_l is the Fourier transform of the cell aperture.

Results are summarized in Fig. (2.10).

Since the redshift of the sources is lower with respect to the CMB case (typically $z \leq 1$ for surveys such as the ones of Fig. (2.10)), weak lensing on the background galaxies is sensitive to more recent epochs, at least for the presently available catalogs. However, constraints coming from those observations are independent of other kind of probes, and thus combination of different measurements of the dark energy parameters brings a significant increase in the available precision, as shown in Fig. (2.11). Here the dark energy equation of state is parametrized as a Taylor expansion in redshift, and the first two terms, w_0 and w_a, are kept (a detailed discussion of this parametrization is given in Chapter 4). The estimate is for the Supernovæ data, the unlensed CMB spectra (without the inclusion of the BB modes), and the lensing on the background galaxies.

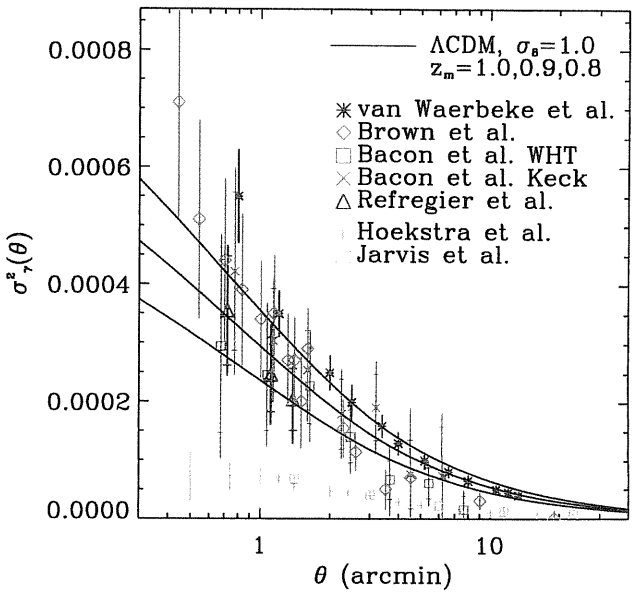

Figure 2.10: Shear variance σ_γ^2 as a function of the radius θ of a circular cell. The data points correspond to recent results from different groups: van Waerbeke et al. (2002a), Brown et al. (2003), Bacon et al. (2002, WHT and Keck), Refregier et al. (2002), Hoekstra et al. (2002b), Jarvis et al. (2002). When relevant, the inner error bars correspond to noise only, whereas the outer error bars correspond to the total error (noise + cosmic variance). The measurements by Hämmerle et al. (2002) and Hamana et al. (2003) are not displayed. The solid curves show the predictions for a ΛCDM model with $\Omega_m = 0.3$, $\sigma_8 = 1$, and $\Gamma = \Omega_0 h = 0.21$. The galaxy median redshift was taken to be $z_m = 1.0, 0.9$, and 0.8, from top to bottom, respectively, corresponding approximately to the range of depth of the top five surveys. The bottom two surveys (Hoekstra et al. 2002b; Jarvis et al. 2002) have a median redshift in the range $z_m \simeq 0.6$–0.7 and, as expected, yield lower shear variances. From [51].

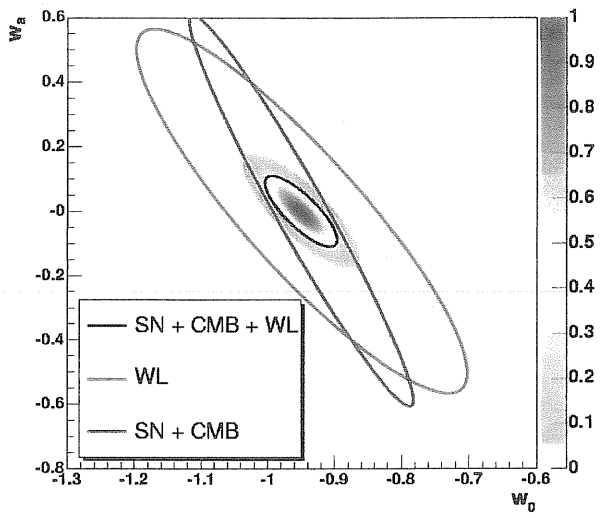

Figure 2.11: Projected constraints for the dark energy parameters for the weak lensing alone and in combination with other probes. From [52].

Chapter 3

Lensing in generalized cosmologies

This Chapter is devoted to the formal derivation of the lensing theory in the models we have chosen to study. We will present the most relevant dark energy as well as modified gravity scenarios, highlighting the possible relative differences in the history of expansion and structure growth, and the way they propagate through the lensing observables. This treatment is introductory to the redefinition and discussion of the lensing variables in these models that we have performed. Most of the work presented in this Chapter was carried out in [56].

3.1 Why not a cosmological constant?

The picture of the universe which has been traced in the previous Chapters and is generally thought of as the "Concordance" is however far from being satisfactory: in particular, without a better insight into the nature of the dark cosmological component, we cannot claim to have a satisfactory physical understanding of cosmology. In fact, the simplest description of the vacuum energy responsible for cosmic acceleration via a Cosmological Constant providing about the 75% of the critical density today raises two problems. The first is the fine tuning required to fix the vacuum energy scale about 120 orders of magnitude less than the Planck energy density which is supposed to be the unification scale of all forces in the early Universe. The second is a coincidence issue, namely why among all the small (but non-zero) available values for the vacuum energy, its was chosen to be

comparable to the critical energy density today. These questions, still largely unsolved, may find a satisfactory answer if the concept of Cosmological Constant is extended to a more general one, admitting some dynamics of the vacuum energy, known now as the dark energy (see [58, 59, 11] and references therein).

The simplest generalization, already introduced well before the present experimental evidences for cosmic acceleration [60, 61], is a scalar field, dynamical and fluctuating, with a background evolution slow enough to mimic a constant vacuum energy given by its potential, providing cosmic acceleration. As soon as the latter was discovered, a renewed interest in these models appeared immediately [62, 63]. In particular, it was demonstrated how the dynamics of this component, under suitable potential shapes inspired by super-symmetry and super-gravity theories (see [64] and [65], respectively, and references therein), can possess attractors in the trajectory space, named tracking solutions, capable to reach the present dark energy density starting from a wide set of initial conditions in the very early universe, thus alleviating, at least classically, the problem of fine-tuning [66, 67]. The scalar field playing the role of the dark energy was named Quintessence. Its coherent insertion among the other cosmological components allowed to constrain it from the existing data [16],[68]-[74], as well as to investigate the relation of the dark energy with the other cosmological components: the explicit coupling with baryons is severely constrained by observations [75], while the possible coupling of the Quintessence with the Ricci scalar [76]-[84],[85]-[92] and the dark matter [96]-[99], as well as the phenomenology arising from generalized kinetic energy terms [100]-[102] have been extensively studied.

The generalization of cosmology that we consider here concerns the Quintessence field as well as the gravitational sector of the fundamental Lagrangian, admitting a general dependence on the Ricci and Brans-Dicke scalar fields. The latter subject is interesting per se (see [103, 104] and references therein), and is receiving more attention after the discovery of cosmic acceleration, with the attempt to interpret the evidence for dark energy as a manifestation of gravity; this scenario has been recently proved to have relevant consequences for what concerns the dark energy fine-tuning problem mentioned above [92].

3.2 Dark energy or modified gravity?

We want to stress here that our aim in studying the gravitational lensing by large scale structure in the generalized scenario described above is not only to have evidence against or in favour of the Cosmological Constant with respect to a dynamical scenario, but also to discriminate between a dark energy component and a modification of gravity. In fact, it has been shown [106] that this distinction is possible only if we consider observables which are sensitive at the same time to the background expansion and to the growth of structures. This is indeed intuitive because it is possible to impose, for instance, that Quintessence and modified gravity scenarios give rise to the same evolution of the Hubble parameter; this would fix the distance to last scattering, and thus the position of the CMB peaks (assuming that the sound horizon is not influenced by the late-time behaviour of whatever mechanism is causing the present observed acceleration). However, the behavior of the cosmological perturbations would be different due to the change in the matter-to-gravity coupling: an example of such feature is given in Fig. 3.1. This would result in a different lensing effect, as already pointed out. The latter is therefore a suitable observable in order to distinguish between the two cases.

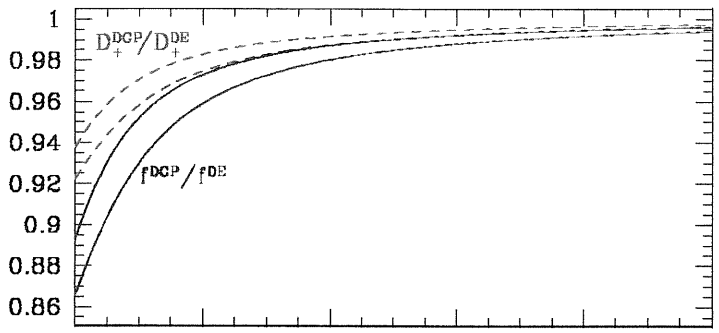

Figure 3.1: The different growth of structures (D_+, blue) and peculiar velocities (f, red) in the Dvali-Gabadadze-Porrati model and in a Quintessence one with the same expansion history. From [106].

3.3 Generalized cosmologies

We will consider a class of theories of gravity whose action is written in natural units as

$$S = \int d^4x\sqrt{-g}\left[\frac{1}{2\kappa}f(\phi,R) - \frac{1}{2}\omega(\phi)\phi^{;\mu}\phi_{;\mu} - V(\phi) + \mathcal{L}_{\rm fluid}\right], \tag{3.1}$$

where g is the determinant of the background metric, R is the Ricci scalar, ω generalizes the kinetic term, and $\mathcal{L}_{\rm fluid}$ includes contributions from the matter and radiation cosmological components; $\kappa = 8\pi G_*$ plays the role of the "bare" gravitational constant, [83]. Here as throughout the following Greek indexes run from 0 to 3, Latin indexes from 1 to 3.
The usual gravity term $R/16\pi G$ has been generalized by the general function $f/2\kappa$ [104, 80]. Note that the formalism adopted is suitable for describing non-scalar-tensor gravity theories, i.e. without ϕ, where however the dependence on R is generic.

3.3.1 Einstein equations

By defining $F(\phi,R) = (1/\kappa)\partial f/\partial R$, the Einstein equations $G_{\mu\nu} = \kappa T_{\mu\nu}$ take the following form [104]:

$$G_{\mu\nu} = T_{\mu\nu} = \frac{1}{F}\left[T^{\rm fluid}_{\mu\nu} + \omega\left(\phi_{,\mu}\phi_{,\nu} - \frac{1}{2}g_{\mu\nu}\phi_{,\sigma}\phi^{,\sigma}\right) + g_{\mu\nu}\frac{f/\kappa - RF - 2V}{2} + F_{,\mu;\nu} - g_{\mu\nu}F^{;\sigma}_{;\sigma}\right],$$

where again one can recognize a part depending on the fluid variables, and a part relative to the non-minimally coupled scalar field of the theory plus a contribution arising from the generalized gravity coupling represented by the function $1/F$; for practical purposes we will render this splitting explicit rewriting $T_{\mu\nu}$ as

$$T_{\mu\nu} = \frac{1}{F}T^{\rm fluid}_{\mu\nu} + \mathcal{T}^{\rm gc}_{\mu\nu}\,. \tag{3.2}$$

Note that in our scheme the generalized cosmology term is active also if gravity is the same as in general relativity, and a minimally coupled scalar field, like in the Quintessence models, represents the only new ingredient with respect to the ordinary case. This is true also in the limiting case where the scalar field reduces to a Cosmological Constant. Moreover, notice that $\mathcal{T}^{\rm gc}_{\mu\nu}$ is not conserved if gravity differs from general relativity; nonetheless, contracted Bianchi identities still hold and ensure

$$(T^{\rm fluid}_{\mu\nu})^{;\mu} = 0\,, \tag{3.3}$$

which allows to derive the equations of motion for the matter variables only, leading to a remarkable simplification [105]. The expression for the stress-energy tensor relative to the scalar field which is conserved in the generalized scenarios described by the action (3.1) must include the term accounting for the interaction with the gravitational field [89]. It is also worth to notice how the equations (3.2) get simplified if the function f is a product of R times a function of the field only:

$$\frac{f}{\kappa} = RF \ . \tag{3.4}$$

In the following, we will refer to this class of cosmologies as Non-Minimally Coupled (NMC) models.

3.4 Formal setting

The first step of the analysis was the development of the formal apparatus needed to have the lensing variables correctly defined in the context given by the action (3.1); this included the generalization of the Einstein equations and the lensing ones. This work was carried out in [56], and we report it here without the need of choosing a specific model among those above, because we willingly kept the notation as general as possible.
We will consider the case of the Extended Quintessence (EQ [90, 82]) scenario, as a representative of NMC models, as an example to illustrate the new aspects of the weak lensing process with respect to ordinary cosmologies; in that cases, the field ϕ, non-minimally coupled to gravity, also represents the dark energy, providing acceleration through its potential V. Specifically, the original EQ works considered a NMC model defined as

$$F(\phi) = \frac{1}{\kappa} + \zeta\phi^2 \ , \tag{3.5}$$

and an inverse power law potential $V(\phi) = M^{4+\alpha}/\phi^{\alpha}$ providing cosmic acceleration today. As we will see later in this thesis, the constraints from solar-system experiments force the correction to the gravitational constant to be small in these specific models. Therefore it is suitable to make approximations in the form of a "first order variation" of the weak lensing observables in generalized gravity theories with respect to the ordinary ΛCDM model.

3.4.1 Background

As a reminder of the notation, we rewrite the unperturbed Friedmann Robertson Walker metric in spherical coordinates as:

$$ds^2 = a^2(\tau)\left(-d\tau^2 + \frac{1}{1-Kr^2}dr^2 + r^2 d\Omega\right), \tag{3.6}$$

where K is the uniform spatial curvature of a spherically symmetric three-space, $d\Omega$ is the metric of the two-sphere, and τ stands for the conformal time variable, related to cosmic time by the usual relation $dt = a(\tau)\,d\tau$.

The energy-momentum tensor (3.2) can be recast in a perfect-fluid form [105]:

$$T_{\mu\nu} = (p+\rho)u_\mu u_\nu + p\, g_{\mu\nu}\,; \tag{3.7}$$

the corresponding background energy density and pressure are easily computed to be:

$$\rho = \frac{1}{F}\left(\rho_{\rm fluid} + \frac{\omega}{2a^2}\phi'^2 + \frac{RF - f/\kappa}{2} + V - \frac{3\mathcal{H}F'}{a^2}\right) = \frac{1}{F}\rho_{\rm fluid} + \rho_{\rm gc}\,, \tag{3.8}$$

$$p = \frac{1}{F}\left(p_{\rm fluid} + \frac{\omega}{2a^2}\phi'^2 - \frac{RF - f/\kappa}{2} - V + \frac{F''}{a^2} + \frac{\mathcal{H}F'}{a^2}\right) = \frac{1}{F}p_{\rm fluid} + p_{\rm gc}\,; \tag{3.9}$$

again the prime denotes differentiation with respect to conformal time and $\mathcal{H}$ is the conformal Hubble factor a'/a. As above, $\rho_{\rm gc}$ and $p_{\rm gc}$ do not obey the conservation law in ordinary cosmologies, $\rho'_{\rm gc} + 3\mathcal{H}(\rho_{\rm gc} + p_{\rm gc}) \neq 0$.

In FRW cosmologies the expansion equation reads

$$\mathcal{H}^2 = a^2\rho - K\,, \tag{3.10}$$

and it cannot be solved directly due to the appearance of $\mathcal{H}$ in $\rho_{\rm gc}$, which is explicit in the last term but is also contained in $RF - f/\kappa$ through

$$R = \frac{6}{a^2}\left(\dot{\mathcal{H}} + \mathcal{H}^2\right). \tag{3.11}$$

Note that this is true also in theories where $f \equiv f(R)$ and no scalar field is present.

On the other hand, NMC scenarios admit a formal solution, which is

$$\mathcal{H} = -\frac{3}{2}\frac{F'}{F} + \sqrt{\frac{9}{4}\left(\frac{F'}{F}\right)^2 + \frac{1}{F}\left(a^2\rho_{\rm fluid} + \frac{\omega}{2}\phi'^2 + a^2V\right) - K}\,, \tag{3.12}$$

where we have selected the expansion solution with positive $\mathcal{H}$. Note that the dependence of the comoving distances r on the redshift $z = 1/a - 1$ gets also modified, according to (3.12):

$$r = \int_0^z \frac{dz}{H(z)} . \tag{3.13}$$

We generically indicate the single components in the fluid with x. Since $T^{\mu\nu}_{\text{fluid}}$ is conserved, energy density, pressure, equation of state and sound velocity, defined as

$$\rho_x = -T^0_{0x} \ , \ p_x = 1/3\, T^i_{ix} \ , \ w_x = p_x/\rho_x \ , \ c_s^2 = p_x'/\rho_x' \ , \tag{3.14}$$

give rise to conservation equations for each non-interacting component having the familiar form:

$$\rho_x' + 3\mathcal{H}\rho_x(1 + w_x) = 0 \ . \tag{3.15}$$

The last ingredient is the Klein-Gordon equation for the evolution of the field, which is substantially different from the case of ordinary cosmologies:

$$\phi'' + 2\mathcal{H}\phi' + \frac{1}{2\omega}\left(\omega_{,\phi}\phi'^2 - a^2\frac{f_{,\phi}}{\kappa} + 2a^2V_{,\phi}\right) = 0 . \tag{3.16}$$

As we will point out in greater detail in the next Section, the relevant changes with respect to the standard picture are represented by the change in time of the function f. In EQ scenarios the dynamics of the field possesses two distinct regimes. At low redshift, the behavior of the energy density coincides with the corresponding one in the tracking trajectories in ordinary quintessence models. At high redshift, generally much earlier than the epoch of structure formation, eventually the effective potential coming from the non-minimal interaction with gravity takes over ($R-$boost), and imprints a behavior $w_\phi = -1/3$ for the quadratic coupling (3.5) [82, 92, 93].

3.4.2 Linear cosmological perturbations

We will describe the linear cosmological perturbations in the real as well as in the Fourier space. For this reason, we follow a notation close to the one introduced recently by Liddle and Lyth [94], which allows not to make explicit the Laplace operator eigenfunctions when working in the Fourier space, minimizing the formal changes needed to go from the

real to the Fourier space and vice versa. See [95] for the usual formulation cast in the Fourier space.

The general expression for the linear perturbation to the metric (3.6) can be written as [94]

$$ds^2 = a^2(\tau)\{-(1+2A)d\tau^2 - B_i d\tau dx^i + [(1+2D)\delta_{ij} + 2E_{ij}]dx^i dx^j\}, \tag{3.17}$$

where the function E_{ij} is chosen to be traceless in order to uniquely identify the non-diagonal spatial perturbation.

It is usual to further decompose the above quantities B_i and E_{ij} into pure scalars (S), scalar-type (S) and vector-type (V) components of vectors, scalar-type (S), vector-type (V) and tensor-type (T) components of tensors, according to their behavior with respect to a spatial coordinate transformation:

$$A = A^S; \tag{3.18}$$

$$B_i = B_i^S + B_i^V; \tag{3.19}$$

$$E_{ij} = E_{ij}^S + E_{ij}^V + E_{ij}^T; \tag{3.20}$$

where

$$B_i^S = \nabla_i B, \quad E_{ij}^S = \left(\nabla_i\nabla_j - \frac{1}{3}\delta_{ij}\nabla^2\right) E\ , \tag{3.21}$$

$$\nabla^i B_i^V = 0, \quad E_{ij}^V = \frac{1}{2}\left(\nabla_i E_j + \nabla_j E_i\right)\ ,\ E_i^{iV} = 0\ , \tag{3.22}$$

$$E_i^{jT} = 0, \quad \nabla^i E_{ij}^T = 0, \tag{3.23}$$

and E, B are scalar functions. Our notation slightly differs from the one of Liddle and Lyth which is given in the Fourier space: the quantities E, E_i and B we use here correspond to the original ones divided by $k^2 = k_i k^i$ and k, respectively. In the linear theory the different types of perturbations evolve independently of each other and can thus be treated separately.

An analogous decomposition can be performed for the stress-energy tensor, whose expression

up to the first perturbative order is:

$$\tilde{T}^0_0 = -(\rho + \delta\rho) \,, \tag{3.24}$$

$$\tilde{T}^0_i = (\rho + p)(v_i - B_i) \,, \tag{3.25}$$

$$\tilde{T}^i_0 = -(\rho + p)v^i \,, \tag{3.26}$$

$$\tilde{T}^i_j = (p + \delta p)\delta^i_j + p\Pi^i_j \,, \tag{3.27}$$

where the fluid velocity v_i and the anisotropic stress Π_{ij} can be split as

$$v_i = v^S_i + v^V_i; \tag{3.28}$$

$$\Pi_{ij} = \Pi^S_{ij} + \Pi^V_{ij} + \Pi^T_{ij}, \tag{3.29}$$

with the same properties of their metric counterparts:

$$v^S_i = \nabla_i v \,, \quad \Pi^S_{ij} = \left(\nabla_i\nabla_j - \frac{1}{3}\delta_{ij}\nabla^2\right)\Pi \,, \tag{3.30}$$

$$\nabla^i v^V_i = 0 \,, \quad \Pi^V_{ij} = \frac{1}{2}\left(\nabla_i\Pi_j + \nabla_j\Pi_i\right) \,, \quad \Pi^{iV}_i = 0 \,, \tag{3.31}$$

$$\nabla^i\Pi_i = \nabla^i\Pi^T_{ij} = 0 \,, \tag{3.32}$$

where again Π is a scalar quantity and the same differences of our notation with the one by Liddle and Lyth hold here for the stress-energy tensor perturbations.

In this thesis we will take into account only density (i.e. scalar-type) perturbations. The reason is that also in the generalized scenarios we consider here they play the dominant role. In fact, as we stress in detail in the following, the scalar-tensor coupling does generate a non-null anisotropic stress already at the linear level, but that is of scalar-type only, and therefore does not act as a source for gravitational waves.

We work in the so called conformal Newtonian gauge, where the non-diagonal perturbations to the metric are set to zero:

$$B = E = 0 \,. \tag{3.33}$$

Furthermore, we will rename the lapse function A and the spatial diagonal perturbation D after the widely used gauge-invariant potentials [86]:

$$A \rightarrow \Psi\,; \qquad D \rightarrow \Phi\,. \tag{3.34}$$

We thus recover the line element of Eq. (2.1):

$$ds^2 = a^2[-(1+2\,\Psi)d\tau^2 + (1+2\,\Phi)dl^2]\,, \tag{3.35}$$

where dl^2 is the unperturbed spatial length element from (3.6).

We now write down the main equations driving the evolution of the perturbed quantities defined above. For each fluid component, the evolution of the scalar perturbed quantities can be followed through the dynamical variables $\delta_x = \delta\rho_x/\rho_x$, v_x, δp_x, Π_x, defined in terms of the stress energy tensor as

$$\delta\rho_x = -\delta T^0_{0\,x}\ ,\ \delta p_x = 1/3\,\delta T^i_{i\,x}\ ,\ \nabla^i v_x = -\delta T^i_{0\,x}/(\rho_x + p_x)\ ,\ p_x \nabla_i \nabla^{j\neq i}\Pi_x = \delta T_i^{j\neq i}\ . \tag{3.36}$$

Note that from now on we do drop the subscript S meaning that we always treat scalar cosmological perturbations, unless otherwise specified. In the Fourier space, the equations for δ_x and v_x take the form

$$\delta_x' - 3\mathcal{H}w_x\,\delta_x = k^2(1+w_x)v_x - 3(1+w_x)\Phi' - 3\mathcal{H}w_x\,p_x\,\delta p_x; \tag{3.37}$$

$$v_x' + \mathcal{H}(1-3w_x)v_x + \frac{w_x'}{1+w_x}v_x = -\frac{\delta p_x}{\rho_x(1+w_x)} - \Psi + \frac{2}{3}\left(1 - \frac{3K}{k^2}\right)\frac{w_x}{1+w_x}\Pi_x\,, \tag{3.38}$$

while δp_x and Π_x depend on the particular species considered. The perturbed Klein-Gordon equation can be written in terms of two equations formally equivalent to (3.37,3.38) by building the conserved expression for the perturbed energy density, pressure and anisotropic stress perturbations [89]. Their combination leads to the Klein-Gordon equation at first perturbative order:

$$\delta\phi'' + \left(2\mathcal{H} + \frac{\omega_{,\phi}}{\omega}\phi'\right)\delta\phi' + \left[k^2 + \frac{1}{2}\left(\frac{\omega_{,\phi}}{\omega}\right)_{,\phi}\phi'^2 + \left(\frac{-a^2 f_{,\phi}/\kappa + 2a^2 V_{,\phi}}{2\omega}\right)_{,\phi}\right]\delta\phi =$$
$$(\Psi' - 3\Phi')\phi' + \left(2\phi'' + 4\mathcal{H}\phi' + \frac{\omega_{,\phi}}{\omega}\phi'^2\right)\Psi + \frac{1}{2\omega\kappa}\frac{\partial^2 f}{\partial\phi\,\partial R}\delta R\,; \tag{3.39}$$

the perturbation in the Ricci scalar can be expressed in terms of those in the metric variables as

$$\delta R = \frac{2}{a^2}\left[-6\mathcal{H}'\Psi - 6\mathcal{H}^2\Psi + 3\Phi'' - 3\mathcal{H}\Psi' + 9\mathcal{H}\Phi' + k^2\Psi + 2(k^2 - 3K)\Phi\right]. \tag{3.40}$$

3.5 Generalized Poisson equation

In this Section we work out the equations relating the stress-energy tensor perturbations to the scalar metric gravitational potentials, which, together with the background cosmic geometry and expansion, determine entirely the lensing process.

We start writing the generalized expression of the density fluctuation [105]:

$$\delta\rho = \rho\cdot\delta = -\delta T^0_0 = \frac{1}{F}\Big[\delta\rho_{\rm fluid} + \frac{\omega}{a^2}\phi'\delta\phi' + \frac{1}{2}\left(\frac{\omega_{,\phi}}{a^2}\phi'^2 - \frac{f_{,\phi}}{\kappa} + 2\,V_{,\phi}\right)\delta\phi$$
$$- \left(\frac{\rho+3p}{2} - \frac{1}{a^2}\nabla^2\right)\delta F - 3\frac{\mathcal{H}\delta F'}{a^2} + 6\frac{\mathcal{H}\Psi F'}{a^2} - 3\frac{\Phi' F'}{a^2} - \frac{\omega}{a^2}\Psi\phi'^2\Big]. \tag{3.41}$$

We can focus on two main aspects of the generalized expression above, playing the major role into the generalization of the Poisson equation: the contribution from the field fluctuations $\delta\phi$ and the $1/F$ term in front of the expression for $\delta\rho$, which acts as an effective time varying gravitational constant. As we shall see below, the latter is the relevant effect in typical Extended Quintessence models.

The Poisson equation relates the fluctuations in the time-time component of the metric to the usual combination of density and scalar-type velocity perturbations, named Δ, whose expression in Newtonian gauge is [95]:

$$\Delta = \delta - 3\,\mathcal{H} w\, v\,. \tag{3.42}$$

We follow as much as possible the notation of earlier works [39]. The $\delta G^0_0 = \delta T^0_0$ equation can be cast in such a way that formally it coincides with the case of ordinary cosmologies. In the Fourier space it is

$$\frac{2}{a^2}\left(k^2 - 3\,K\right)\Phi = 3\,\Delta\left(H^2 + \frac{K}{a^2}\right), \tag{3.43}$$

so that we can exploit our distinction between fluid and generalized cosmology terms. Note that the Hubble expansion rate is evaluated with respect to the ordinary time, $H = \dot{a}/a =$

$a'/a^2 = \mathcal{H}/a$. By using equations (3.8,3.10), we can write $H^2 = H^2_{\rm fluid} + H^2_{\rm gc}$, where

$$H^2_{\rm fluid} = \frac{1}{F}\frac{\rho_{\rm fluid}}{3} = \frac{F_0}{F}H_0^2\left[\Omega_{0m}\,(1+z)^3 + \Omega_{0r}\,(1+z)^4 + (1-\Omega_0)\,(1+z)^2\right]\,, \qquad (3.44)$$

and Ω_{0m}, Ω_{0r} and Ω_0 are the contribution to the present expansion rate from the matter, radiation and the total density respectively, while F_0 is the actual value of the gravitational coupling strength, and can be replaced with $1/8\pi G$. It is important to note that $H^2_{\rm fluid}$ is linked to the energy density of the fluid components, all them but the scalar field, but it contains a most important generalization, represented by the F_0/F term, which plays the role of a time dependent gravitational constant into the Friedmann equation. Moreover, using the relation $K/a^2 = H_0^2(\Omega_0 - 1)(1+z)^2$, we included the effect of the spatial curvature into $H_{\rm fluid}$. The expressions for $H^2_{\rm gc}$ and $\Omega_{\rm gc}$ can be easily obtained by making use of the equations (3.8,3.10):

$$H^2_{\rm gc} = \rho_{\rm gc}\ \ ,\ \ \Omega_{\rm gc} = \frac{H^2_{\rm gc}}{H_0^2}\,. \qquad (3.45)$$

Starting from (3.43), let us write down the relation between the power spectra of Φ, $P_\Phi = k^3\Phi^2/2\pi^2$, and the one of Δ:

$$P_\Phi = \frac{9}{4}\left(\frac{H_0}{k}\right)^4\left(1 - \frac{3(1-\Omega_0){H_0}^2}{k^2}\right)^{-2}\cdot$$
$$\left[\frac{F_0}{F}\Omega_{0m}(1+z) + \frac{F_0}{F}\Omega_{0r}(1+z)^2 + (1-\Omega_0)\left(\frac{F_0}{F} - 1\right) + \frac{1}{(1+z)^2}\Omega_{\rm gc}\right]^2 P_\Delta \qquad (3.46)$$

This is the equation which generalizes the link between time-time metric fluctuations with density and scalar-type velocity perturbations. The new effects arise from the scalar field contribution, encoded in $H^2_{\rm gc}$, the $1/F$ term behaving as a time dependent gravitational constant, as well as from the fluctuations of the scalar field, contained in Δ, both in $\delta\rho$ and v.

Let us check the most relevant corrections to the quantities above in flat EQ models we take as reference [90, 82]. The scalar field fluctuations $\delta\phi$ exhibit a behavior which is close to that of ordinary Quintessence [89], since they are still driven by the potential V in the limit of small coupling. In these conditions, the most important correction is represented by the $1/F$ term, effectively representing the time variation of the gravitational constant.

The expression for F in (3.5) can be conveniently rewritten as

$$F = \frac{1}{8\pi G} + \zeta(\phi^2 - \phi_0^2) \,, \tag{3.47}$$

to make explicit that at the present $F = 1/8\pi G$. The observational constraints [87, 88] usually are expressed as bounds on the quantities

$$\frac{1}{G}\frac{dG}{dt} \simeq -\frac{1}{F}\frac{dF}{dt} = \frac{2}{\phi}\frac{d\phi}{dt} \quad , \quad \omega_{JBD} = \frac{F}{F_\phi^2} = \frac{F}{4\zeta^2\phi^2} \,, \tag{3.48}$$

calculated at the present time, where the $\simeq$ sign above is due to the slight difference with the gravitational constant measured in Cavendish like experiments [83] and ω_{JBD} is the usual Jordan-Brans-Dicke parameter, which usually implies the strongest constraint. Typically [80, 82] the correction to the $1/8\pi G$ term is small, so that

$$\frac{1}{F} \simeq 8\pi G[1 - 8\pi G\zeta(\phi^2 - \phi_0^2)] \,. \tag{3.49}$$

Moreover, in tracking trajectories with inverse power law potentials, the field approaches ϕ_0 of the order of $1/\sqrt{G}$ from below, being generally much smaller than that in the past, when $1/F$ freezes to the value $8\pi G(1 + 8\pi G\zeta\phi_0^2)$ [82]. The magnitude of the correction is therefore

$$8\pi G\zeta\phi_0^2 = \frac{1}{4\zeta\omega_{JBD}} = \phi_0\sqrt{\frac{2\pi G}{\omega_{JBD}}} \,; \tag{3.50}$$

note that as ω_{JBD} approaches infinity, recovering general relativity, the correction may still be relevant depending on the values of ζ or ϕ_0. The gravitational potential receives a contribution which is

$$\delta\Phi = -8\pi G\zeta(\phi^2 - \phi_0^2)\Phi_{\text{fluid}+\phi} \,. \tag{3.51}$$

The subscript $()_{\text{fluid}+\phi}$ represents all the terms coming from the fluid quantities as well as the scalar field ones from the minimal coupling, i.e. not involving F explicitly:

$$k^2\Phi_{\text{fluid}+\phi} = 4\pi G\Delta_{\text{fluid}+\phi}H_0^2[\Omega_{0m}(1+z)^2 + \Omega_{0r}(1+z)^4 + \Omega_\phi] \,. \tag{3.52}$$

Note also that if the field trajectory has an almost constant equation of state w_ϕ, the expression above reduces to

$$k^2\Phi_{\text{fluid}+\phi} = 4\pi G\Delta_{\text{fluid}+\phi}H_0^2[\Omega_{0m}(1+z)^2 + \Omega_{0r}(1+z)^4 + \Omega_{\phi 0}(1+z)^{3(1+w_\phi)}] \,; \tag{3.53}$$

in order to keep the notation simple, we drop such subscript in the following, always meaning that it is there when discussing approximate expressions in EQ models. Similarly, the gravitational potential power spectrum gets an extra contribution which at the first order in the correction to $1/8\pi G$ is

$$\delta P_\Phi = -16\pi G\zeta(\phi^2 - \phi_0^2)P_\Phi \,, \tag{3.54}$$

where

$$P_\Phi = \frac{9}{4}\left(\frac{H_0}{k}\right)^4 \left[\Omega_{0m}\,(1+z) + \Omega_{0r}\,(1+z)^2 + \Omega_{\phi 0}\,(1+z)^{3(1+w_\phi)}\right] P_\Delta \tag{3.55}$$

is the expression in minimally coupled scenarios.

In general, another important effect which arises in cosmology from the generalization of the underlying gravity physics is represented by the relation between Ψ and Φ. The difference between f and R, which may arise from a scalar-tensor coupling as well as a non-standard dependence of f from R itself, gives origin to tidal forces exciting the anisotropic stress of scalar origin [105]; in the Fourier space its simple form is

$$p_\phi \Pi_\phi = \frac{k^2}{a^2}\frac{\delta F}{F} \,, \tag{3.56}$$

and implies a shift between the two gauge independent scalar metric perturbations, which in our gauge takes the form

$$\Psi + \Phi = -\frac{a^2}{k^2} p\Pi = -\frac{\delta F}{F} \,, \tag{3.57}$$

where the last equality holds if the anisotropic stress is due to the generalization of gravity and is does not come from matter or radiation. This is an important new aspect of generalized cosmologies which implies a change in almost all the equations describing the weak lensing effect in cosmology, to be discussed next. For this reason, it is convenient to give a name to the $\Psi + \Phi$ combination, valid both for the real and the Fourier space:

$$\Xi = \Psi + \Phi \,. \tag{3.58}$$

One has $\Xi = 0$ in ordinary cosmology, and $\Xi = -\delta F/F$ in the generalized scenarios of interest here. As we already stressed, Ξ is excited both by a scalar-tensor coupling like in

EQ models, and a generalized dependence of the gravitational Lagrangian term on R; its expression in terms of f is

$$\Xi = -\left(\frac{\partial f}{\partial R}\right)^{-1}\left[\frac{\partial^2 f}{\partial\phi\partial R}\delta\phi + \frac{\partial^2 f}{\partial R^2}\delta R\right] . \tag{3.59}$$

While in the first case the correction is small because of the smallness of the scalar field fluctuations $\delta\phi$ [89, 80], the contribution from the second term has not been investigated yet.

3.6 Lensing equation

We follow the notation introduced in the previous Chapter for the lensing variables, accounting now for the new degrees of freedom defined above. In terms of Ξ, defined in (3.58), the geodesic equation assumes the familiar form [36, 32] plus the perturbation coming from the anisotropic stress (i stands now for x or y):

$$\frac{d^2\theta_i}{d\tau^2} = \frac{K}{\sin^2\sqrt{K}\chi}\partial_{\theta_i}(2\Phi - \Xi) - 2\sqrt{K}\frac{\cos\sqrt{K}\chi}{\sin\sqrt{K}\chi}\frac{d\theta_i}{d\tau} . \tag{3.60}$$

This equation generalizes eq. (2.18) of the previous Chapter; the gravitational potentials differ from each other in absolute value so that the quantity $\Phi - \Psi$ is not simply 2Φ any more; the new relevant combination $2\Phi - \Xi$ propagates through all the lensing variables below.

The effects coming from the modified cosmological expansion are encoded in χ, through the modified dependence of the distances r given by (3.12,3.13) with respect to the redshift z. Using again the comoving displacement from the polar axis, $x_i = \theta_i \sin\sqrt{K}\chi/\sqrt{K}$, the equation (3.60) now reads

$$x_i'' + K\, x_i = -\frac{\partial(\Psi - \Phi)}{\partial x_i} = 2\partial_i\Phi - \partial_i\Xi ; \tag{3.61}$$

and its general solution is now

$$x_i + A\frac{\sin\sqrt{K}\chi}{\sqrt{K}} + B\,\cos\sqrt{K}\chi = -\int_0^\chi d\chi'\partial_i[\Psi(\hat{n},\chi') - \Phi(\hat{n},\chi')]\,\frac{\sin\sqrt{K}\chi'}{\sqrt{K}} =$$

$$= \int_0^\chi d\chi' \partial_i [2\Phi(\hat{n}, \chi') - \Xi(\hat{n}, \chi')] \frac{\sin\sqrt{K}\chi'}{\sqrt{K}}, \tag{3.62}$$

where A and B are integration constants, and the position $\vec{x}$ on the light cone is completely specified by the line of sight direction $\hat{n}$ and the generalized radial coordinate χ.

3.7 Weak lensing observables

In this section we generalize the expressions computed in Sec. 2.4 of the previous Chapter for the lensing variables: we keep the notation close to that one, so that the new contributions can be easily identified as the corrections.

3.7.1 Distortion tensor

From eq. (2.27) the above expressions we can rederive the appropriate expression for the distortion tensor:

$$\psi_{ij}(\hat{n}, \chi) = \frac{1}{\sqrt{K}} \int_0^\chi d\chi' \frac{\sin\sqrt{K}\chi' \sin\sqrt{K}(\chi - \chi')}{\sin\sqrt{K}\chi} \partial_i \partial_j [\Psi(\hat{n}, \chi') - \Phi(\hat{n}, \chi')] =$$

$$= \frac{1}{\sqrt{K}} \int_0^\chi d\chi' \frac{\sin\sqrt{K}\chi' \sin\sqrt{K}(\chi - \chi')}{\sin\sqrt{K}\chi} \partial_i \partial_j [-2\Phi(\hat{n}, \chi') + \Xi(\hat{n}, \chi')], \tag{3.63}$$

which will then be evaluated along the integral of the possible source distribution, as already pointed out.

Let us evaluate the correction to the distortion tensor in EQ models. The contribution from Ξ is negligible in these scenarios, since it arises from the scalar field fluctuations $\delta\phi$, yielding a correction which is small with respect to the one coming from the variation of $1/F$, as we already discussed [89]. Therefore, in flat cosmologies and at a given χ, the correction to $\psi_{ij}(\hat{n}, \chi)$ is due only to the shift in the gravitational potential, represented by (3.51):

$$\delta\psi_{ij}(\hat{n}, \chi) = 16\pi G\zeta\phi_0^2 \int_0^\chi d\chi' \frac{\chi'(\chi - \chi')}{\chi} \left(\frac{\phi^2}{\phi_0^2} - 1\right) \partial_i \partial_j \Phi(\hat{n}, \chi'). \tag{3.64}$$

Note however that integrating in the χ variable, although convenient in order to minimize the formal corrections to ψ_{ij}, hides the effect of the varying gravitational constant on χ itself; in flat cosmologies the latter coincides with r given by (3.13), which has to be corrected as

$$\delta r = 4\pi G\zeta\phi_0^2 \int_0^z \frac{dz}{H(z)} \left(\frac{\phi^2}{\phi_0^2} - 1\right), \tag{3.65}$$

as it can be easily verified since H (which denotes the unperturbed Hubble parameter) is $\propto 1/\sqrt{F}$.

3.7.2 Generalized lensing potential

Finally, we can generalize the expression (2.34) for the lensing potential, which becomes

$$\phi(\hat{n}) = \int_0^{\chi_\infty} d\chi f_K(\chi) \left[-2\Phi(\hat{n},\chi) + \Xi(\hat{n},\chi)\right] \int_\chi^{\chi_\infty} d\chi' \frac{f_K(\chi'-\chi)}{f_K(\chi')} g(\chi') \,, \tag{3.66}$$

or, in the compact form which makes use of the integral source distribution $g'(\chi)$,

$$\phi(\hat{n}) = \int_0^{\chi_\infty} d\chi\, g'(\chi) \left[\Psi(\hat{n},\chi) - \Phi(\hat{n},\chi)\right] = \int_0^{\chi_\infty} d\chi\, g'(\chi) \left[-2\Phi(\hat{n},\chi) + \Xi(\hat{n},\chi)\right] \,. \tag{3.67}$$

The expression above acquires several new contributions in the generalized scenarios of interest here. The modified background expansion affects the angular diameter distance as well as the effective gravitational constant; the perturbations get new contributions from the field fluctuations affecting Φ and exciting the metric fluctuation mode represented by Ξ.

In EQ models, if the integration is made on the variable χ, the main correction is due to the time variation of the effective gravitational constant:

$$\delta\phi(\hat{n}) = 16\pi G\zeta\phi_0^2 \int_0^{\chi_\infty} d\chi\, g'(\chi) \left(\frac{\phi^2}{\phi_0^2} - 1\right) \Phi(\hat{n},\chi) \,. \tag{3.68}$$

In this equation, and in Eqs. (3.76),(3.81),(3.84), the quantity Φ is meant to be $\Phi_{\text{fluid}+\phi}$ as defined in Eq. (3.51) .

We need now to track these effects into the angular power spectrum of the projected lensing potential. That is defined as usual as

$$C_l^{\phi\phi} = \langle\, |\phi_{lm}|^2 \,\rangle \quad , \quad \phi_{lm} = -2 \int d\Omega_{\hat{n}}\, \phi(\hat{n})\, Y_{lm}(\hat{n}) \tag{3.69}$$

where the -2 is purely conventional in order to keep the notation consistent with earlier works [39]. One needs now to expand the metric fluctuations in the Fourier space with respect to the position $\vec{x} = r \cdot \hat{n}$. The expansion functions are just the eigenfunctions $Y_{\vec{k}}(\vec{x})$

of the Laplace operator in curved spacetime, defined in general in curved FRW geometry [95]. Their radial and angular dependences are further expanded in ultra-spherical Bessel functions u_l and scalar spherical harmonics, by exploiting the relation

$$Y_{\vec{k}}(\vec{x}) = 4\pi \sum_{l,m} i^l u_l(k\,x) Y_{lm}(\hat{k})\, Y_{lm}(\hat{x})\,, \tag{3.70}$$

where k and x denote the modulus of the corresponding vectors. By using the completeness of the spherical harmonics, and the fact that x coincides with the radial distance $f_K(\chi)$, the final expression for ϕ_{lm} is

$$\phi_{lm} = \sqrt{\frac{8}{\pi}} \int_0^{\chi_\infty} d\chi\, g'(\chi) \int d^3k \left[2\Phi(\vec{k},\chi) - \Xi(\vec{k},\chi)\right] i^l u_l(k\, f_K(\chi)) Y_{lm}(\hat{k})\, Y_{lm}(\hat{n})\,. \tag{3.71}$$

The lensing potential angular power spectrum (3.69) is therefore

$$\begin{aligned} C_l^{\phi\phi} = {} & \frac{32}{\pi} \int_0^{\chi_\infty} d\chi\, g'(\chi) \int_0^{\chi_\infty} d\chi' g'(\chi') \cdot \\ & \cdot \int d^3k \int d^3k' u_l[k\, f_K(\chi)] u_l[k' f_K(\chi')] Y_{lm}(\hat{k}) Y^*_{lm}(\hat{k}') \cdot \\ & \cdot \left[\langle \Phi(\vec{k},\chi)\Phi(\vec{k}',\chi')^* - \frac{1}{2}\Xi(\vec{k},\chi)\Phi(\vec{k}',\chi')^* - \frac{1}{2}\Xi(\vec{k}',\chi')^*\Phi(\vec{k},\chi) + \frac{1}{4}\Xi(\vec{k},\chi)\Xi(\vec{k}',\chi')^*\rangle\right]\,. \end{aligned} \tag{3.72}$$

Assuming that the statistical average above eliminates the correlation between different Fourier modes, as well as the dependence on the direction of the wavenumbers,

$$\langle \mathcal{A}(\vec{k},\chi)\, \mathcal{B}(\vec{k}',\chi')\rangle = \langle \mathcal{A}(k,\chi)\mathcal{B}(k,\chi')\rangle \delta(\vec{k} - \vec{k}')\,, \tag{3.73}$$

where $\mathcal{A}$ and $\mathcal{B}$ represent either Ψ or Ξ and they are meant to be ensemble averaged, one finally gets

$$\begin{aligned} C_l^{\phi\phi} = {} & \frac{32}{\pi} \int_0^{\chi_\infty} d\chi\, g'(\chi) \int_0^{\chi_\infty} d\chi' g'(\chi') \int k^2 dk\, u_l[k\, f_K(\chi)] u_l[k\, f_K(\chi')] \cdot \\ & \cdot \left[\langle \Phi(k,\chi)\Phi(k,\chi')\rangle - \langle \Xi(k,\chi)\Phi(k,\chi')\rangle + \frac{1}{4}\langle \Xi(k,\chi)\Xi(k,\chi')\rangle\right]\,. \end{aligned} \tag{3.74}$$

It is also useful to write down explicitly the equivalent form of the expression above which contains the gravitational potentials only:

$$\begin{aligned} C_l^{\phi\phi} = {} & \frac{32}{\pi} \int_0^{\chi_\infty} d\chi\, g'(\chi) \int_0^{\chi_\infty} d\chi' g'(\chi') \int k^2 dk\, u_l[k\, f_K(\chi)] u_l[k\, f_K(\chi')] \cdot \\ & \cdot \left[\frac{1}{4}\langle \Psi(k,\chi)\Psi(k,\chi')\rangle + \frac{1}{4}\langle \Phi(k,\chi)\Phi(k,\chi')\rangle - \frac{1}{2}\langle \Psi(k,\chi)\Phi(k,\chi')\rangle\right]\,, \end{aligned} \tag{3.75}$$

putting in evidence the correlation between Ψ and Φ.

From this expression we can easily infer the main correction to the lensing potential angular power spectrum arising in EQ cosmologies, using (3.54):

$$\begin{aligned}\delta C_l^{\phi\phi} &= -512 G\zeta\phi_0^2 \int_0^{\chi_\infty} d\chi\, g'(\chi) \int_0^{\chi_\infty} d\chi' g'(\chi') \cdot \\ &\left(\frac{\phi^2}{\phi_0^2} - 1\right) \int k^2 dk\, u_l[k\, f_K(\chi)] u_l[k\, f_K(\chi')] \langle \Phi(k,\chi)\Phi(k,\chi')\rangle \,. \end{aligned} \tag{3.76}$$

Note that the numbers here conspire to yield a quite large factor in front of this expression, which may render the correction above relevant even for values of the product $G\zeta\phi_0^2$ as small as 10^{-3}.

In the following we further specialize our results computing the generalized expression of some quantity particularly relevant for observations, as well as their main corrections in EQ models.

3.7.3 Convergence power spectrum

The convergence, represented by the trace of the distortion tensor, is usually used as a main magnitude of the weak lensing distortion.

The expression we need to compute is given by

$$\kappa = \frac{1}{2}(\psi_{11} + \psi_{22}) \tag{3.77}$$

which will be averaged over the source distribution as usual. We get

$$\begin{aligned}\kappa &= \frac{1}{2}\int_0^{\chi_\infty} d\chi'\, g(\chi') \int_\chi^{\chi_\infty} \frac{f_K(\chi)\, f_K(\chi'-\chi)}{f_K(\chi')} \partial^i\, \partial_i \left[\Psi(\hat{n},\chi) - \Phi(\hat{n},\chi)\right] = \\ &= \frac{1}{2}\int_0^{\chi_\infty} d\chi'\, g(\chi') \int_\chi^{\chi_\infty} \frac{f_K(\chi)\, f_K(\chi'-\chi)}{f_K(\chi')} \partial^i\, \partial_i \left[-2\Phi(\hat{n},\chi) + \Xi(\hat{n},\chi)\right] = \\ &= \frac{1}{2}\int_0^{\chi_\infty} d\chi\, g'(\chi) \partial^i\, \partial_i \left[-2\Phi(\hat{n},\chi) + \Xi(\hat{n},\chi)\right] . \end{aligned} \tag{3.78}$$

The two-dimensional Laplacian appearing in this equation can be safely replaced with its three-dimensional analogue, as argued before. Once this substitution has been made, we can expand the generalized gravitational potential in Fourier harmonics transforming with respect to the spatial point $\hat{n}\cdot\chi$, and transform the Laplacian in a multiplication by $(-k^2)$:

$$\kappa = \frac{1}{2(2\pi)^{3/2}} \int_0^{\chi_\infty} d\chi\, g'(\chi) \int d^3k\, k^2 \left[2\Phi(\vec{k},\chi) - \Xi(\vec{k},\chi)\right] Y_{\vec{k}}(\vec{x}) \,. \tag{3.79}$$

Comparing this expression with the ones for the lensing potential power spectrum (3.74,3.75) we can immediately infer the result:

$$\begin{aligned} P_\kappa(l) &= \frac{8}{\pi}\int_0^{\chi_\infty} d\chi\, g'(\chi)\int_0^{\chi_\infty} d\chi' g'(\chi')\int dk\, k^8\, u_l(k\, f_K(\chi))u_l(k\, f_K(\chi'))\cdot \\ &\cdot \left[\langle\Phi(k,\chi)\Phi(k,\chi')\rangle - \langle\Xi(k,\chi)\Phi(k,\chi')\rangle + \frac{1}{4}\langle\Xi(k,\chi)\Xi(k,\chi')\rangle\right] = \\ &= \frac{8}{\pi}\int_0^{\chi_\infty} d\chi\, g'(\chi)\int_0^{\chi_\infty} d\chi' g'(\chi')\int dk\, k^8\, u_l(k\, f_K(\chi))u_l(k\, f_K(\chi'))\cdot \\ &\cdot \left[\frac{1}{4}\langle\Psi(k,\chi)\Psi(k,\chi')\rangle + \frac{1}{4}\langle\Phi(k,\chi)\Phi(k,\chi')\rangle - \frac{1}{2}\langle\Psi(k,\chi)\Phi(k,\chi')\rangle\right], \end{aligned} \tag{3.80}$$

which generalizes eq. (2.43).

In EQ cosmologies, using again (3.54), one finds

$$\begin{aligned} \delta P_\kappa(l) &= -128 G\zeta\phi_0^2\int_0^{\chi_\infty} d\chi\, g'(\chi)\int_0^{\chi_\infty} d\chi' g'(\chi')\left(\frac{\phi^2}{\phi_0^2}-1\right)\cdot \\ &\int dk\, k^8\, u_l(k\, f_K(\chi))u_l(k\, f_K(\chi'))\langle\Phi(k,\chi)\Phi(k,\chi')\rangle, \end{aligned} \tag{3.81}$$

where the correction to χ must be taken into account following (3.65) if the integration is made on the redshift.

3.8 An example of correlation with other CMB secondary anisotropies

The lensing potential correlates significantly with secondary anisotropies of the CMB, because it arises much later than the decoupling; here we generalize the lensing cross-correlation with the Integrated Sachs-Wolfe effect (ISW, see [39] for a comparison with the case of ordinary cosmologies).

The latter can be represented in terms of temperature fluctuations as

$$\Theta^{ISW}(\hat{n}) = -\int_0^{\infty} d\chi[\dot{\Phi}(\hat{n},\chi) - \dot{\Psi}(\hat{n},\chi)] = -\int_0^{\infty} d\chi\,[2\dot{\Phi}(\hat{n},\chi) - \dot{\Xi}(\hat{n},\chi)]\,. \tag{3.82}$$

Note that, in order to avoid confusion with the integration variable χ', in this paragraph only we will denote with an overdot the derivative with respect to conformal time.

Again using the expressions for the lensing potential power spectra (3.74,3.75), and making use of the statistical independence of different Fourier modes, we are able to write

immediately the cross-correlated spectrum:

$$C^{\Theta\phi} = \frac{8}{\pi}\int_0^{\chi_\infty} d\chi\, g'(\chi)\int_0^{\chi_\infty} d\chi' \int k^2\, dk\, u_l(k\, f_K(\chi))u_l(k\, f_K(\chi'))\cdot$$
$$\cdot\left[\langle\Phi(k,\chi)\dot{\Phi}(k,\chi')\rangle - \frac{1}{2}\langle\Xi(k,\chi)\dot{\Phi}(k,\chi')\rangle - \frac{1}{2}\langle\dot{\Xi}(k,\chi')\Phi(k,\chi)\rangle + \frac{1}{4}\langle\Xi(k,\chi)\dot{\Xi}(k,\chi')\rangle\right] =$$
$$= \frac{2}{\pi}\int_0^{\chi_\infty} d\chi\, g'(\chi)\int_0^{\chi_\infty} d\chi' \int k^2\, dk\, u_l(k\, f_K(\chi))u_l(k\, f_K(\chi'))\cdot$$
$$\cdot\left[\langle\Psi(k,\chi)\dot{\Psi}(k,\chi')\rangle + \langle\Phi(k,\chi)\dot{\Phi}(k,\chi')\rangle - \langle\Psi(k,\chi)\dot{\Phi}(k,\chi')\rangle - \langle\dot{\Psi}(k,\chi')\Phi(k,\chi)\rangle\right]. \quad (3.83)$$

The main correction in EQ cosmologies is obtained again by using (3.54). Interestingly, the time derivative reintroduces a term proportional to $|\Phi|^2$:

$$\delta C^{\Theta\phi} = -128G\zeta\phi_0^2\int_0^{\chi_\infty} d\chi\, g'(\chi)\int_0^{\chi_\infty} d\chi'\left(\frac{\phi^2}{\phi_0^2}-1\right) \quad (3.84)$$
$$\cdot\int k^2\, dk\, u_l(k\, f_K(\chi))u_l(k\, f_K(\chi'))\langle\Phi(k,\chi)\dot{\Phi}(k,\chi')\rangle$$
$$-256G\zeta\phi_0^2\int_0^{\chi_\infty} d\chi\, g'(\chi)\int_0^{\chi_\infty} d\chi'\frac{\phi\dot{\phi}}{\phi_0^2}\int k^2\, dk\, u_l(k\, f_K(\chi))u_l(k\, f_K(\chi'))\langle\Phi(k,\chi)\Phi(k,\chi')\rangle.$$

These expressions can be further simplified noticing that for lensing on the CMB signal the source distribution is well represented by a delta function at the last scattering (LS) surface; thus the averaging function $g'(\chi)$ can be written as

$$g'(\chi) = f_K(\chi)\int_\chi^{\chi_\infty} d\chi'\frac{f_K(\chi'-\chi)}{f_K(\chi')}\,\delta(\chi'-\chi_{\rm LS}) = \frac{f_K(\chi)\, f_K(\chi_{\rm LS}-\chi)}{f_K(\chi_{\rm LS})}. \quad (3.85)$$

3.9 Summary

In this Chapter we have developed the theoretical instruments that we will need in order to proceed with our analysis of the CMB lensing impact in the task of understanding the nature of the dark energy. We have fixed the contributions from the modified background expansion as well as the fluctuations, both in the Ricci scalar and in the scalar field responsible for the scalar-tensor coupling, and showed that both of them are responsible for an anisotropic stress of scalar origin, causing the gravitational potentials to be different already at the linear level.

We have studied in particular the modifications induced by the time variation of the effective gravitational constant, which are most relevant in non-minimally coupled models in

which the gravitational Lagrangian sector is a product of a function depending on a scalar field and on the Ricci scalar, focusing on Extended Quintessence (EQ) scenarios, where the scalar field, playing the role of the dark energy and responsible for cosmic acceleration today, possesses a quadratic coupling with the Ricci scalar.

Finally, we have specialized our results with two examples yelding two quantities which are most relevant for observations, i.e. the lensing convergence power spectrum as well as the correlation between the lensing potential and the Integrated Sachs-Wolfe (ISW) effect affecting the total intensity and polarization anisotropies in the cosmic microwave background radiation, and have computed the relative corrections with respect to ordinary cosmology. We have showed that in this case the order of magnitude of these effects is of the order of $8\pi G\zeta\phi_0^2$, where ζ is the coupling constant and ϕ_0 is the present value of the dark energy field: such correction may be relevant even if the underlying theory is close to general relativity, i.e. if the Jordan-Brans-Dicke parameter $\omega_{JBD} = 1/32\pi G\zeta^2\phi_0^2$ is large, depending on the relative balance between ζ and ϕ_0.

Despite of these interesting indications in the particular case of EQ cosmologies, the formulas we developed here have great generality, and we will apply the results presented above starting from the case of scalar-field dark energy cosmologies, which are the target of next Chapter.

Chapter 4

Lensing in Quintessence models

In this Chapter we present the analysis of the CMB lensing in minimally coupled Quintessence scenarios. The phenomenology of these models is relatively simple, since there is no anisotropic stress, the gravitational coupling is the same as in General Relativity, and acceleration is provided by the dynamics of a scalar field representing the dark energy. We will describe the numerical achievements that made possible the study of the CMB lensing in these models, and accurately examine the different mechanisms contributing to the global effect and their phenomenological interpretation. Finally, we provide a statistical analysis of these models via a dark energy parametrization and a Fisher matrix treatment, dealing with the issue of how future surveys devoted to the CMB polarization may help in constraining the dark energy behavior. Most of the content of this Chapter is the result of the work [107].

4.1 Dark energy cosmology

Here we will review the tracking Quintessence scenarios, where the dark energy is described through a scalar field ϕ (see e.g. [59]). The associated action is of the form:

$$S = \int d^4x\sqrt{-g}\cdot \left[\tfrac{1}{2\kappa}R - \phi^{;\mu}\phi_{;\mu}\tfrac{1}{2} - V(\phi) + \mathcal{L}_{\rm fluid}\right] . \tag{4.1}$$

In order to highlight the general phenomenology, we will consider two representative models where the equation of state has a mild and violent redshift behavior, respectively for

the inverse power law potentials, (IPL [61]) and those inspired by super-gravity theories (SUGRA [65]):

$$V(\phi) = \frac{M^{4+\alpha}}{\phi^{\alpha}} \quad , \quad V(\phi) = \left(\frac{M^{4+\alpha}}{\phi^{\alpha}}\right) e^{4\pi G\phi^2} \; ; \tag{4.2}$$

the field motion and its tracking trajectories will be reviewed in Sec. 4.3. For what concerns the background evolution, a variety of models including the ones above are well described by essentially two parameters: the present value w_0 of the equation of state and its first derivative with respect to the scale factor a, $-w_a$ [110, 111].

In this framework, the evolution of the equation of state with the scale factor can be written as

$$w(a) = w_0 + w_a(1-a) = w_\infty + (w_0 - w_\infty)a \; , \tag{4.3}$$

where w_∞ is the asymptotic value of w in the past. We will exploit the parameterization above in Section 4.4, in order to evaluate the precision achievable with the lensing on the measure of w_0 and w_∞ from the CMB total intensity and polarization angular power spectra.

4.2 CMB lensing and Boltzmann numerical codes in cosmology

The effect of gravitational lensing on the CMB spectra had been first introduced in the CMBfast code by Zaldarriaga and Seljak [112] for Cold Dark Matter cosmologies including a Cosmological Constant (ΛCDM). In their formalism the lensing effect on the angular power spectra of the anisotropies can be understood as the convolution of the unlensed spectra with a Gaussian filter determined by the lensing potential [32] (the validity of the Gaussian filter approximation will be discussed in the last Chapter, in the part dedicated to the nonlinear evolution). The expression for the lensing potential has to be generalized in scalar-tensor cosmologies because of the presence of anisotropic stress already at a linear level [56]. In the present scenario, however, this is not required and the structure of the quantities relevant for computing the lensing effect is formally unchanged.

We carry out the exact evolution of density perturbations, also including Quintessence fluctuations, using a modified version of the code DEFAST, based on CMBFAST [108] and

originally written to study quintessence scenarios where the dark energy scalar field is minimally [89] or non-minimally [80] coupled to the Ricci scalar. The architecture of DEFAST is based on the version 4.0 of CMBFAST, although there has been a progressive code fork in the subsequent versions.

We follow the notation of the original paper [112]; an important simplification with respect to the spectra defined in Chapter 2 is the use of the flat-sky formalism, since we don't expect considerable lensing effects on such large scales to spoil this approximation. Therefore, the expansion in spherical harmonics can be replaced by a two-dimensional multipole expansion in which the Fourier-conjugate variables are the multipole vector $\mathbf{l}$ and the angular position $\hat{\mathbf{n}}$ [39]:

$$\Theta(\hat{\mathbf{n}}) = \int \frac{d^2\mathbf{l}}{(2\pi)^2}\Theta(\mathbf{l})e^{i\mathbf{l}\cdot\hat{\mathbf{n}}}, \tag{4.4}$$

for the temperature, and

$${}_{\pm}X(\hat{\mathbf{n}}) = -\int \frac{d^2\mathbf{l}}{(2\pi)^2}{}_{\pm}X(\mathbf{l})e^{\pm 2i(\varphi_l-\varphi)}e^{i\mathbf{l}\cdot\hat{\mathbf{n}}}, \tag{4.5}$$

where φ_l is azimuthal angle of $\mathbf{l}$, for the polarization. Again one separates the Stokes moments as

$${}_{\pm}X(\hat{\mathbf{n}}) = Q(\hat{\mathbf{n}}) \pm iU(\hat{\mathbf{n}}) \tag{4.6}$$

in the real space.

Under the assumption of Gaussian statistics, the power spectra and cross correlations will be now defined as

$$\left\langle X^*(\mathbf{l})X'(\mathbf{l}')\right\rangle = (2\pi)^2\delta(\mathbf{l}-\mathbf{l}')C_{(l)}^{XX'}. \tag{4.7}$$

The observed CMB temperature in the direction $\hat{\mathbf{n}}$ is $T(\hat{\mathbf{n}})$ (we call it T from now on in order to stick to the most common notation for the spectra) and equals the unobservable temperature at the last scattering surface $\tilde{T}(\hat{\mathbf{n}}+\delta\hat{\mathbf{n}})$, where $\delta\hat{\mathbf{n}}$ is the angular excursion of the photon as it propagates from the last scattering surface until the present. In terms of Fourier components we have

$$\begin{aligned} T(\hat{\mathbf{n}}) &= \tilde{T}(\hat{\mathbf{n}}+\delta\hat{\mathbf{n}}) \\ &= (2\pi)^{-2}\int d^2\mathbf{l}\; e^{i\mathbf{l}\cdot(\hat{\mathbf{n}}+\delta\hat{\mathbf{n}})}\; T(\mathbf{l}). \end{aligned} \tag{4.8}$$

An analogous relation applies to the two Stokes parameters Q and U that describe linear polarization, and in the real space measure the difference in the light intensity along the x and y (and their rotations of 45°) axes (in analogy with the shear components, as already pointed out when they were first introduced). They can be decomposed in their opposite parity Fourier components $E(\mathbf{l})$ and $B(\mathbf{l})$ [48]

$$\begin{aligned} Q(\hat{\mathbf{n}}) &= \tilde{Q}(\hat{\mathbf{n}}+\delta\hat{\mathbf{n}}) \\ &= (2\pi)^{-2}\int d^2\mathbf{l}\; e^{i\mathbf{l}\cdot(\hat{\mathbf{n}}+\delta\hat{\mathbf{n}})}\,[E(\mathbf{l})\cos(2\phi_{\mathbf{l}}) - B(\mathbf{l})\sin(2\phi_{\mathbf{l}})] \\ U(\hat{\mathbf{n}}) &= \tilde{U}(\hat{\mathbf{n}}+\delta\hat{\mathbf{n}}) \\ &= (2\pi)^{-2}\int d^2\mathbf{l}\; e^{i\mathbf{l}\cdot(\hat{\mathbf{n}}+\delta\hat{\mathbf{n}})}\,[E(\mathbf{l})\sin(2\phi_{\mathbf{l}}) + B(\mathbf{l})\cos(2\phi_{\mathbf{l}})]. \end{aligned} \tag{4.9}$$

We want to compute the correlation functions of two light rays at directions, say, $\hat{\mathbf{n}}^A$ and $\hat{\mathbf{n}}^B$ in the sky, with relative deviations $\delta\hat{\mathbf{n}}^A$ and $\delta\hat{\mathbf{n}}^B$. With an appropriate choice of coordinate the two rays can be represented to be respectively at the origin and at another point separated by an angle θ along the $\mathbf{x}$ axis [49]:

$$\begin{aligned} C_T T(\theta) &= \int \frac{d^2\mathbf{l}}{(2\pi)^2}\, e^{il\theta\cos\phi_l}\langle e^{i\mathbf{l}\cdot(\delta\hat{\mathbf{n}}^A-\delta\hat{\mathbf{n}}^B)}\rangle\; C_{\tilde{T}Tl} \\ C_Q(\theta) &= \int \frac{d^2\mathbf{l}}{(2\pi)^2}\, e^{il\theta\cos\phi_l}\langle e^{i\mathbf{l}\cdot(\delta\hat{\mathbf{n}}^A-\delta\hat{\mathbf{n}}^B)}\rangle\; [C_{\tilde{E}El}\cos^2(2\phi_{\mathbf{l}}) + C_{\tilde{B}Bl}\sin^2(2\phi_{\mathbf{l}})] \\ C_U(\theta) &= \int \frac{d^2\mathbf{l}}{(2\pi)^2}\, e^{il\theta\cos\phi_l}\langle e^{i\mathbf{l}\cdot(\delta\hat{\mathbf{n}}^A-\delta\hat{\mathbf{n}}^B)}\rangle\; [C_{\tilde{E}El}\sin^2(2\phi_{\mathbf{l}}) + C_{\tilde{B}Bl}\cos^2(2\phi_{\mathbf{l}})] \\ C_C(\theta) &= \int \frac{d^2\mathbf{l}}{(2\pi)^2}\, e^{il\theta\cos\phi_l}\langle e^{i\mathbf{l}\cdot(\delta\hat{\mathbf{n}}^A-\delta\hat{\mathbf{n}}^B)}\rangle\; C_{\tilde{T}El}\cos(2\phi_{\mathbf{l}}). \end{aligned} \tag{4.10}$$

The expectation value in the above equation can be computed using the equation for the deflection angle given in Chap. 2, Eq. (2.25), where now $\alpha(\mathbf{n},\chi) \to \delta\hat{\mathbf{n}}$, and calculating its auto-correlation function. The result is

$$\langle e^{i\mathbf{l}\cdot(\delta\hat{\mathbf{n}}-\delta\hat{\mathbf{n}}')}\rangle = \exp^{-\frac{l^2}{2}[\sigma_0^2(\theta)+\cos(2\phi_{\mathbf{l}})\sigma_2^2(\theta)]}, \tag{4.11}$$

where the Gaussian function in the multipole space on the right hand side is, in this formalism, the equivalent of the lensing potential power spectrum introduced in the previous Chapter: its variance gives a measure of the mixing between different Fourier modes (*i.e.* [32]), as we explain below.

The resulting power spectra in terms of the unlensed ones can finally then found to be (we don't report the lengthy calculation [112])

$$\begin{aligned} C_{TTl} &= C_{\tilde{T}Tl} + \mathcal{W}^{l'}_{1l}\, C_{\tilde{T}Tl'} \\ C_{EEl} &= C_{\tilde{E}El} + \frac{1}{2}[\mathcal{W}^{l'}_{1l} + \mathcal{W}^{l'}_{2l}]\, C_{\tilde{E}El'} + \frac{1}{2}[\mathcal{W}^{l'}_{1l} - \mathcal{W}^{l'}_{2l}]\, C_{\tilde{B}Bl'} \\ C_{BBl} &= C_{\tilde{B}Bl} + \frac{1}{2}[\mathcal{W}^{l'}_{1l} - \mathcal{W}^{l'}_{2l}]\, C_{\tilde{E}El'} + \frac{1}{2}[\mathcal{W}^{l'}_{1l} + \mathcal{W}^{l'}_{2l}]\, C_{\tilde{B}Bl'} \\ C_{TEl} &= C_{\tilde{T}El} + \mathcal{W}^{l'}_{3l}\, C_{\tilde{T}El'}, \end{aligned} \tag{4.12}$$

where the sum over l' is implicit, and the functions $\mathcal{W}$ are defined to be

$$\begin{aligned} \mathcal{W}^{l'}_{1l} &= \frac{l'^3}{2}\int_0^\pi \theta d\theta\; J_0(l\theta)\; \{\sigma_2^2(\theta)J_2(l'\theta) - \sigma_0^2(\theta)J_0(l'\theta)\} \\ \mathcal{W}^{l'}_{2l} &= \frac{l'^3}{2}\int_0^\pi \theta d\theta\; J_4(l\theta)\; \{\frac{1}{2}\sigma_2^2(\theta)[J_2(l'\theta) + J_6(l'\theta)] - \sigma_0^2(\theta)J_4(l'\theta)\} \\ \mathcal{W}^{l'}_{3l} &= \frac{l'^3}{2}\int_0^\pi \theta d\theta\; J_2(l\theta)\; \{\frac{1}{2}\sigma_2^2(\theta)[J_0(l'\theta) + J_4(l'\theta)] - \sigma_0^2(\theta)J_2(l'\theta)\}. \end{aligned} \tag{4.13}$$

The quantities $\sigma_0^2(\theta)$ and $\sigma_2^2(\theta)$ are given by

$$\begin{aligned} \sigma_0^2(\theta) &= 16\pi^2 \int_0^{\chi_{\rm rec}} W^2(\chi, \chi_{\rm rec})d\chi \int_0^\infty k^3 dk \cdot \\ &\cdot\; P_\Phi(k, \tau = \tau_0 - \chi)[1 - J_0(k\theta\chi)]\;, \end{aligned} \tag{4.14}$$

and

$$\begin{aligned} \sigma_2^2(\theta) &= 16\pi^2 \int_0^{\chi_{\rm rec}} W^2(\chi, \chi_{\rm rec})d\chi \int_0^\infty k^3 dk \cdot \\ &\cdot\; P_\Phi(k, \tau = \tau_0 - \chi)J_2(k\theta\chi)\;. \end{aligned} \tag{4.15}$$

Here k is the wavenumber absolute value, J_l is the Bessel function of order l, χ is the comoving radial distance, τ is the conformal time, P_Φ is the power spectrum of the gravitational potential, and W is a function accounting for the cosmic curvature, which amounts to $1 - \chi/\chi_{\rm rec}$ for a flat universe (it is the integrand of the weight function $g'(\chi)$ in eq. (2.37) of the previous Chapter). The above equations tell us that the lensed power spectra C_{XXl}, where X runs over the possible spectra types, are obtained from their unlensed ancestors $C_{\tilde{X}Xl}$ after a convolution the some window functions W, which account for the contribution of the lensing potential. The latter appears in the window functions through σ_0 and σ_2,

where however its power spectrum has been rewritten in terms of that of the gravitational potential P_Φ according to the prescription of Eq. (2.37) in Chap. 2: this explains our previous statement that the functions σ_0 and σ_2 appearing in Eq. (4.11) are the equivalent of the lensing potential with the present notation. The mixing of the primordial EE and BB spectra, which is evident from these formulæ, depends on the fact that the real-space quantities around which one Taylor-expands in powers of the deflection angle are not EE and BB themselves, but their combination forming the Stokes parameters Q and U.

In ΛCDM cosmologies and most of the numerical codes dealing with them, including CMB-fast, the quantities appearing in the above equations may be computed independently of the main routine which performs the integration of the cosmological perturbations equations. This can be done because the power spectrum of matter density perturbations Δ_m can be factorized in two terms, depending respectively only on the wavenumber and the redshift:

$$P_{\Delta_m}(k,\chi) = Ak^n \cdot T^2(k,0)g^2(\chi) \ . \tag{4.16}$$

Ak^n here represents the primordial power, T is the transfer function of density perturbations taking into account the evolution on sub-horizon scales, and g is the overall linear growth factor. However, this separation is only convenient if one is provided with a satisfactory analytical fit of the growth of perturbations, which is not the case unless we ignore the influence of Quintessence fluctuations, which do make a non-negligible effect on large scales [113]. To account for these changes, we evaluate numerically the density contrast from all fluctuating components Δ. This quantity is computed and saved while the main routine performs the integration of the equations of motions, and used later for the computation of the quantities (4.14) and (4.15), which include all fluctuating components.

A separate issue concerns the normalization constant A above when lensing is taken into account. The lensed perturbation spectra no longer depend linearly on the primordial normalization, since the lensing is a second order effect; consequently, the normalization has to be treated as the other parameters, having no trivial impact on the perturbations. In Section 4.3 the models under examination have been set to have the same amplitude of the primordial perturbations, in order to highlight the differences arising due to the later lensing dynamics, while in Section 4.4 the primordial normalization is among the

cosmological parameters to be constrained.

4.3 Lensed CMB polarization power spectra

In this section we describe the phenomenology of the two dark energy models discussed in the previous Section, as they well represent the different dynamics that the dark energy might have. We study the behavior of the relevant lensing quantities, showing results for the corresponding lensed CMB power spectra. In particular, we focus on the effect induced by the dark energy behavior at the epoch when the lensing power injection is effective. We give a qualitative description of how the lensing breaks the degeneracy between w_0 and w_∞ affecting the unlensed TT, TE and EE spectra.

Both the SUGRA and the IPL models are characterized by two parameters, the index of the power-law α, and the mass of the field M. As it is well known [66, 67] they both admit attractor trajectories for the field dynamics in the early universe, known as tracking solutions. For field values much smaller than the Planck mass, the two potentials converge to the shape of a pure inverse power law. In this regime, and as long as the field is not the dominant cosmological component, the field energy density scales in redshift with an almost constant equation of state, depending on the power law only: $w = -2/(\alpha+2)$. For suitable values of α, which in our example is set respectively as -2.21 and -0.34 for the SUGRA and IPL models this implies a shallower scaling with respect to matter and radiation, so that the field eventually comes to dominate the expansion. When this happens is determined by the potential amplitude, governed by the mass parameter, for both cases; it is adjusted to yield the observed dark energy density today. The difference between IPL and SUGRA arises in this last part of the evolution, since in the SUGRA case the exponential becomes effective flattening the shape of the potential.

First of all we want to discuss qualitatively the effects on the corresponding background evolution, where we expect to see the most relevant differences between the two models; the key point of the comparison is the behavior of the dark energy component, which will characterize the scaling of the expansion factor. We consider models where the present equation of state of the dark energy is $w_0 = -0.9$, in agreement with the present constraints [20].

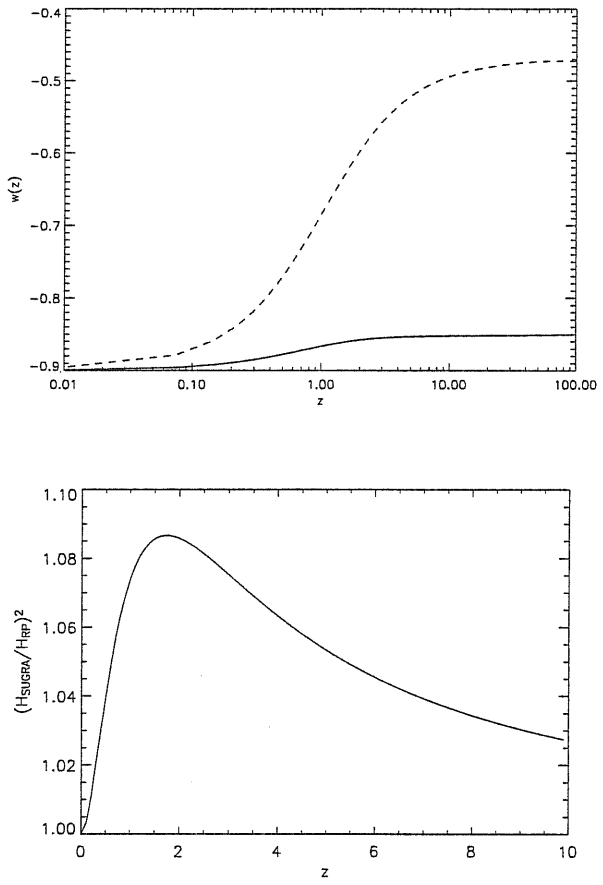

Figure 4.1: UPPER PANEL: Evolution of the equation of state of dark energy for the SUGRA (dashed line) and IPL (solid line) models. LOWER PANEL: Ratio of the squared Hubble parameters for the same models: the line H = 1 corresponds to the IPL case.

The redshift evolution of $w(z)$ is shown in Fig. 4.1, showing that while in the IPL model it is mildly departing from its present value at high redshifts, in the SUGRA one it rapidly gets to higher values. We also plot the squared ratio of the Hubble parameters, which enters directly in the distance measurements, for the two models.

The remaining cosmological parameters are chosen accordingly to the concordance cosmological model, see the first column of Table 4.1.

Since in the SUGRA model the dark energy becomes relevant at higher redshifts with respect to the ΛCDM and IPL cases, the inhibition of structure formation starts earlier (see [114] and references therein); thus, for fixed primordial normalization, we expect two effects.

The first is a smaller lensing signal, since clustering of structures will be lower in this model (see [32]). The second is that the lensing cross section, namely the redshift region where the lensing signal picks most of its power, is shifted towards earlier epochs, in consequence of the structure formation process occurring at higher redshift following the earlier dark energy dominance.

These features can be verified analyzing the function $\sigma_0(\theta)$; we choose a reference value of the angle, say $\theta \simeq 14$ arcminutes, corresponding roughly to the middle of the range suitable for CMB computations. We consider the function $\sigma_0(\theta_0, z)$ for this angle and assume a unitary power spectrum fixing $P_\Phi(k, \tau) = 1$ for the gravitational potential fluctuations. We call the resulting quantity the *lensing kernel*, $k_0(\theta_0, z)$; its dimensions are the inverse of a volume, and it gives a measure of the whole lensing effect coming from the background. The expected plot for σ_2 is similar, because the shape of the lensing kernel is governed by the quantity $W^2 = (1 - \chi/\chi_{\rm rec})^2$, and thus the relevant feature of the peak at $z \simeq 1$ is conserved. For reference, we plot $\sigma_2(\theta_0, z)$ (and we call the corresponding kernel $k_2(\theta_0, z)$) for the same angle as in the σ_0 case. The results are shown in Fig. 4.2.

Both our expectations are verified; note how the two cosmological models, although having

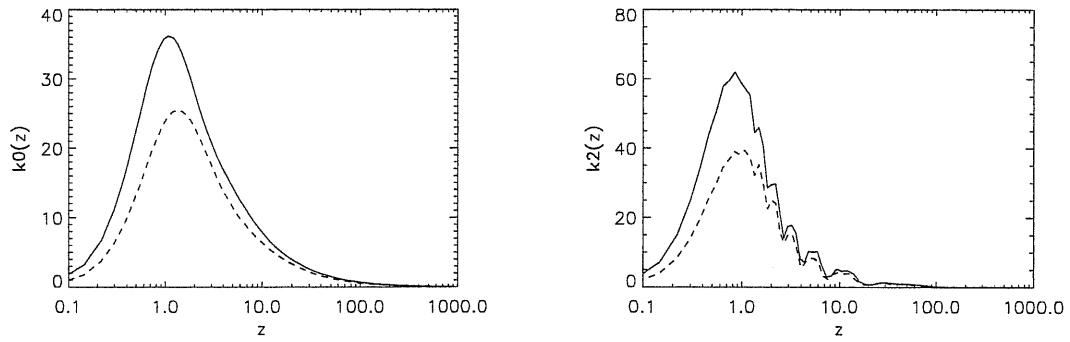

Figure 4.2: Lensing kernel k_0 (upper panel) and k_2 (lower panel) for $\theta \simeq 14'$, for the SUGRA (dashed line) and IPL (solid line) models, having the same equation of state today.

the same values of all cosmological parameters today, differ substantially (30%) at the epoch of structure formation entirely because of the difference in the cosmological distances.

Let us now turn to analyze the impact of the different perturbation growth rate, influencing $\sigma_0(\theta)$ and $\sigma_2(\theta)$ through the power spectrum of the gravitational potential. It

is convenient to plot the linear growth factor, $g(z,k) = T(k,z)/T(k,z=0)$, for the two models at a fixed wavenumber; the behavior is qualitatively the same for any k. The result is shown in Fig. 4.3. The phenomenology is the following. In the matter dominated era,

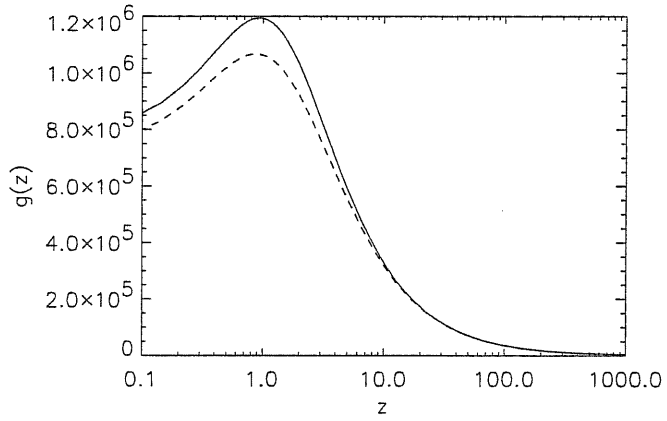

Figure 4.3: Growth factor of the perturbations for a comoving wavenumber $k = 0.1$ Mpc^{-1}, for the SUGRA (dashed line) and IPL (solid line) models. In the two models, g has the same value at infinity.

say at redshifts between 1000 and a few in the figure, g has the well known scaling as $a = 1/(1+z)$. At the onset of acceleration, its growth is inhibited and eventually it starts to decrease. The effect is of the order of 10%, and goes in the same direction as the one in Fig. 4.2: the solid line (IPL) lies above the dashed (SUGRA) one, so that the combination of the two effects of background evolution and perturbations growth contributing to the expressions of σ_0 and σ_2 is indeed large. As expected, this effect is stronger in the SUGRA case, as dark energy dominance takes place earlier.

On the basis of the issues outlined above, it is crucial to fix CMB observables purely sourced by gravitational lensing. The BB modes in the CMB represent an almost ideal candidate for this, since the lensing is the only known mechanism injecting power on scales smaller than $l \simeq 200$, where the imprint from primordial gravitational waves starts to drop. In the following we give a qualitative illustration of its relevance, leaving a more quantitative discussion for the next Section.

The TT, TE and EE CMB spectra are dominated by primary anisotropies, imprinted at last scattering, where in most models the dark energy is not yet effective. The lensing contributes

smoothing a bit the acoustic peaks, and moving some power to the damping tail [112]. The location of the acoustic peaks depends on the different cosmological expansion histories, as a result of the modification in the comoving distance to last scattering d_{LS}, which is written as

$$d_{LS} = H_0^{-1} \int_0^{z_{LS}} dz[\Omega_m(1+z)^3 + +(1-\Omega_m)e^{3\int_0^z dz' \frac{1+w(z')}{1+z'}}]^{-1/2} . \qquad (4.17)$$

where H_0 is the Hubble parameter, Ω_m is the matter abundance today relative to the critical density and the contributions from radiation and curvature are neglected. It does not come as a surprise that this quantity depends very weakly on different forms of $w(z)$, since those are washed out by two integrals in redshift; nonetheless, such projection effect is the main visible difference between unlensed and lensed spectra for TT, TE and EE modes. The Integrated-Sachs-Wolfe effect acts on large scales only, responding to the change in the cosmic equation of state; although promising results may be obtained correlating the ISW with the large scale structure data [115], from a pure CMB point of view the cosmic variance represents a substantial limiting factor.

The BB phenomenology is utterly different. Here the lensing is the only source of power on sub-degree angular scales, and the lensing cross section is largest at structure formation, where the dark energy might differ significantly from a Cosmological Constant, even for the same expansion rate today. The lensed CMB power spectra are shown in Figs. 4.4 and 4.5. It is immediately evident how the sensitivity of the BB power to the dark energy at high redshifts is sensibly altered with respect to the small projection affecting all the other spectra. Indeed, the BB peak traces directly the perturbation growth rate and background expansion at the epoch of structure formation. For the cosmological parameters at hand, the effect is of the order of several ten percent, consistently with the results in Figs. 4.2, 4.3. We remark that the C_ls have been obtained with the same value of all cosmological parameters, including the primordial normalization, and differ only in the value of the dark energy equation of state at intermediate redshifts. For comparison we also plot, in Fig. 4.6, the BB modes with a different normalization, fixed by the same $\sigma_8 = 0.76$. Notice that the spectra are switched, since the SUGRA model requires a larger primordial power in order to achieve the same amount of clustering at present, but the difference in the amplitude of the BB modes spectrum is still large, confirming that the amplitude effect is not an artifact

due to the normalization procedure.

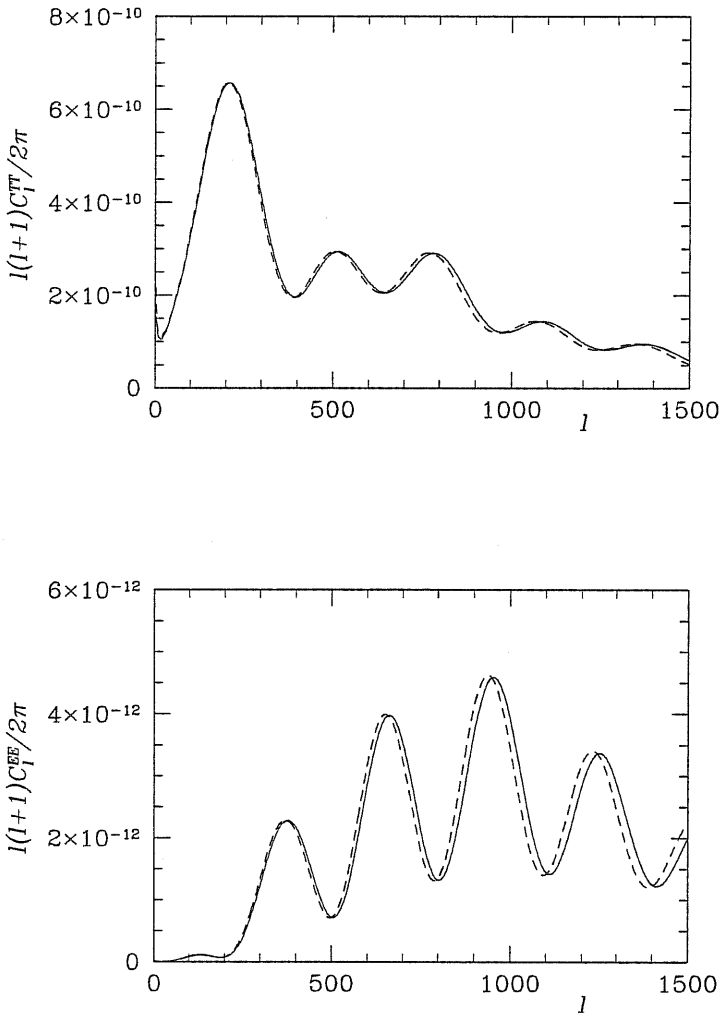

Figure 4.4: TT (upper panel) and EE (lower panel) lensed power spectra for the SUGRA (dashed line) and IPL (solid line) models with fixed primordial normalization.

To make the projection degeneracy breaking more apparent, we also consider dark energy models featuring the same value of d_{ls} in (4.17), with different values of w_0 and w_∞. The TT and BB spectra are shown in Fig. 4.7 , showing clearly the same pattern in the TT acoustic peaks, apart from the different ISW effect on very large scales, but markedly different BB amplitude, reflecting the enhanced dependence of the latter on w_∞. We will

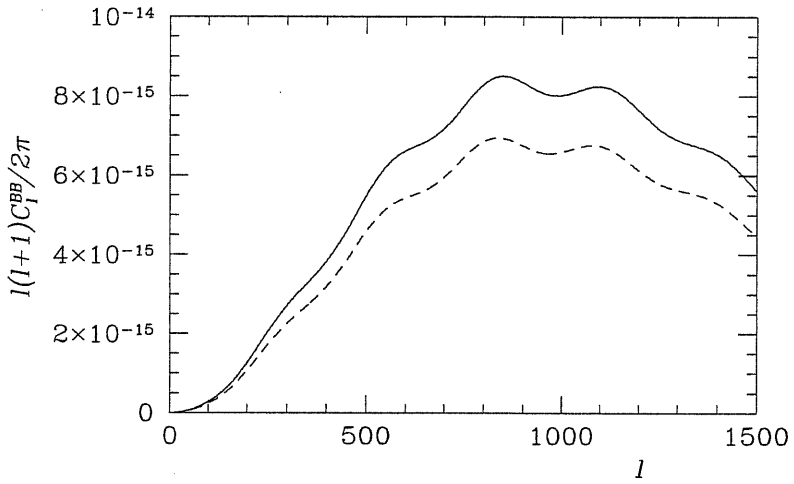

Figure 4.5: BB lensed power spectra for the same SUGRA (dashed line) and IPL (solid line) models of Fig. 4.4.

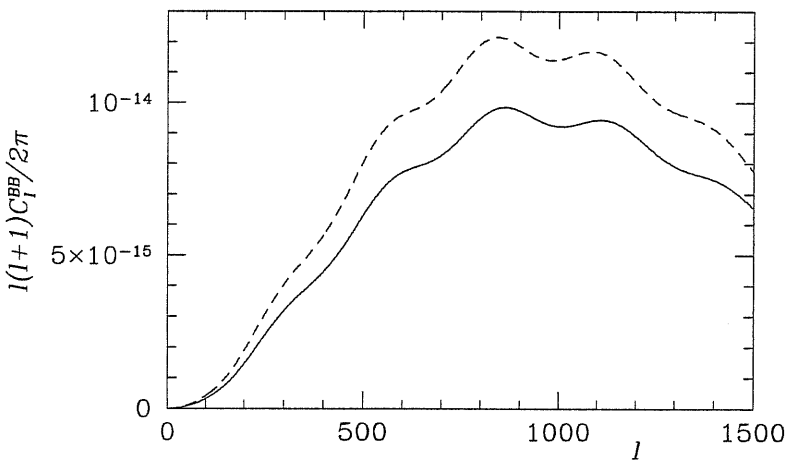

Figure 4.6: BB lensed power spectra for the SUGRA (dashed line) and IPL (solid line) models, but with normalization fixed by the same σ_8.

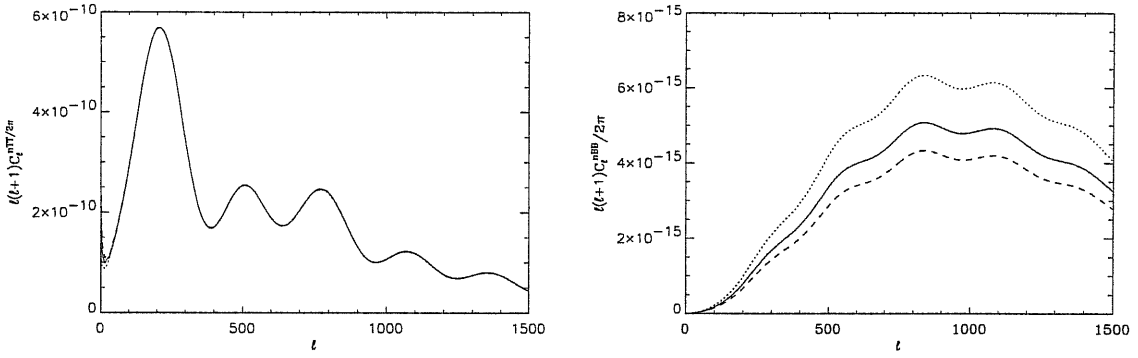

Figure 4.7: Lensed TT (left) and BB (right) power spectra for dark energy models with $w_0 = -0.9$, $w_\infty = -0.4$ (solid line), $w_0 = -0.965$, $w_\infty = -0.3$ (dashed line), $w_0 = -0.8$, $w_\infty = -0.56$ (dotted line).

quantify the relevance of this effect in the next Section.

4.4 Fisher matrix analysis

Here we give a first quantitative evaluation of the benefit that the knowledge of the lensing effect, and the inclusion of the BB spectrum in particular, has on the CMB capability of constraining the dark energy dynamics. Our approach is based on a Fisher matrix analysis, reviewed in Section 4.4.1; in Section 4.4.3 we show the results.

4.4.1 Method

In a CMB analysis involving the polarization power spectra [48], the Fisher matrix takes the form

$$\mathrm{F}_{ij} = \sum_{\ell} \sum_{XY} \frac{\partial C_\ell^{XY}}{\partial \alpha_i} \left[\Xi_\ell\right]^{-1}_{XY,X'Y'} \frac{\partial C_\ell^{X'Y'}}{\partial \alpha_j}, \tag{4.18}$$

where XY and $X'Y'$ are either TT, EE, TE or BB and $\Xi_{XY,X'Y'} \equiv \mathrm{Cov}(C_\ell^{XY} C_\ell^{X'Y'})$ is the power spectra covariance matrix:

$$\Xi_\ell = \begin{pmatrix} \Xi_\ell^{TT,TT} & \Xi_\ell^{TT,EE} & \Xi_\ell^{TT,TE} & 0 \\ \Xi_\ell^{TT,EE} & \Xi_\ell^{EE,EE} & \Xi_\ell^{EE,TE} & 0 \\ \Xi_\ell^{TT,TE} & \Xi_\ell^{EE,TE} & \Xi_\ell^{TE,TE} & 0 \\ 0 & 0 & 0 & \Xi_\ell^{BB,BB} \end{pmatrix}. \tag{4.19}$$

The terms in the power spectra covariance matrix are given by

$$\begin{aligned}\Xi_\ell^{xy,x'y'} &= \frac{1}{(2\ell+1)f_{sky}\Delta\ell} \\ &\times [(C_\ell^{xy'}+N_\ell^{xy'})(C_\ell^{yx'}+N_\ell^{yx'}) \\ &+(C_\ell^{xx'}+N_\ell^{xx'})(C_\ell^{yy'}+N_\ell^{yy'})],\end{aligned} \tag{4.20}$$

The noise covariance is given by N_ℓ^{xy}, which also contains the effect of the instrumental beam. The inverse of the Fisher matrix gives the uncertainty on the theoretical parameters:

$$\mathcal{C}_{ij} \equiv \langle \Delta\alpha_i \Delta\alpha_j \rangle = \mathrm{F}_{ij}^{-1} \ . \tag{4.21}$$

$\Delta\alpha_i$ is the marginalized 1-σ error on the i^{th} parameter, and is given by the square root of the diagonal elements of the inverse of the Fisher matrix.

As a representative of the forthcoming CMB polarization probes capable to detect the BB spectrum we consider a post-Planck all-sky experiment. We conservatively consider a Gaussian, circular beam with angular resolution of 7 arcminutes, considering multipoles up to $l = 1800$. We assume an instrumental detector noise of 1 μ K, and cut the galactic plane assuming a sky fraction of 0.66 (a more rigorous definition of these quantities will however be given in Sec. 4.5).

A delicate issue in applying a Fisher matrix analysis to the CMB lensing is represented by the non-Gaussianity of the lensing effect, due to the correlation of cosmological perturbations on different angular scales; the lensing statistics have been recently receiving increasing attention in view of the incoming precision polarization experiments [118, 119, 122, 116]. In particular, Smith et al. [119] achieved a first quantification of the increase in the covariance matrix due to the non-Gaussian nature of the lensing signal in the BB modes, giving a pipeline to estimate the resulting achievable accuracy.

For our study their most relevant result is the behavior of the so called *degradation factor*, the ratio between the squared sample covariance in the case of this non Gaussian signal and the corresponding Gaussian case. This is shown to depend both on the instrumental error (the degradation increases with the signal-to-noise ratio of the experiment, as expected because the instrumental error is close to Gaussian) and on the maximum available multipole (again increasing with $l_{\max}$, because of the stronger effect of the correlation between neigh-

boring band powers).
According to their worst case scenario, we make a conservative choice enlarging by a factor 10 the covariance contribution to the BB spectrum in the covariance matrix (4.20).
A step further has been made in [117], who suggested a way of taking into account the non-Gaussian correlations of the lensed BB spectra, with special regard on the issue of degeneracies between the dark energy parameters and the neutrino mass. This approach goes however beyond the scope of the present analysis, and may be considered in further work.

4.4.2 Preliminary considerations

We analyze four flat cosmological models, corresponding to a pure ΛCDM, and inverse power law, and two SUGRA cases, specified by eight cosmological parameters, including the two specifying the dark energy equation of state:

w_0	present e.o.s. of dark energy	
w_∞	asymptotic past e.o.s. of dark energy	
h	present value of reduced Hubble parameter	(0.72)
$\Omega_B h^2$	fractional baryon density $\times\ h^2$	(0.022)
$\Omega_C h^2$	fractional CDM density $\times\ h^2$	(0.12)
n_S	perturbation spectral index	(0.96)
τ	reionization optical depth	(0.11)
A_S	density perturbation amplitude	(1.)

All the cosmological parameters, except the dark energy ones for the last SUGRA case, are chosen consistently with the current observations of CMB and large scale structure [20, 16]; we use the CMBFAST normalization for the reference models and consider the reelative parameter as their ratio) and assume the same values, indicated in parenthesis in the table above, for the non-dark-energy parameters for all the models, while the dark energy parameters are the following:

	ΛCDM	IPL	SUGRA1	SUGRA2
w_0	-1.	-0.9	-0.9	-0.82

w_∞	-1.	-0.8	-0.4	-0.24

The choice of the reference models reflected our will to check not only what kind of precision the lensing and the BB modes may bring in the knowledge of the cosmological parameters, but also whether the numerical results themselves presented any model-dependent feature. For this reason, we progressively deviated from the Cosmological Constant model, considering increasing dark energy dynamics for the IPL and the two SUGRA model, up to the last one which, as already said, lies on the edge of the allowed range of dark energy parameters but is useful in order to understand the effect of a violently varying Quintessence component.

As a first, qualitative estimate of the relative importance of the different spectra for the final result, we considered the relative change in the three spectra TT, EE and BB due to a order percent shift in the w_∞ parameter around the reference model (this can be considered a sort of weighted derivative, although the expression on the left hand side is not divided by δw_∞), specifically:

$$(C^{\mathrm{XX}}(w_\infty^+) - C^{\mathrm{XX}}(w_\infty^-))/C^{\mathrm{XX}}(w_\infty^{\mathrm{ref}}) \tag{4.22}$$

for the four cases, where X stands for T, E or B respectively and w_∞^+, w_∞^- are the values at which the double-sided derivative is evaluated. We chose this parameter since it represents the asymptotic dark energy equation of state in the past, and thus is suitable to track the dark energy behaviour at redshifts relevant for lensing. The reason why we don't include the correlation is that the denominator approaches zero several times, making the corresponding plot falsely unreadable; however, we verified that the order of magnitude is the same as the other weighted derivatives. Even if the derivatives with respect to different spectra are partially mixed in the covariance matrix, this plot gives a reasonable flavour of how much the four components concur to build the global Fisher matrix. Figure 4.8 shows that the relative change in the spectra are comparable for all the models under examination; naively, this would correspond to a 25% improvement due to the inclusion of the the BB modes spectrum. A further important remark in favor of the BB modes may be that while for the TT and EE components the effect is maximum around the peaks

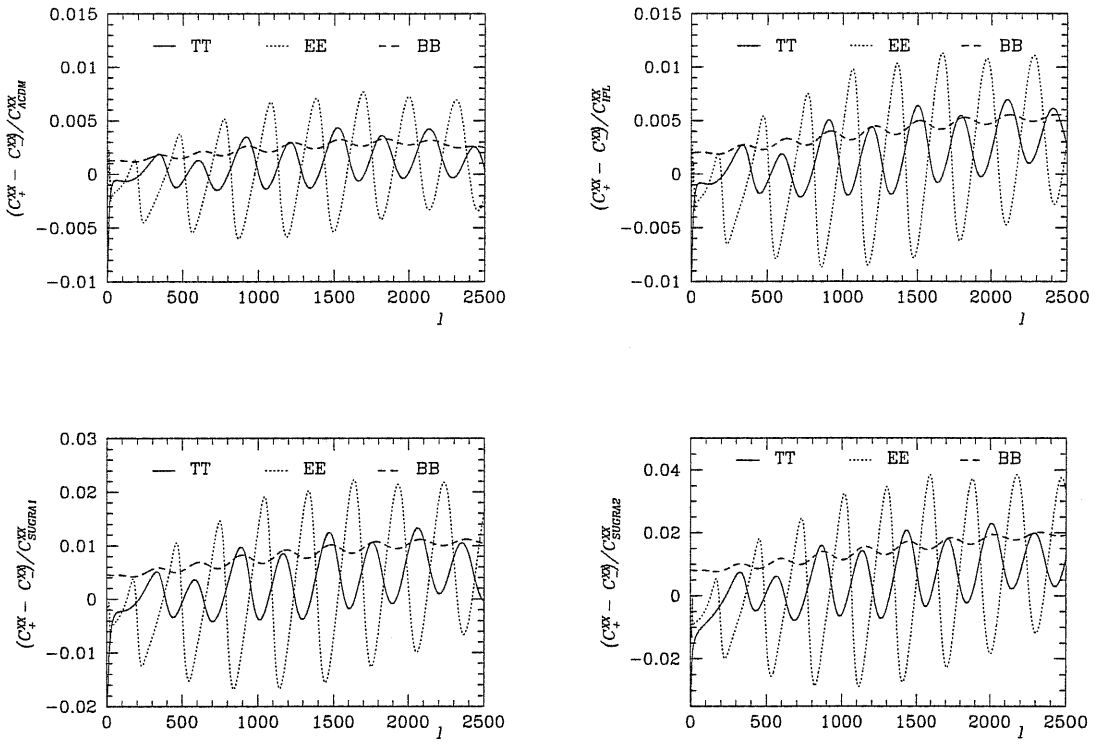

Figure 4.8: Weighted derivatives of the TT, EE and BB spectra with respect to the w_∞ parameter for the four models under study.

and valleys of the unlensed distribution as expected, since the main effect of the lensing is a smoothing of the oscillations in the acoustic regime, for the BB case the derivative is always positive and presents less marked features. This maybe relevant, for example, in the evaluation of the constraints from experiments limited to a small fraction of the sky, such as the polarization-oriented EBex [120] or PolarBEar [121], for which the binning procedure which has necessary to be applied in order to avoid fake correlations of the data points could reduce the statistical significance of the TT and EE modes, but not that of the BB ones.

The plot in Fig. 4.8 also suggests an interesting feature of the covariance matrix. In fact, it is easily seen that the reaction of the spectra to the change in w_∞ is larger with increasing dark energy dynamics (in the lower panels). The difference $w_\infty^+ - w_\infty^-$ has been fixed to 0.02 for all the four models, implying that the evidence arising from the Figure is

that the derivative of the lensed spectra with respect to w_∞ is a growing function of the Quintessence abundance. Such anticipation, *i.e.* that these more dynamical models can be better constrained through the lensing of the CMB, will find confirmation in the Fisher matrix results, as we discuss in the following.

Table 4.1: Results from the Fisher matrix analysis for the four models.

	ΛCDM		IPL		SUGRA1		SUGRA2	
	value	σ_{Fisher}	value	σ_{Fisher}	value	σ_{Fisher}	value	σ_{Fisher}
w_0	$-1.$	0.12	-0.9	9.7×10^{-2}	-0.9	6.1×10^{-2}	-0.82	3.5×10^{-2}
w_∞	$-1.$	0.27	-0.8	0.19	-0.4	6.9×10^{-2}	-0.24	1.9×10^{-2}
$\Omega_B h^2$	0.022	5.7×10^{-5}	0.022	6.0×10^{-5}	0.022	5.7×10^{-5}	0.022	5.9×10^{-5}
$\Omega_C h^2$	0.12	7.0×10^{-4}	0.12	7.3×10^{-4}	0.12	6.6×10^{-4}	0.12	5.0×10^{-4}
h	0.72	5.0×10^{-2}	0.72	4.5×10^{-2}	0.72	2.9×10^{-2}	0.72	1.5×10^{-2}
n_S	0.96	2.1×10^{-3}	0.96	2.2×10^{-3}	0.96	2.1×10^{-3}	0.96	2.0×10^{-3}
τ	0.11	3.1×10^{-3}	0.11	3.0×10^{-3}	0.11	3.1×10^{-3}	0.11	3.2×10^{-3}
A	1.0	5.6×10^{-3}	1.0	5.5×10^{-3}	1.0	5.5×10^{-3}	1.0	5.6×10^{-3}

4.4.3 Marginalized errors on cosmological parameters

The results of the analysis are shown in table 4.1, reporting the $1-\sigma$ marginalized errors for each parameter, according to the present Fisher matrix approach. For the ΛCDM model there is an important indication of an achievable precision smaller than 20% on the w_0 parameter, while the limit on w_∞ is considerably weaker. The accuracy on the others is in agreement with previous similar analysis, which was indeed expected because the BB modes statistics have large error bars and trace the physics at late redshifts so that their influence on other parameters is smaller. Results are increasingly better for the IPL and the two SUGRA cases; this can be attributed to the more and more violent redshift behavior of the equation of state of these models, making them increasingly sensitive to the redshift region probed by lensing. In particular, the achievable precision on the w_∞ parameter appears to be growing faster, so that for the SUGRA cases the results for the two dark energy parameters are comparable.

As we have already mentioned, a relevant issue in the interpretation of the results is rep-

resented by degeneracies; we have emphasized in the previous discussion that the CMB spectra without account of the lensing signal are affected by a projection degeneracy concerning the distance to the last scattering surface. Indeed, there is a curve in the plane (w_0, w_∞) for which d_{LS} in Eq. (4.17) is the same, resulting in almost complete degeneracy of these two parameters which is only alleviated by the difference in the ISW effect. Therefore, if they were the only statistical data to be used in the dark energy parameter forecast, the reliability of the Fisher matrix method itself would be jeopardized, since one of the conditions for its applicability is for the parameters to be as uncorrelated as possible. In this respect, the addition of the lensing and in particular that of the BB power spectrum, which introduces an amplitude effect and thus removes this degeneracy, has to be seen not only as an improvement in the statistical quality of the data, but first of all as a conceptual achievement ensuring the goodness of the analysis method.

A more rigorous check that this statement is correct can be obtained comparing the result of the Fisher matrix with and without the addition of the BB modes power spectrum. For this purpose we will need not only, or better not as the primary source of information, the 1-σ expected constraints, but first of all the change in the eigenvalues of the Fisher matrix. In fact, the degree of degeneracy of the Fisher matrix, which is the most immediate indicator of problems in the analysis, is given by the size of its eigenvalues; the σs alone are less indicative because they are further filtered by the remixing of parameter axes into eigenvectors. In other words, although it is true that the smallest and thus more problematic eigenvalue is related to w_∞ in the sense that the latter is the principal component of the corresponding eigenvector, the alleviation of the degeneracy that it measures may not be exactly reflected by change in $\sigma(w_\infty)$ if the chosen set of parameters does not bear good enough resemblance to the principal components.

Therefore, we present and comment here both the change in the smallest eigenvalue, $e_{\rm small}$ (here below) and that in the 1-σ expected precision (in Tabs. 4.2,4.3), for the four cases.

	ΛCDM	IPL	SUGRA1	SUGRA2
$e_{\rm small}$ (no BB)	9.85	15.7	108.7	597.7
$e_{\rm small}$ (with BB)	13.28	26.7	155.9	695.0

From the numbers above it appears clear that the improvement is often (in three cases out of four) even larger than the naive 25% expected from the "weighted derivative" test. Significantly, the models that get the largest benefit from the inclusion of the BB modes spectrum are those which are worse globally determined, so that the result gains even more importance. The last SUGRA model is probably so extreme that the ISW effect in the temperature spectrum, which is the main dark energy indicator for the other three spectra, suffices to give a good determination of w_∞ by itself, so that the BB modes are still important, with a variation of the 15%, but less crucial than in other cases.

As for the change in the diagonal terms of the Fisher matrix, only in the case of IPL the change in e_{small} is directly translated into a change in $\sigma(w_\infty)$, and we have indeed verified that the relative eigenvector is very close to w_∞ for that model. In the other cases the degeneracy improvement is still more evident in $\sigma(w_\infty)$ than in the others, but is in part spread over the cosmological parameters that present a non-negligible correlation with w_∞: w_0, and h in particular.

Table 4.2: Results from the Fisher matrix analysis in absence or presence of the BB modes for the ΛCDM and IPL models.

	ΛCDM		**IPL**	
	σ (no BB)	σ (with BB)	σ (no BB)	σ (with BB)
w_0	0.13	0.12	0.11	9.7×10^{-2}
w_∞	0.31	0.27	0.24	0.19
$\Omega_B h^2$	6.4×10^{-5}	5.7×10^{-5}	6.5×10^{-5}	6.0×10^{-5}
$\Omega_C h^2$	7.9×10^{-4}	7.0×10^{-4}	7.8×10^{-4}	7.3×10^{-4}
h	5.6×10^{-2}	5.0×10^{-2}	5.4×10^{-2}	4.5×10^{-2}
n_S	2.3×10^{-3}	2.1×10^{-3}	2.3×10^{-3}	2.2×10^{-3}
τ	3.2×10^{-3}	3.1×10^{-3}	3.0×10^{-3}	3.0×10^{-3}
A	5.7×10^{-3}	5.6×10^{-3}	5.6×10^{-3}	5.5×10^{-3}

Table 4.3: Results from the Fisher matrix analysis in absence or presence of the BB modes for the two SUGRA models.

	SUGRA1		SUGRA2	
	σ (no BB)	σ (with BB)	σ (no BB)	σ (with BB)
w_0	$0.6.6 \times 10^{-1}$	6.1×10^{-2}	3.7×10^{-2}	3.5×10^{-2}
w_∞	7.9×10^{-2}	6.9×10^{-2}	2.1×10^{-2}	1.8×10^{-2}
$\Omega_B h^2$	6.4×10^{-5}	5.7×10^{-5}	6.5×10^{-5}	5.9×10^{-5}
$\Omega_C h^2$	7.5×10^{-4}	6.6×10^{-4}	7.0×10^{-4}	5.0×10^{-4}
h	3.3×10^{-2}	2.9×10^{-2}	1.6×10^{-2}	1.5×10^{-2}
n_S	2.2×10^{-3}	2.1×10^{-3}	2.3×10^{-3}	2.0×10^{-3}
τ	3.2×10^{-3}	3.1×10^{-3}	3.2×10^{-3}	3.2×10^{-3}
A	5.8×10^{-3}	5.5×10^{-3}	6.0×10^{-3}	5.6×10^{-3}

4.5 How to observe the B-modes

In this section we want to very briefly present the result of a study oriented to understand what kind of experiment is more suitable to the search for the lensing-born BB modes of polarization. In the analysis above we have considered as a target experiment a conservative version of a CMB-polarization satellite. This choice was motivated on one hand by the direct comparison with similar papers which conducted Fisher matrix analysis with similar sets of parameters ([122, 123, 124]), and on the other by this study that showed that experiments aiming at the detection and measurement of B modes around the lensing peak need to be calibrated over a significant fraction of the sky.
The detailed form of the instrumental noise N_ℓ^{xy} is (*i.e.* [125])

$$N_\ell^{xy} = \frac{f_{\rm sky}}{w\, B_l^2}, \tag{4.23}$$

where beyond the sky fraction we find the relevant quantities

$$w^{-1} = \frac{4\pi\sigma^2}{N} \tag{4.24}$$

and

$$B_l = \exp^{-\sigma_b^2 l(l+1)/2}. \tag{4.25}$$

Here σ is the r.m.s. noise in any of the global N pixels, and B_l is the experimental beam function. The latter depends on the standard deviation of the beam

$$\sigma_B = \frac{\theta_B}{\sqrt{8 \log 2}}, \tag{4.26}$$

where θ_B is the full width half maximum beam size.

For a given experiment the *integrated sensitivity* depends on the instruments and thus is fixed: it corresponds to the ratio $\sigma^2/f_{\rm sky}$. Therefore, the experimental setup can be modified through the quantities σ and $f_{\rm sky}$, keeping the integrated sensitivity constant: one can choose a scan of the sky to be either deeper but smaller, or shallower but larger. The plots that we show here in Fig. 4.9 have been done for the PolarBearII experiment [121], which is presently forecast to bet set at sky fraction of $\simeq 1$ %, and we have explored the 1-σ precisions on w_0 and w_∞ for 500 cases with$f_{\rm sky}$ varying from approximately 1/1000 to 0.5, for the ΛCDM and IPL models. The main feature of the results is that there is an "elbow" in the curves for both parameters, so that the precision is rapidly improving increasing the sky fraction up to a certain value, after which the achieved result stays basically constant. The reliability of these results has been recently confirmed in [123], which make a similar plot in their Fig. 15 (though for a single dark energy parameter), finding the elbow in roughly the same position as ours around $f_{\rm sky} \simeq 0.05$.

4.6 Some final considerations

The results obtained in this Chapter can be divided in two parts. One is completely model-independent, and consists in the detailed study of how the dynamics of the expansion and those of the perturbations merge in order to give the global lensing effect. This has been done isolating and analyzing the two effects, but the formal description is valid in any generalized cosmology scenario.

The second part is more specific to the scalar field dark energy case, for which we have used the Fisher matrix method in order to quantify the benefit of the inclusion of the lensing effect for constraining the dark energy parameters. However, the remarkable indication of increasing precision for increasing dynamics that we obtained is plausibly valid for any

deviation from the Cosmological Constant case, so that the results encourage the extension of the analysis to modified gravity models, and we may expect that models which couple a scalar field to the Ricci scalar, such as the NMC models introduced in the previous Chapter, benefit the most from the CMB lensing observables, which are sensitive at the same time to both the expansion history and the density fields evolution.

The first step in this direction is described in the next Chapter, which however deals with one of the simplest scalar-tensor gravity scenario, the Jordan-Brans-Dicke model.

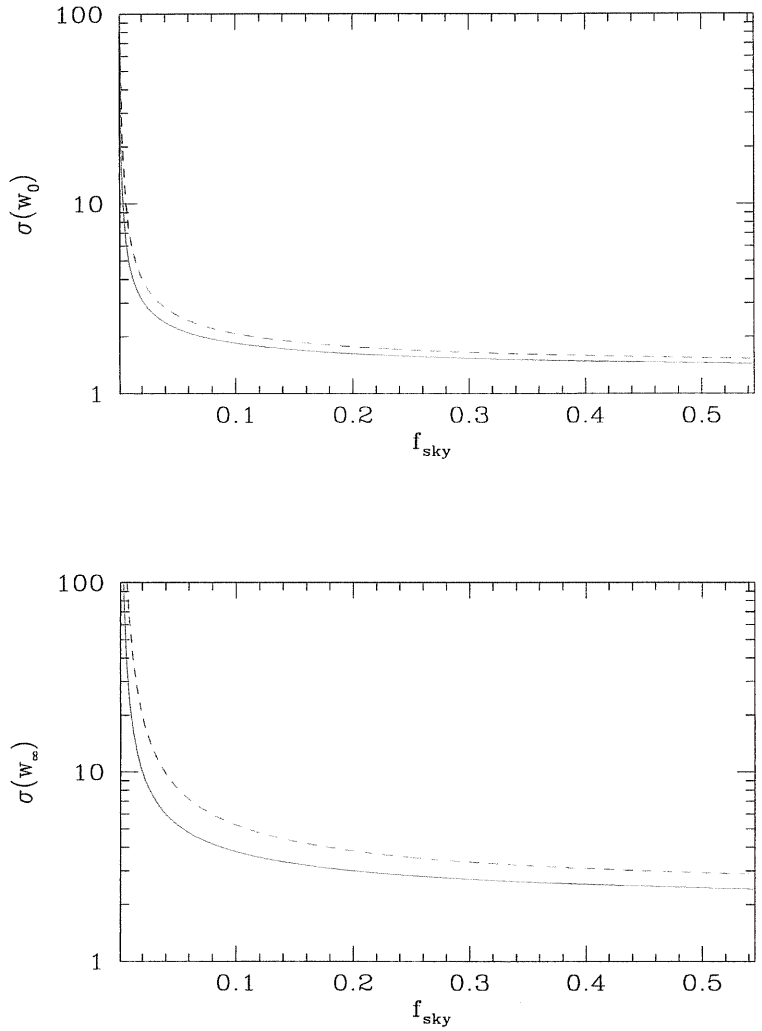

Figure 4.9: Expected 1-σ precision for different sky fraction for the w_0 (upper panel) and w_∞ (lower panel) parameters. The red, dashed curve is for the ΛCDM model, the blue, solid curve for the IPL model.

Chapter 5

The Jordan-Brans-Dicke cosmology: constraints and lensing signal

In the first part of this Chapter we report the results of an analysis of a simple model of Modified Gravity, the Jordan-Brans-Dicke theory [57]. This work, whose main result was a consistent improvement of the constraint on the Jordan-Brans-Dicke parameter on cosmological scales, was carried out in [129] and intended as a preliminary step for the treatment of the CMB lensing in this scenario. In fact, the DEfast code (introduced in the previous Chapter) did not feature a routine for the integration of the associated set of equation, and this numerical work was carried out in the paper above and incorporated into the main routine. This model was regarded as particularly interesting in the perspective of the study of the CMB lensing signal because it allows to isolate the effects coming from the modifications of gravity through only one additional parameter, and it features the anisotropic stress as a new degree of freedom with respect to the ΛCDM or ordinary Quintessence models, as previously commented.

We have used cosmic microwave background data from WMAP 1st year [18], ACBAR [141], VSA [139] and CBI [140], and galaxy power spectrum data from 2dF [143], to constrain flat cosmologies based on the Jordan–Brans–Dicke theory, using a Markov Chain Monte Carlo

approach, and obtained a 95% marginalized probability lower bound on the Brans–Dicke parameter $\omega > 120$.

In the second part of the Chapter we present our preliminary results for the CMB lensing in these scenarios. Results are preliminary since we have not included the anisotropic stress yet as a source for the quantities σ_0 and σ_2 of the previous Chapter, which, as we have discussed, can be regarded as the most representative quantities for the evaluation of the lensing contribution. However, the estimate of the order of magnitude of the lensed CMB spectra should be substantially correct for the range of allowed values of the coupling parameter, since the anisotropic stress in this model is significantly smaller, by three order of magnitude in any regime, than the gravitational potential Φ (which amounts to say that the relative difference in absolute value between Φ and Ψ, which we have denoted as Ξ, is that small). Nonetheless, the analysis of the anisotropic stress is this and other models is being presently performed and we will talk more diffusely about it in the next Chapter, dedicated to the work in progress and the most immediate future directions.

5.1 The model

Jordan–Brans–Dicke (JBD) theory [57, 130] is the simplest extended theory of gravity, depending on one additional parameter, the Brans–Dicke coupling ω, as compared to General Relativity. As Einstein's theory is recovered in the limit $\omega \to \infty$, there will always be viable JBD theories as long as General Relativity remains so too. As such, it acts as a laboratory for quantifying how accurately the predictions of General Relativity stand up against observational tests. The most stringent limits are derived from radar timing experiments within our Solar System, with measurements using the Cassini probe [88] now giving a two-sigma lower limit $\omega > 40,000$ (improving pre-existing limits [87] by an order of magnitude).

With precision cosmological data now available, particularly on cosmic microwave background (CMB) anisotropies from WMAP [18, 16], it has become feasible to obtain complementary constraints from the effect of modified gravity on the structure formation process, as suggested in Ref. [131]. That paper focused on the way that ω alters the

Hubble scale at matter–radiation equality, which is a scale imprinted on the matter power spectrum, in an attempt to identify how large an effect can be expected. Subsequently, the expected total intensity and polarization microwave anisotropy spectra in the JBD theory were computed, and a forecast of the sensitivity to ω of data from the WMAP and Planck satellites carried out exploiting a Fisher matrix approach [132].

Here we make a comprehensive comparison of predictions of the JBD theory to current observational data, using WMAP 1st year data and other CMB data plus the galaxy power spectrum as measured by the two-degree field (2dF) galaxy redshift survey. We define JBD models in terms of eight parameters, which are allowed to vary simultaneously. Our procedure is closest in spirit to work by Nagata et al. [133], who considered a more general model, the so-called *harmonic attractor model*, which includes JBD as a special case. However their dataset compilation was restricted to the WMAP 1st year temperature power spectrum.

The constraint we will obtain is not competitive with the very stringent solar system bound given above (though the analysis of Ref. [132] indicates that a limit as high as 3000 might eventually be reached by the measurements of the Planck satellite), but it is complementary in that it applies on a completely different length and time scale. Such constraints can therefore still be of interest in general scalar–tensor theories where ω is allowed to vary; for instance Nagata et al. [133] find that in some parameter regimes of their harmonic attractor model the cosmological constraint is stronger than the Solar System one. In that regard, our result is most comparable to cosmological constraints imposed on ω from nucleosynthesis, which give only a weak lower limit of $\omega > 32$ [134].

5.1.1 Background cosmology

The Lagrangian for the JBD theory is

$$\mathcal{L} = \frac{m_{\rm Pl}^2}{16\pi}\left(\Phi R - \frac{\omega}{\Phi}\partial_\mu\Phi\partial^\mu\Phi\right) + \mathcal{L}_{\rm matter}\,, \tag{5.1}$$

where the Brans–Dicke coupling ω is a constant, and $\Phi(t)$ is the Brans–Dicke (BD) field whose present value must give the observed gravitational coupling. With reference to the general Lagrangian which is the integrand of eq. (3.1), here $f(\Phi, R) = \Phi\, R$ and we use the

Planck mass m_P defined as $m_P = 1/\sqrt{G_*}$; we have included factors of $m_{\rm Pl}$ to define Φ as dimensionless. The equations for a spatially-flat Friedmann universe are [57, 130, 135]

$$\left(\frac{\dot{a}}{a}\right)^2 + \frac{\dot{a}}{a}\frac{\dot{\Phi}}{\Phi} = \frac{\omega}{6}\left(\frac{\dot{\Phi}}{\Phi}\right)^2 + \frac{8\pi}{3m_{\rm Pl}^2\Phi}\rho\,; \tag{5.2}$$

$$\ddot{\Phi} + 3\frac{\dot{a}}{a}\dot{\Phi} = \frac{8\pi}{(2\omega+3)m_{\rm Pl}^2}(\rho - 3p)\,, \tag{5.3}$$

with the usual notation for the scale factor $a(t)$, and where ρ and p are the energy density and pressure summed over all types of material in the Universe.

The Universe is assumed to contain the same ingredients as the WMAP 1st year concordance model [18], namely dark energy, dark matter, baryons, photons and neutrinos. We make the simplifying assumptions of spatial flatness, dark energy in the form of a pure cosmological constant, and effectively massless neutrinos whose density is related to that of photons by the usual thermal argument. The present value of Φ must correctly reproduce the strength of gravity seen in Cavendish-like experiments, which requires [130]

$$\Phi_0 = \frac{2\omega+4}{2\omega+3}\,, \tag{5.4}$$

where here and throughout a subscript '0' indicates present value. We will assume that the value of Φ_0 in our Solar System is representative of the Universe as a whole, though this may not be absolutely accurate [136]. We also assume that the initial perturbations are given by a power-law adiabatic perturbation spectrum.

When the Universe is dominated by a single fluid there are a variety of analytic solutions known [137], where Φ is typically constant during a radiation era, slowly increasing during a matter era, and then more swiftly evolving as dark energy domination sets in. However we need solutions spanning all three eras and so will solve the equations numerically, for which we use the integration variable $N \equiv \ln a/a_0$. An example of the evolution is shown in Fig. 5.1.

The basic parameter set we use to build our cosmological models contains the following parameters

- ω Brans–Dicke coupling
- H_0 present Hubble parameter [$\mathrm{km\,s^{-1}Mpc^{-1}}$]

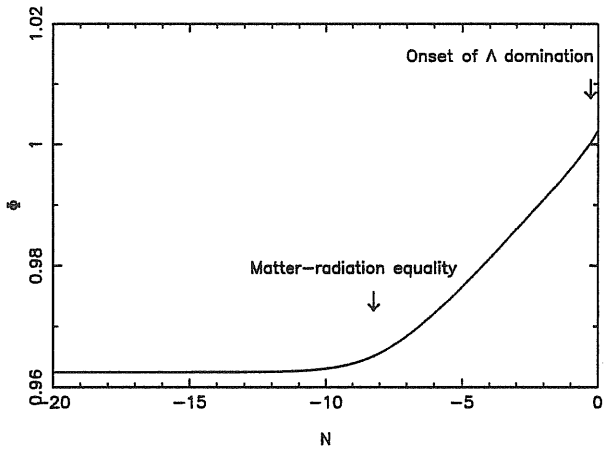

Figure 5.1: Evolution of the BD field from early in radiation domination to the present. It is just possible to see the evolution of Φ increase as Λ domination sets in. The cosmological parameters are $\omega = 200$, $H_0 = 72$, and $\rho_{\mathrm{m},0} = 0.3$ in units of the standard cosmology critical density.

ρ_{B}	baryon density
ρ_{C}	cold dark matter density
A_{S}	curvature perturbation amplitude
n_{S}	perturbation spectral index
τ	reionization optical depth
b	galaxy bias parameter, $P_{\mathrm{gg}}/P_{\mathrm{mm}}$

where $b^2 = P_{\mathrm{gg}}/P_{\mathrm{mm}}$ is the ratio of the (observed) galaxy power spectrum to the (calculated) matter power spectrum. Other parameters are fixed by the assumptions above, and the radiation energy density is taken as fixed by the direct observation of the CMB temperature $T_0 = 2.725\mathrm{K}$ [138].

An important subtlety that must be taken into account is that the extra terms in Eq. (5.2), plus the Cavendish-like correction to the present value of Φ, mean that the usual relation between the Hubble parameter and density, used to define the critical density and hence density parameters, no longer applies. Generically, the extra terms require an increase in the present value of ρ to give the same expansion rate, the correction being of order $1/\omega$. Because of this subtlety, we define the density parameters $\Omega_{\mathrm{B,C}}$ by dividing by the critical density for the standard cosmology, meaning that the density parameters don't

quite sum to one for a spatially-flat model.

Operationally, we proceed as follows. We seek a background evolution corresponding to a particular value of $h = H_0/100$ and of the present physical matter density. We can assume the initial velocity of the BD field $\dot{\Phi}$ is zero deep in the radiation era, which leaves us two parameters, the early time value of Φ and the value of the cosmological constant, to adjust in order to achieve the required values. This is a uniquely-defined problem, with the necessary values readily found via an iterative shooting method.

5.1.2 Perturbation evolution

We carry out the evolution of density perturbations using a modified version of the code DEFAST.

DEFAST takes as input the parameter set described in the previous subsection, and returns the microwave anisotropy spectra (for temperature and polarization) and the matter power spectrum. A dynamical and fluctuating scalar field, playing the role of the dark energy and/or the BD field, is included into the analysis together with the other cosmological components, following the existing general scheme [105].

In order to bring the model description into the formalism used by DEFAST, we redefine the BD field and coupling according to

$$\phi^2 = \omega\,\Phi\frac{m_{\rm Pl}^2}{2\pi} \quad ; \quad \xi = \frac{1}{4\omega}\,, \tag{5.5}$$

which brings the Lagrangian into the form

$$\mathcal{L} = \frac{1}{2}\xi\phi^2 R - \frac{1}{2}\partial_\mu\phi\partial^\mu\phi + \mathcal{L}_{\rm matter}\,, \tag{5.6}$$

where ϕ is now a canonical scalar field non-minimally coupled to gravity (Notice however that this model is different from the more complex NMC model introduced as an example in Chap. 3, where the $\omega_{\rm JBD}$ parameter was time-varying). We implement the cosmological constant in the code by giving ϕ a constant potential energy.

Our calculations include the effect of perturbations, with the initial perturbations in ϕ fixed by the requirement of adiabaticity. The correction to the background expansion rate from the dynamics of ϕ is the most relevant effect on the CMB power spectrum,

appearing as a projection plus a correction to the ISW effect, as discussed in detail in Refs. [80, 82].

5.1.3 Data analysis

The data we use are taken from WMAP 1st year [142] and the 2dF galaxy redshift survey expressed as 32 bandpowers in the range $0.02 < k < 0.15h^{-1}\mathrm{Mpc}$ [143]. In order to incorporate the 2dF data, the galaxy bias parameter b is taken to be a free parameter for which the analytic marginalization scheme of Ref. [144] can be applied. We also consider the effect of including the high-ℓ CMB data from VSA [139], CBI [140], ACBAR [141].

Our present analysis does not include supernovae data. Inclusion of the modification to the luminosity distance from ω would be straightforward. However the variation of the gravitational coupling G means that supernovae can no longer be assumed to be standard candles, and Ref. [145] suggests that the effect from varying G dominates. Further, inclusion of supernovae data may be particularly susceptible to the possibility that the local value of Φ in the vicinity of the supernova may not match the global cosmological value [136]. Nevertheless, it would be interesting to investigate robust methods for including such data, also in connection with alternative observational strategies [146].

We carry out the data analysis using the now-standard Markov Chain Monte Carlo posterior sampling technique, by modifying the June 2004 version of the CosmoMC program [147] to call DEFAST to obtain the spectra. CosmoMC computes the likelihood of the returned model and assembles a set of samples from the posterior distribution. For the purposes of posterior sampling, we have parametrized the JBD cosmology using $\ln\xi \equiv -\ln 4\omega$ simply because it is more straightforward to obtain the samples we need, while simultaneously suppressing the possibility of jumping to regions with $\omega < 1$. Specifically, we use a flat prior on $\ln\xi \in [-9, -3]$ where the lower cutoff has been adjusted to the point where the likelihood function is no longer sensitive to the effect of varying the Brans–Dicke parameter and the ΛCDM model is thereby recovered. As usual, this Jeffreys prior, which is defined here as a flat prior on the logarithm of a parameter of unknown scale, has the interesting property of invariance under scale reparametrizations [148]. For this reason it serves as a reasonable substitute for working with a more desirable physical parameter

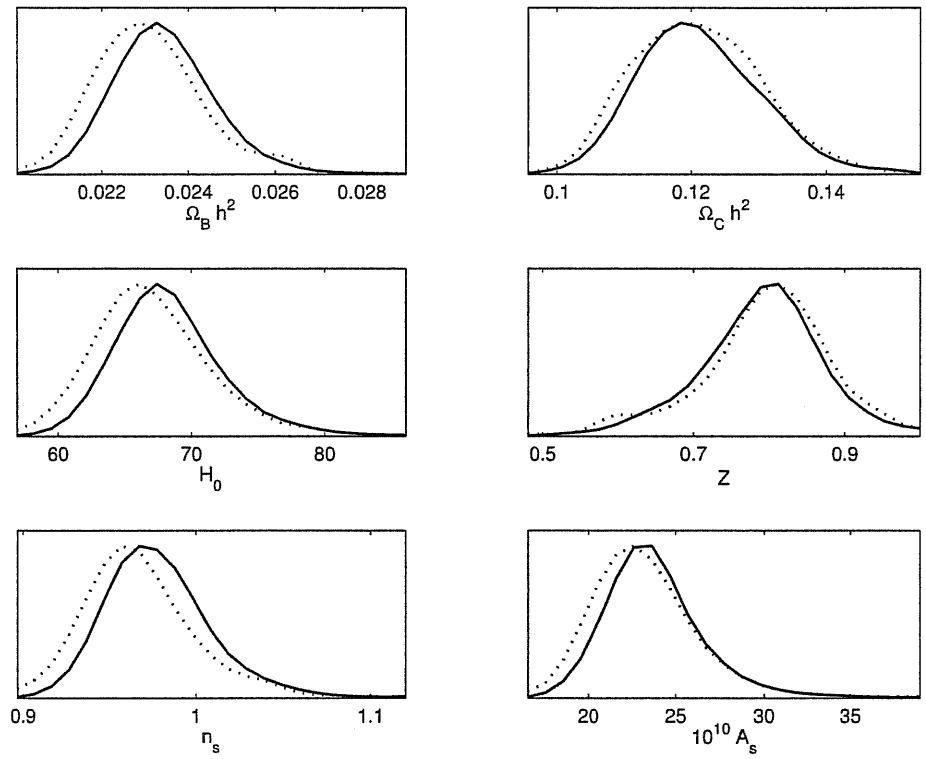

Figure 5.2: Marginalized 1D posterior distributions (solid lines) on the base parameters as listed in the text. Also displayed is the mean likelihood of the binned posterior samples (dotted lines).

which could be identified to isolate and give a linear response in the ISW effect, mainly responsible for the upper bound on $\ln \xi$.

The optical depth τ is parametrized using $\mathcal{Z} = \exp[-2\tau]$, where $\mathcal{Z}^{1/2}$ is the fraction of photons that remain unscattered through reionization, since the combination $A_S\mathcal{Z}$ is well constrained by the CMB.

The results that we present are based on around 100,000 raw posterior samples, and while the basic constraints can be derived with significantly fewer samples, this large number assures more robust constraints on the derived parameter ω when we use importance sampling in order to adjust for the change in prior density [147].

5.2 Observational constraints

Turning first to the constraints on the basic parameter set, from Figure 5.2 we note the overall consistency of our results with the current observational picture (see for example Ref. [16] and a work by two of the current authors Ref. [149]), finding the 99% marginalized probability regions to be

$$\begin{aligned} 0.021 < \Omega_{\rm B} h^2 < 0.027, \quad & 0.10 < \Omega_{\rm C} h^2 < 0.15\,, \\ 61 < H_0 < 80, \quad & 0.57 < \mathcal{Z} < 0.97\,, \\ 0.92 < n_{\rm S} < 1.07, \quad & 19 < A_{\rm S} < 33\,. \end{aligned} \tag{5.7}$$

Note that part of our allowed region lies outside the priors assumed by Nagata et al. [133]. As usual for joint analyses of CMB and galaxy power spectrum data, it is unnecessary to impose a further constraint on H_0.

The primary focus of our study has been to derive constraints on the JBD parameter for which, from the outset, we have expected only to find a one-sided bound; the situation can only become more interesting when both the angular diameter distance and the recombination history become much better probed by the CMB. This expectation is indeed confirmed by the data, as shown in Figure 5.3 in which we display the region of highest posterior density. The lower panel detailing the posterior constraint on ω has been obtained by importance sampling to correct for the change in prior density when changing parameters from $\ln\xi$ to ω (we note that the mean likelihood of the binned posterior obtained from sampling $\ln\xi$ performs well for putting a bound on ω, demonstrating less sensitivity to the details of the prior density).

We obtain marginalized probability upper bound, as the main result of this analysis, to be

$$\begin{aligned} \ln\xi \; &< \; -6.2, \quad 95\%, \\ \ln\xi \; &< \; -5.7, \quad 99\%. \end{aligned} \tag{5.8}$$

The corresponding marginalized probability lower bounds on the JBD parameter are found to be

$$\omega \; > \; 120, \quad 95\%,$$

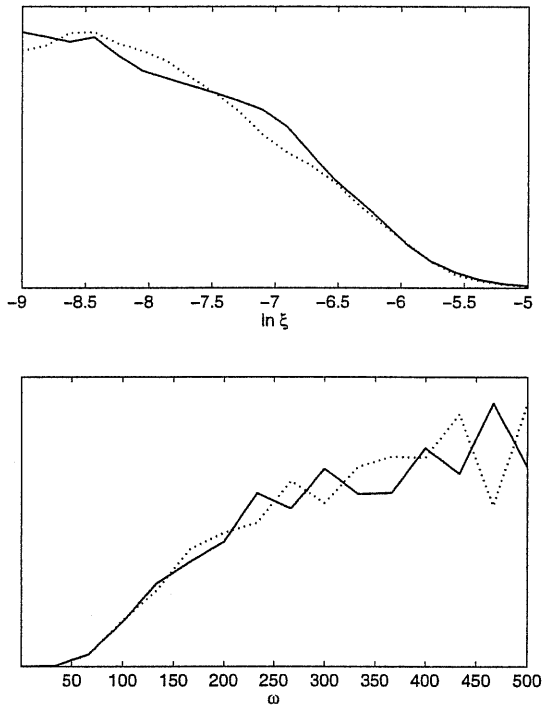

Figure 5.3: Marginalized 1D posterior distributions (solid lines) on the JBD parameter $\ln\xi$ (upper panel). Also displayed are the derived importance sampled constraints (correcting for the change in prior density) on the more familiar ω (lower panel, no smoothing). We obtain a 95% marginalized probability bound of $\ln\xi > -6.2$, corresponding to a bound on the JBD parameter $\omega > 120$.

$$\omega > 80, \quad 99\%. \tag{5.9}$$

This bound is nicely consistent with the expectation for WMAP given by the Fisher matrix analysis of Ref. [132].

We report in Figure 5.4 the 2D posterior constraints in the $\ln\xi$–H_0 plane, in order to demonstrate the degeneracy and covariance between these two parameters. In a more refined analysis, one could replace H_0 with the dimensionless parameter r_s/D_A more appropriate to the study of the CMB, where r_s is the sound horizon at recombination and D_A is the angular diameter distance to the last-scattering surface [150]. Finally, in Figure 5.5 we display two models, our best-fit ΛCDM model with parameters $\theta\equiv\{\Omega_B h^2, \Omega_C h^2, H_0, \mathcal{Z}, n_S, 10^{10}A_S, \omega\}= \{0.023, 0.12, 66,\ 0.79, 0.96, 23.2, \infty\}$, and a best-fit JBD model with parameters $\theta= \{0.024, 0.13, 79, 0.80, 1.03, 24, 70\}$, in order to illustrate how the observables change at finite ω. Here the JBD model lies in the vicinity of the contour

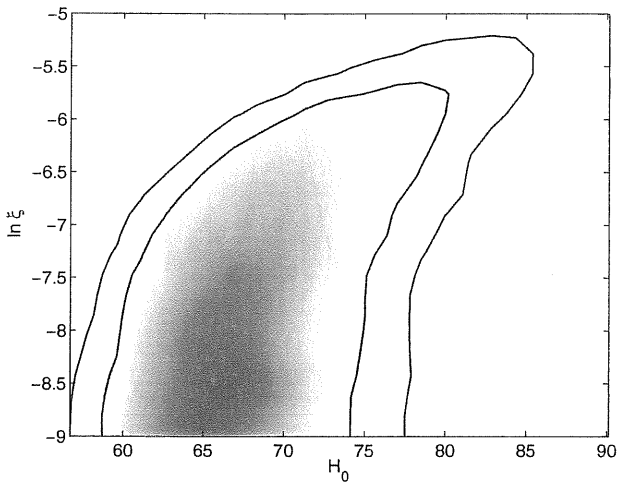

Figure 5.4: Marginalized 2D posterior distribution in the $\ln\xi$–H_0 plane. The solid lines enclose 95% and 99% of the probability. Under this parametrization there is clearly a geometrical degeneracy.

enclosing 99% of the posterior probability distribution and was selected by running a short Monte Carlo exploration at fixed $\omega = 70$. Note that although in principle the parameter $\ln\xi$ could be extended to $-\infty$, whereby the bulk of the parameter space would be composed of the ΛCDM model, in practice it is reasonable to adjust the lower cutoff to the point where the likelihood function loses sensitivity to the variation of $\ln\xi$ so that the Brans–Dicke model alone is explored by the MCMC. Consequently, the probability contours can reasonably be interpreted to describe the most credible region of the Brans–Dicke model parameter space.

Our current analysis leaves the bias parameter free, and so constrains only the shape of the matter power spectrum. We note however that the JBD model has a significantly higher amplitude, indeed requiring a modest antibias $b \simeq 0.98$, which at least in part is due to the more rapid perturbation growth ($\delta \propto a^{1+1/\omega}$ during matter domination [131]) in the JBD theory. For comparison the ΛCDM model has a best-fit bias $b = 1.2$. This suggests that precision measures of the present-day matter spectrum amplitude, as for instance may become available via gravitational lensing, could significantly tighten constraints. We also note that there is a shift in the location of the baryon oscillations in the matter power spectrum as compared to the ΛCDM model; these are mostly erased by the 2dF window

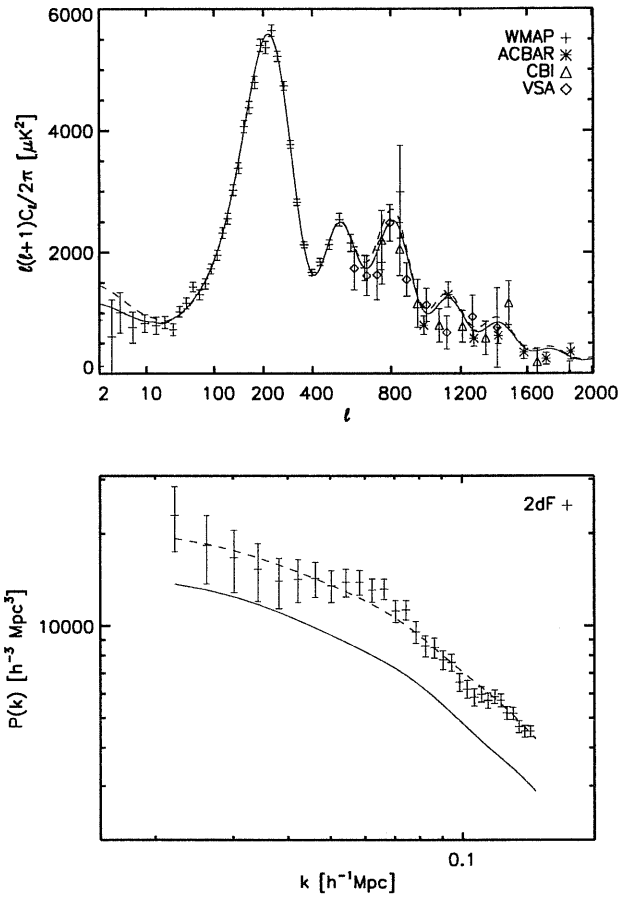

Figure 5.5: A comparison between a ΛCDM model (solid line) and a JBD ΛCDM model with $\omega = 70$ (dashed line). The data are the 2dF galaxy power spectrum and the models the matter power spectrum convolved with the 2dF window functions, and whose overall amplitude is left as a free parameter. Detailed parameters are given in the text.

function,[1] but future high-precision measurements of those may also assist in constraining ω.

We have carried out the same analysis including also the data from VSA, CBI and ACBAR in the multipole range $600 < \ell < 2000$. This high-ℓ data leads to a slightly tighter bound on the Brans–Dicke parameter, $\ln \xi < -6.4$ corresponding to $\omega > 177$ at 95% marginalized probability. However, at the same time inclusion of this new data leads to an unexpectedly large shift in the spectral index, to $0.90 < n_S < 1.00$ at 95% marginalized

[1] Our analysis used 2dF data from Percival et al. [143], preceding the more recent 2dF data analysis which shows evidence of baryon oscillations [19]. We would not expect inclusion of these data to significantly change our results.

probability, so that the Harrison–Zel'dovich spectrum is only just included (this statement remains true in the general relativity limit). Whether this points to some emerging tension in the combined dataset, a harmless statistical fluctuation, or a hint of the breaking of scale-invariance, can be addressed only in the light of the next round of CMB observations. While our constraint on $\ln \xi$ marginalizes over n_S, in the interests of quoting a robust bound we have given as our main result the weaker limit obtained without including the high-ℓ data.

Our ultimate constraint $\omega > 120$ can be compared with that of Nagata et al. [133], who quote results corresponding to $\omega > 1000$ at two-sigma and $\omega > 50$ at four-sigma. The former constraint is much stronger than projected in Ref. [132], and stronger than one would expect from a naïve assessment that the corrections to observables should be of order $1/\omega$. If we plotted a model with $\omega = 1000$ in our Figure 5.5, it would lie practically on top of the ΛCDM model. However their latter constraint is in reasonable agreement with ours, and they do highlight that it is this constraint which corresponds to a sharp ridge of deteriorating chi-squared in their analysis, indicating that their constraint should conservatively be taken as $\omega > 50$.

5.3 Lensing signal in JBD models - preliminary

The strategy for obtaining the lensed spectra in the JBD models closely follows the one described in detail for the Quintessence case. However, in the previously considered scenario of dark energy with a (w_0, w_∞) parametrization, the observed alleviation of the degeneracy on the latter parameter was an intuitive consequence of the inclusion of the lensing effect, since we expect the associated observables to be mostly sensitive to the $z \simeq 1$ region, where w_∞ actually plays the most important role in assessing the dark energy behavior. On the other hand, in the present case it is less obvious to quantify *a priori* the benefit of taking into account the lensing contribution (and the BB modes spectrum in particular) since the additional parameter of this theory, ω_{JBD}, is constant in time. Nonetheless, the trajectory of the field is influenced by the coupling parameter at late redshifts, around the onset of the dark energy domination, indicated in Fig. 5.1, so that we can expect a good

sensitivity of the lensed spectra to ω_{JBD} as well.

The inclusion of the lensing effect is *per se* an important result since it leads to an improvement of the reliability of any CMB-based analysis. Moreover, a simple plot of the temperature and polarization spectra with fixed primordial normalization, in the same fashion of what has been done in the previous Chapter for the SUGRA and IPL models, shows that the amplitude of the BB modes spectrum is visibly sensitive to a change in the $\omega_{\rm JBD}$ parameter even well within the range of allowed values established by our work described above. We present the results here (with the conceptually important, but numerically harmless, remark that the anisotropic stress source has not been considered yet; a visual justification of this statement is given in Fig. 5.9, whereas the issue will be treated with greater detail in the next Chapter) for three models with ω_{JBD} respectively equal to 100, 200 and 10^5: the first is basically excluded at the 95% confidence level by our analysis, while the second is inside the allowed parameter space and the last one is meant to recover the ordinary General Relativity case and thus resembles an ordinary ΛCDM model.

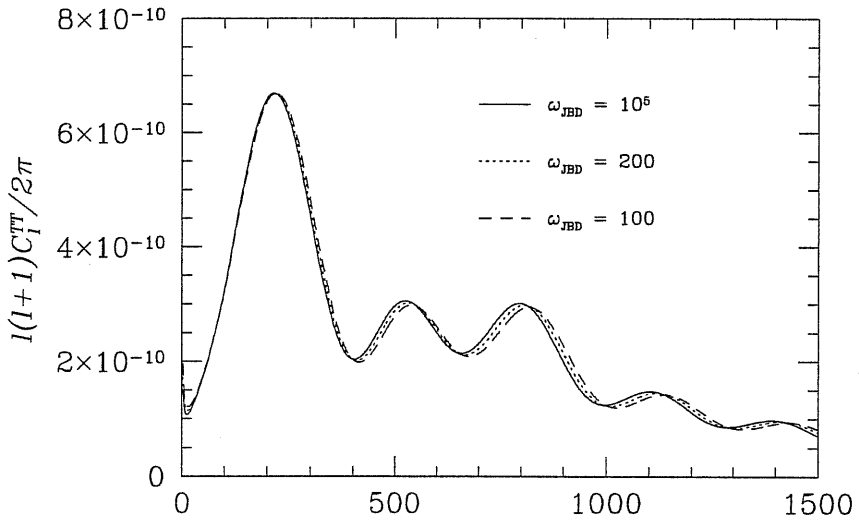

Figure 5.6: Temperature power spectra for three JBD models.

A naive estimation of how much the different lensed power spectra are sensitive to

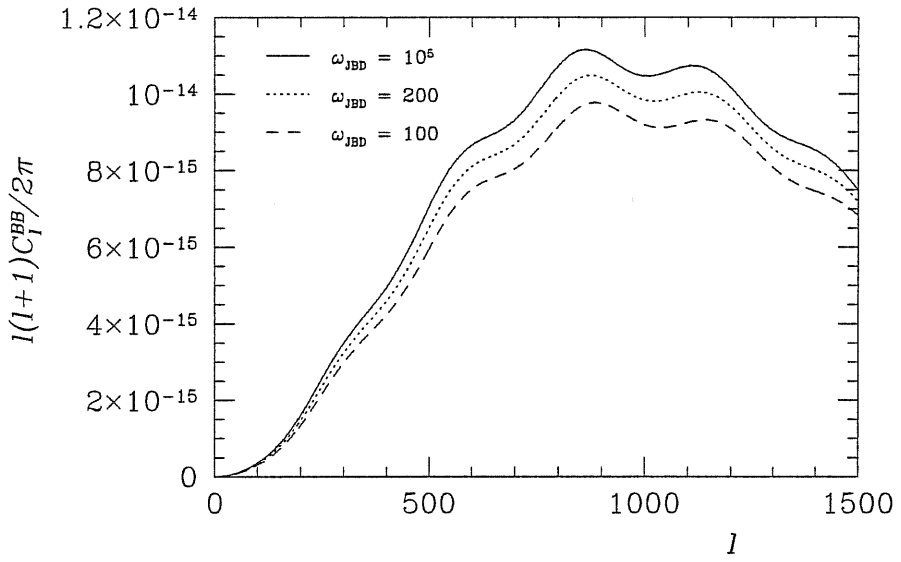

Figure 5.7: B-type polarization power spectra for the same JBD models as above.

the variation of the ω_{JBD} parameter can be obtained, as already noticed for the ordinary Quintessence scenarios, evaluating the "weighted derivative" of the TT, EE and BB spectra with respect to it; we want to measure

$$\frac{C^{XX}(\omega^{+}_{\rm JBD}) - C^{XX}(\omega^{-}_{\rm JBD})}{C^{XX}(\omega^{\rm ref}_{\rm JBD})}, \tag{5.10}$$

where again XX runs over the possible spectra and the variation of $\omega_{\rm JBD}$ are chosen to be of the order of 5%. The plot that we present here is for $\omega_{\rm JBD} = 200$, and shows that in this case (with respect to the Quintessence one) the EE modes spectrum play a larger role (with the caveats about the binning procedure which we have already pointed out), while the BB modes contribution is still significant but slightly smaller, and comparable to that of the temperature spectrum. However, the effect on the structure of the Fisher matrix comes from the combination of the four derivatives, and, as indeed verified in the previous Chapter, a plot like this can be only be regarded as an order of magnitude check.

As a further comment, let us mention that the effect of the coupling parameter can be read as a time variation of the effective strength of the gravitational constant, G,

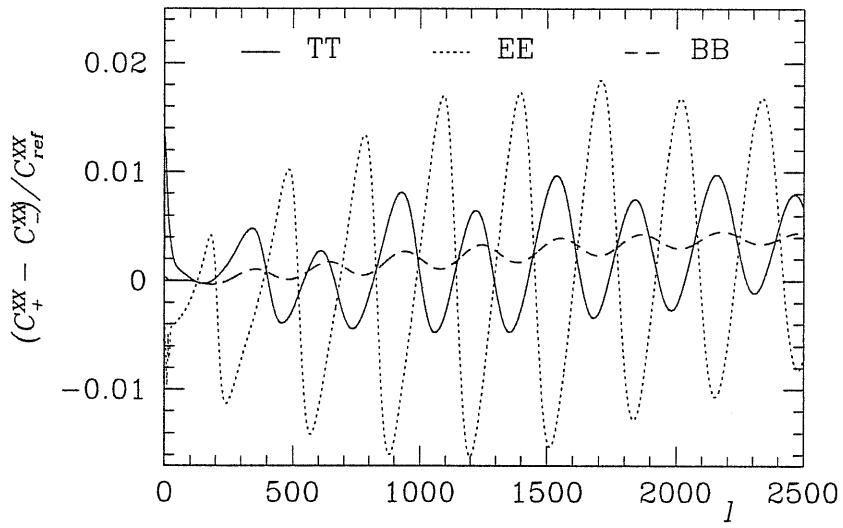

Figure 5.8: The weighted variation of the TT, EE and BB power spectra for the $\omega_{\rm JBD} = 200$ model in response to a double-sided 5% variation of the parameter.

which corresponds to the function 1/F with the notation convention

$$f(\Phi, R) = F(\Phi)R. \tag{5.11}$$

Therefore, as anticipated in Chap. 3, the main effect of the field is a change in the Hubble parameter with respect to ordinary cosmology

$$H \rightarrow H(new) = \frac{F_0}{F}, \tag{5.12}$$

influencing the distance measurements since

$$d(z) = c \int_0^z \frac{dz'}{H(z')}. \tag{5.13}$$

Such a behaviour of the Hubble parameter may be reproduced by a ad-hoc dark energy model. As a result, in order to break this degeneracy between dark energy and modified gravity, any observation revealing the presence of anisotropic stress would be extremely important, since it is known that the anisotropic stress vanishes for the ordinary Quintessence case. The CMB lensing may not be suitable to this task, since the anisotropic stress is

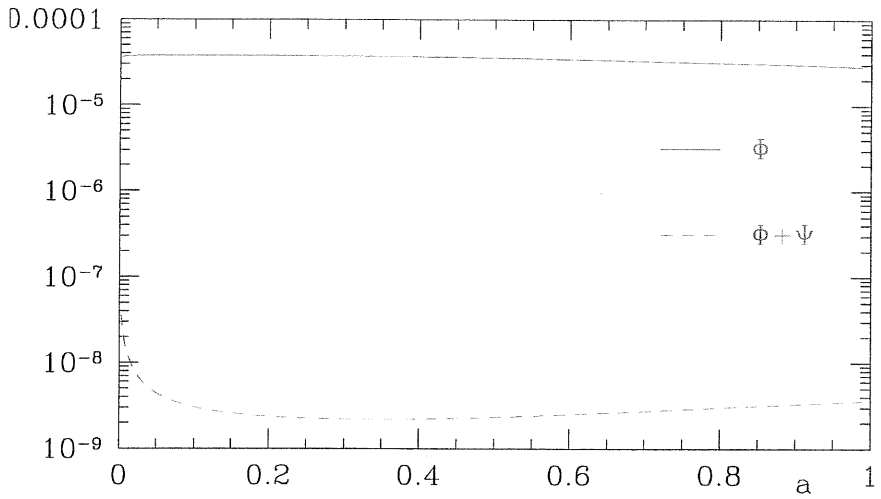

Figure 5.9: A comparison between the gravitational potential Φ and the anisotropic stress $\Xi = \Psi + \Phi$ on large scales, for $\omega_{JBD} = 200$, showing that for this model the contribution of the latter can be as a first approximation neglected.

small in such model and it only appears in the lensed spectra as a small correction to the gravitational potential. Still, the proper account of this degree of freedom in the integration of the equation of motion is in order in the perspective of finding observables capable to discriminate between possible explanation of the cosmic acceleration.

5.4 Final remarks

This discussion, and the plots above, show that the inclusion of the lensing signal in the numerical treatment of this model may help significantly in tightening the constraints on the Jordan-Brans-Dicke parameter, while on the other hand the contribution of the single BB modes power spectrum may be expected to be somehow less remarkable in the present case than it was for the Quintessence case.

The cosmological constraint obtained from the combination of the WMAP 1st year and other CMB datasets with observations from large-scale-structure, $\omega > 120$ at the 95% confidence

level, is destined to improve significantly with a possible reconsideration of the WMAP 3-year results and of new structure formation data. However, before performing this kind of analysis, our aim is to perfect our estimate of the lensed spectra in this scenario. This is part of the work in progress which we describe in the next Chapter, whose main objective are a comprehensive treatment of the anisotropic stress and the extension of our code to nonlinear matter power spectra, which is not contemplated in the present formulation of the lensing routine.

Chapter 6

Work in progress

In this Chapter we want to give a brief account of the principal lines of investigation that we are following in relation to the work previously described.
There are two main issues that we'll treat here: the anisotropic stress, which we have already introduced as a feature of NMC and JBD models, and the impact of nonlinear evolution on the determination of the lensed power spectra, together with a proposed strategy for including it in our investigation.

6.1 Anisotropic stress

The anisotropic stress at the linear level of perturbation theory is an index of whether the modification of the metric with respect to the FRW background change in different directions. This is intuitive recalling its definition from Chap. 3:

$$\tilde{T}^i_j = (p + \delta p)\delta^i_j + p\Pi^i_j \,, \tag{6.1}$$

where it is defined as the scalar part Π of Π^i_j. Therefore, it vanishes unless the pressure of the considered fluids is direction-dependent. This cannot happen for perfect fluids, such as the ordinary matter, radiation and Cosmological Constant components with $p \propto \rho$, and cannot happen for a minimally coupled scalar field as well, since the latter is (non-perturbatively) equivalent to a perfect fluid [152]. Neutrinos are the only species that can have a (decaying) anisotropic stress in these cosmological scenarios (*i.e.* [153]. As a result, the importance of

this variable basically relies in the fact that an indication of non-null anisotropic stress is an indication of gravity modifications.

The DEfast code has been modified in order to include this variable in the perturbations equations; since it is gauge-invariant [95] it can be straightforwardly obtained in the Newtonian gauge (while the code use the sinchronous one, A = B = 0 in our notation) as

$$k^2(\Phi + \Psi) = 8\pi G a^2 p \Pi \tag{6.2}$$

where p is the average pressure of the unperturbed fluid. In our numerical simulations by now we have only used adiabatic initial conditions, in which the primordial excitations of the two gravitational potentials are proportional to each other.

It is now clear why we have often talked interchangeably of anisotropic stress and our variable Ξ defined in Eq. (3.58):

$$\Xi = \Phi + \Psi = \frac{8\pi G a^2 p \Pi}{k^2}, \tag{6.3}$$

which is the one that we usually plot for immediate comparison with the gravitational potential Φ. The expression of Ξ in NMC theories

$$\Xi = -\frac{\delta F}{F} = -\left(\frac{\partial f}{\partial R}\right)^{-1}\left[\frac{\partial^2 f}{\partial\phi\partial R}\delta\phi + \frac{\partial^2 f}{\partial R^2}\delta R\right] \tag{6.4}$$

gives mathematical support to our theoretical interpretation, since in ordinary cosmology $\delta\phi$ and δR, which are the source for the anisotropic stress, both vanish. From the above expression we can also understand why this variable is small in the JBD model treated in the previous Chapter; although the investigation of the second term involving δR is difficult, we have seen that the theory is equivalent to a non-minimally coupled scalar field case with the ordinary $f(R) = R$ term, and we know that the fluctuations of the field for the equivalent model are small, due to the quasi-massless nature of the Quintessence field (*i.e.* [80]).

A more interesting case may be constituted by NMC models more general than the one introduced in Chap. 3, where the two terms in the above equation are both different from zero and the second is potentially large according to the model; this would allow to achieve a prediction for the anisotropic stress the most popular models of modified gravity, such as the Dvali-Gabadadze-Porrati model [154] and the $f(R) \propto R^n$ (*i.e.* [155] and references therein), which have been receiving increasing attention in the recent years.

6.2 Non-linear evolution

The inclusion of nonlinear evolution in our code is one of our primary targets, and goes together with the issue of testing the validity of approximating the deflection angle (or, equivalently, the lensing potential) as a Gaussian field, on which we have based our numerical analysis.

The basic idea is that in the late stage of cosmic evolution, some of the scales which are relevant for the birth of the lensing effect start to enter the nonlinear regime. This problem is less marked for the CMB lensing than it is for the cosmic shear ([33]), since, as we have seen, most of the lensing signal in our case comes from large scales (the peak of the lensing potential power spectrum is at $l \simeq 60$), where the impact of nonlinearity is still quite limited. This can be appreciated from the beautiful plot of Ref. [33], that we report here in Fig. 6.1, which shows the contribution of different wavenumbers to the lensing potential power spectrum, revealing that the largest part comes from scales $10^{-3} < k < 0.1$ Mpc and that the importance of scales $k > 0.1$ Mpc is very limited.

However, even if for the temperature lensed power spectrum the forecast correction due to nonlinear evolution is $< 0.2\%$ up to scales $l \simeq 2000$ ([33]), which include the entire range of our Fisher matrix simulations, for example, on smaller scales the effect can reach the percent level, and thus will be important for those small-sky CMB experiments which can reach very high angular resolution (*i.e.* [120, 156]). Moreover, simulations of lensed CMB have showed that the effect of nonlinearities for the BB modes is indeed more significant [33], of the order of 6% percent on all scales and possibly significantly larger beyond the lensing peak at $l \simeq 1000$; this may be due to the fact that the BB modes are obtained convolving the lensing potential power spectrum with the one of the primordial EE modes, which possess little power on large scales, so that the BB spectrum is almost white for l smaller than a few hundreds and presents its typical oscillation features only at larger multipoles. This latter effect is likely to be even more relevant in modified-gravity theories, where the transition from linear to nonlinear regime may happen earlier with respect to the ΛCDM model, and therefore is crucial for our correct estimation of the impact of lensing measurements in this kind of models.

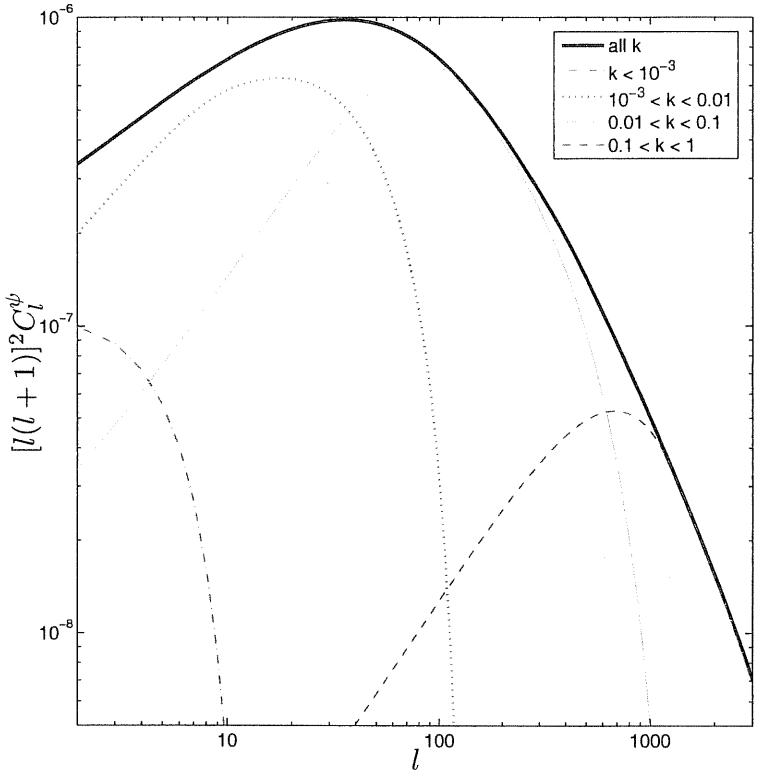

Figure 6.1: Different wavenumbers contributions to the power spectrum of the lensing potential, for a ΛCDM cosmological model. Note that the plot is logarithmic: the impact of the small scales (in magenta, dashed) is very limited.

The issue of the Gaussian approximation is intimately linked to the one depicted above. The non-Gaussian nature of the lensing signal does not depend on nonlinearity exclusively, since the convolution of two Gaussian fields (the unlensed CMB and the lensing potential power spectra) is anyway non Gaussian. However, if the Gaussianity of the lensing potential itself is compromised, we may expect a non-negligible correction to the non-Gaussianity of the lensed spectra as well. However, it was showed in Ref. [32]) that this approximation is harmless, if the deflection-angle variance is small, even if the deflection angle is not Gaussian; therefore we won't any more discuss possible repercussions of nonlinearities in non-Gaussianity, contenting ourselves with the conservative treatment of non-Gaussianity of the BB modes described in Chap. 4.

6.2.1 Proposed treatment

The present way the DEfast code deals with nonlinearities is using the analytical formula of Peacock and Dodds [157], providing a correction to the linear growth function of the perturbations. However, later N-body simulations, especially in connection with the attempt of constraining cosmological parameters through lensing form large-scale structure, have showed that this approximation lacks of precision (*i.e.* [158]). A significant improvement to their fitting formula was given, following the N-body simulations of the Virgo Consortium, in [159] who based their analysis on the *halo model* [160, 161, 162], whose basic idea is to represent the density field as a distribution of isolated halos, describing large-scale correlations as clustering of different halos and small-scale one as clustering within a single halo. Within this formalism the total nonlinear power spectrum $P_{\rm NL}$ is expressed as the sum of two terms

$$P_{\rm NL}(k) = P_Q(k) + P_H(k), \tag{6.5}$$

the first of which accounts for interactions on large scales and the second for those on small scales.

Their work will be considered as our starting point. They use initial power-law matter power spectrum, which is suitable for our purposes, and compiled a large library of simulations for different cosmological models. The most important quantity that distinguishes the models is, as expected, the scale at which the matter perturbations turn nonlinear, $k_{\rm NL}$, or the variance of the linear density field (the latter is indicated as Δ^2_L), defined as a function of the expansion value and a Gaussian filtering of radius R to be

$$\sigma^2(R,a) = \int \Delta^2_L(k,a) e^{(-k^2R^2)} \frac{dk}{k}. \tag{6.6}$$

This allows to give an intuitive physical meaning to the non linear wavenumber $k_{\rm NL}$ through the relation $\sigma^2(k_{\rm NL}^{-1}, a) = 1$. Two further parameters of the halo model are the *effective spectral index* $n_{\rm eff}$ and the curvature parameter C, which refine the dependence of σ on the filter radius (roughly corresponding to a first and second logarithmic derivative).

Given this parameterization, the authors of Ref. [159] provide in their appendix C an accurate (up to a few percent level for a ΛCDM model) fitting function of both the terms of

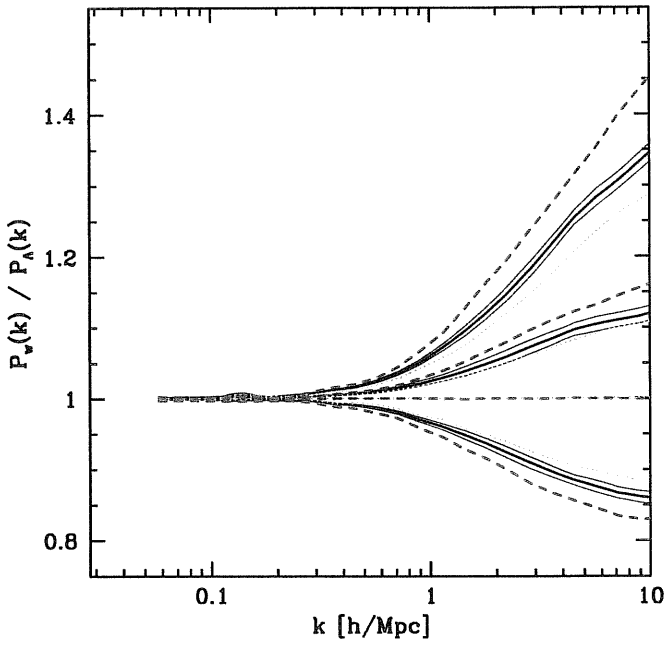

Figure 6.2: Fractional effect of w on the non-linear mass power spectrum, at fixed linear theory power. The thick lines of a given color/type show, from top to bottom, $w = -0.5, -0.75, -1.5$, all relative to $w = -1$. The black, solid line is for $\Omega_m = 0.281$, with red, dashed (green, dotted) showing $\Omega_m = 0.211$ (0.351). Thin black lines show rms statistical error bands. From [163].

the nonlinear power spectrum, together with a publicly available code for generating $\sigma, n_{\rm eff}$ and C, given the cosmological parameters of the model under examination.
The inclusion of this procedure in DEfast should provide us with $P_{\rm NL}(k)$ for the concordance ΛCDM model. The next step is the generalization of their formula to dark energy cosmology, which has been provided for the constant equation-of-state case by Ref. [163]. They have used results of [159] as well, and have built a code that outputs the relative correction of the nonlinear power spectrum $P_{\rm NL}(k)(w)$ with respect to $P_{\rm NL}(k)(w = -1)$. Their plot of this correction, output at $z = 0$, is reported here in Fig. 6.2.

A similar prescription, but including the two-parameters description of dark energy (w_0, w_∞) which is our primary objective, has been subsequently given in Ref. [164], where however the possible range of cosmological parameters appears more limited; on the other hand, the claimed precision of nonlinear power spectra is extremely interesting, around 1%

for models within the allowed range.

The three steps described above should allow us to include the effect of nonlinear evolution in our code at least for the case of the Quintessence models such as the ones exploited in Chap. 4. The analogue treatment for modified gravity cases, which may be even more interesting since they may highlight the presence of a large anisotropic stress component, is among out objectives but is for the time being limited by the absence of appropriate cosmological N-body simulations for these models.

Chapter 7

Conclusions and future prospects

The weak lensing in cosmology is one of the most important tools to investigate the mechanics of the dark cosmological component, which represents almost the 96% of the cosmic budget according to the most recent measurements [16]. The candidates which have been proposed for explaining the dark energy are suitably described in a cosmological context which is generalized with respect to the ordinary one, admitting dark matter-energy couplings as well as generalized theories of gravity.

For these classes of theories, a systematic treatment of the weak lensing process lacked in literature and our work aimed at filling this gap. We considered a Lagrangian where the gravitational sector is made of a function which depends arbitrarily on the Ricci scalar as well as on a scalar field; beyond ordinary Quintessence models, the most general scalar-tensor theory of gravity, as well as any dependence on the Ricci scalar without a scalar field, can be described in full generality in this framework.

Starting from the equation describing the geodesic deviation, we have derived the generalized expressions for distortion tensor and projected lensing potential, tracking the effects due to the background evolution as well as the fluctuating components behavior; contact with the cosmological observables was established through the study of the generalized Poisson equation.

We have exploited the potentiality of the CMB physics, with particular regard to the BB modes of the polarization, which are sourced by gravitational lensing of cosmic structures,

in order to constrain the dynamics of scalar-field dark energy at the epoch of equivalence with the non-relativistic matter component. We focus on the amplitude of the BB angular power spectrum; mapping techniques isolating the lensing power [116] might also be considered for extracting information about the cosmic expansion rate redshift behavior. We have shown how the lensing phenomenology, being directly linked to the cosmic dynamics and linear perturbation growth rate when the dark energy enters the cosmic picture, presents an enhanced sensitivity to the value of the dark energy equation of state at the corresponding epoch. Such feature breaks the so called projection degeneracy, affecting the TT, TE and EE angular power spectra, preventing the possibility of constraining the redshift dependence of the dark energy equation of state from CMB. Analogous studies have been focused on the non-Gaussian power injection into the anisotropy statistics of order larger than the second [127, 126]. Indeed, the outcome of these studies is consistent with the present one, i.e. the lensing power in the CMB bispectrum, the harmonic space analogue to the three point correlation function, presents a remarkable sensitivity to the dark energy equation of state at the onset of acceleration. Thus the present study is related to those, although on a completely different domain. Since we still don't know where the impact of instrumental systematics and foregrounds will be the strongest in a real experiment attempting to detect the CMB lensing signal, it is important to carry out the analysis on all CMB lensing observables. Moreover, the BB modes in CMB polarization at the arcminute scale are the explicit target of forthcoming CMB probes (see *i.e.* [120], [165] and references therein).
We have then quantified the scientific impact of our result in terms of the achievable precision on the cosmological parameters, modeling our assumptions on the specifics of forthcoming probes of CMB polarization, exploring a large part of the allowed dark energy parameters space. The results are strongly encouraging, predicting an accuracy of order 10% on the present value of the dark energy equation of state, and a somehow weaker limit on its first derivative with respect to the scale factor, but with an important indication of better results with increasing dark energy dynamics. This result is comparable with the one quoted in [52], where the authors take into account SNIa data and CMB physics but do not include BB modes into the analysis and with the forecasts in [128] for Quintessence models, where the authors consider SNIa data and weak lensing of background galaxies. In particular, the

prediction of a smaller uncertainty for high dark energy dynamics is reproduced also for the observable considered here.

The predictions of our analysis have also been confirmed by recent works in the same spirit [123, 124], which evaluated the impact of the lensed CMB in combination with other cosmological observables.

We have started an analogous study for scalar-tensor gravity scenarios, aiming at having a solid description of the CMB lensing in these models by the time observations accurate enough for discriminating between dark energy and modified gravity will be available; the study of how to include for nonlinear evolution in our calculations goes in the same direction of enhancing the degree of accuracy of our predictions. Other open problems, such as a better account of the non-Gaussianity arising from the lensing recombination of different wavelengths which avoids the degradation of the quality of the statistical data, and a deeper understanding of the foregrounds for the CMB polarization spectra, may as well help in further improving the reliability of the method.

Our main conclusion is that the work presented here indeed confirmed the weak lensing of the CMB as a potentially powerful probe of the dark energy dynamics, and that our study fits perfectly within the perspectives for the future of the dark energy investigations, both on the theoretical and the experimental side.

Bibliography

[1] Hubble, E. *"A relation between distance and radial velocity among extra-galactic nebulæ"*, *Proc. Natl. Acad. Sci. USA* **15**, 168 (1929).

[2] Freedman W.L., *"The Hubble constant and the expansion age of the universe"*, *Phys. Rep.* **333**, 13, (2000).

[3] Freedman W.L. *et al.* , *"Final results from the Hubble Space Telescope Key Project to measure the Hubble constant"*, *Astrophys. J.* **553**, 47 (2001).

[4] Sandage, A., Tammann, G. A. and Saha, A., *"The time scale test for Ω: the inverse Hubble Constant compared with the age of the Universe"*, *Phys. Rep.* **307**, 4 (1998).

[5] Zwicky, F. *"Spectral displacement of extra galactic nebulae"*, *Helv. Phys. Acta* ***6***, *110 (1933).*

[6] Bahcall, N. A. and Fan, X., "The most massive distant clusters: Determining Ω and σ_8", Astrophys. J. **504**, *1 (1998).*

[7] Mohr, J. J., Mathiesen, B. and Evrard, A. E., "Properties of the intracluster medium in an ensemble of nearby galaxy clusters", Astrophys. J. **553**, *545 (2000).*

[8] White, S. D. M., et al. , "The Baryon content of galaxy clusters: A challenge to cosmological orthodoxy", Nature **429**, *638 (2004).*

[9] Peacock, J. A., and Dodds, S. J., "Reconstructing the linear power spectrum of cosmological mass fluctuations", MNRAS **267**, *1020 (1994).*

[10] *Ellis G. F. R., "Issues in the philosophy of Cosmology", to appear in "Handbook in Philosophy of Physics", astro-ph/0602280.*

[11] *Padmanabhan T., "Cosmological constant - the weight of the vacuum", Phys. Rep.* ***380****, 235, 2003.*

[12] *Hagiwara, K. et al. , "Global cosmological parameters:* H_0, Ω_M *and* Λ*", Phys. Rev. D* ***66****, 010001-1 (2002).*

[13] *Eidelman, S. et al. , "The cosmological parameters", Phys. Lett. B* ***592****, 1(2004).*

[14] *Dodelson, S. and Knox, L., "Dark Energy and the CMB", Phys. Rev. Lett.* ***84****, 3523 (2000).*

[15] *Knox, L., "On Precision Measurement of the Mean Curvature," Phys. Rev. D* **73**, *023503 (2006).*

[16] *Spergel, D. N. et al. , "Wilkinson Microwave Anisotropy Probe (WMAP) Three Year Results: Implications for Cosmology", astro-ph/0603449.*

[17] *Fukugita, M., Hogan, C. J. and Peebles, J. P. E. , "The Cosmic baryon budget", Astrophys. J.* **503**, *518 (1998).*

[18] *Spergel, D.N. et al. , "First-year Wilkinson Microwave Anisotropy Probe (WMAP) observations: determination of cosmological parameters", Astrophys. J. Suppl. Series* ***148****, 175 (2003).*

[19] *Cole, S. et al. , [The 2dFGRS Collaboration], "The 2dF Galaxy Redshift Survey: Power-spectrum analysis of the final dataset and cosmological implications," MNRAS* **362**, *505 (2005).*

[20] *Tegmark M. et al. , "The three-dimensional power spectrum of galaxies from the Sloan Digital Sky Survey", Astrophys. J.* ***606****, 702 (2004).*

[21] *Eiseinstein, D.J. et al. , "Detection of the Baryon Acoustic Peak in the Large-Scale Correlation Function of SDSS Luminous Red Galaxies," Astrophys. J.* **633**, *560 (2005).*

[22] Guth, A. H., *"The Inflationary Universe: A Possible Solution To The Horizon And Flatness Problems"*, Phys. Rev. D **23**, 347 (1981).

[23] Albrecht, A. and Steinhardt, P. J. *"Cosmology For Grand Unified Theories With Radiatively Induced Symmetry Breaking"*, Phys. Rev. Lett. **48**, 1220 (1982).

[24] Schmidt B. P. et al. [Supernova Search Team Collaboration], *"The High-Z Supernova Search: Measuring Cosmic Deceleration and Global Curvature of the Universe Using Type Ia Supernovae"*, Astrophys. J. **507**, 46 (1998).

[25] Riess A.G. et al. , *"Observational evidence from supernovæ for an accelerating universe and a Cosmological Constant"*, Astronom. J. **116**, 1009 (1998).

[26] Perlmutter S. et al. , *"Measurements of Ω and Λ from 42 High-Redshift Supernovæ"*, Astrophys. J. **517**, 565 (1999).

[27] Corasaniti P. S., *"The Impact of Cosmic Dust on Supernova cosmology"*, astro-ph/0603833.

[28] Riess A.G. et al. , *"Type Ia Supernova discoveries at $z > 1$ from the Hubble Space Telescope: evidence for past deceleration and constraints on dark energy evolution"*, Astrophys. J. **607**, 665 (2004).

[29] Filippenko, A. V. and Riess, A. G. *"Results from the High-Z Supernova Search Team"*, Phys. Rep. **307**, 31 (1998).

[30] Petters, A. O., Levine, H. and Wambsganss, J. *"Singularity Theory and Gravitational Lensing"*, Birkhäuser, Boston, 2001.

[31] Misner, C., Thorne, K. and Wheeler, J., *"Gravitation"*, W.H. Freeman and Co., San Francisco, 1973.

[32] Bartelmann M. and Schneider P., *"Weak gravitational lensing"*, Phys. Rep. **340**, 291 (2001).

[33] Lewis, A. and Challinor, A., *"Weak gravitational lensing of the CMB"*, Phys. Rep. **429**, 1 (2006).

[34] Schneider, P., Ehlers, J. and Falco, E. E., *"Gravitational Lenses"*, Springer (1992).

[35] Walsh, D., Carswell, R. F. and Weymann, R. J., *"0957+561 A,B: twin quasistellar objects or gravitational lens?"*, Nature **279**, 381 (1979).

[36] Kaiser, N., *"Weak lensing and Cosmology"*, Astrophys. J. **498**, 26 (1998).

[37] White, M. and Hu, W., *"A new algorithm for computing statistics of weak lensing by large-scale structure"*, Astrophys. J. **537**, 1 (2000).

[38] Metcalf, R. B. and Silk, J., *"Gravitational magnification of the Cosmic Microwave background"*, Astrophys. J. **489**, 1 (1997).

[39] Hu W., *"Weak Lensing of the CMB: a harmonic approach"*, Phys. Rev. D **62**, 043007 (2000).

[40] Silk, J., *"Cosmic black body radiation and galaxy formation"*, Astrophys. J. **151**, 459 (1968).

[41] Coles, P. and Lucchin, F. *"Cosmology: The origin and evolution of cosmic structure"*, Wiley (1995).

[42] Bennett C.L. et al. , *"Cosmic temperature fluctuations from two years of COBE differential microwave radiometers observations"*, Astrophys. J. **436**, 423 (1994).

[43] Penzias A.A. and Wilson R.W., *"A measurement of excess antenna temperature at 4080 Mc/s."*, Astrophys. J. **142**, 419 (1965).

[44] Acquaviva, V., Bartolo, N., Matarrese, S. and Riotto, A., *"Second-order Cosmological Perturbations from Inflation"*, Nucl. Phys. B **667**, 119 (2003).

[45] Maldacena, J. M., *"Non-Gaussian features of primordial fluctuations in single field inflationary models,"*, J. High Energy Phys. **0305**, 013 (2003).

[46] Bartolo N., Komatsu E., Matarrese S. and Riotto A., *"Non-Gaussianity from inflation: theory and observations"*, Phys. Rep. **402**, 103 (2004).

[47] Hu, W. and White, M. J., *"A CMB Polarization Primer"*, New Astron. **2**, 323 (1997).

[48] Zaldarriaga, M. and Seljak, U., *"An All-Sky Analysis Of Polarization In The Microwave Background"*, Phys. Rev. D **55**, *1830 (1997).*

[49] Kamionkowski, M., Kosowsky, A. and Stebbins, A., *"A probe of primordial gravity waves and vorticity"*, Phys. Rev. Lett. **78**, *2058 (1997).*

[50] Kolb, E. W. and Turner, M. S., *"The early Universe"*, Addison Wesley *(1990).*

[51] Refregier, A., *"Weak Gravitational Lensing By Large-Scale Structure"*, Ann. Rev. Astron. Astrophys. **41**, *645 (2003).*

[52] Yeche, C. et al. , *"Prospects for Dark Energy Evolution: a Frequentist Multi-Probe Approach,"*, astro-ph/0507170.

[53] Bernardeau, F., van Waerbeke, L. and Mellier, Y., *"Weak Lensing Statistics as a Probe of Omega and Power Spectrum,"*, Astron. Astrophys. **322**, *1 (1997).*

[54] Hu, W. and Tegmark, M., *"Weak Lensing: Prospects for Measuring Cosmological Parameters"*, Astrophys. J. **514**, *L65 (1999).*

[55] Jain, B. and Seljak, U., *"Cosmological Model Predictions for Weak Lensing: Linear and Nonlinear Regimes"*, Astrophys. J. **484** *(1997) 560.*

[56] Acquaviva, V., Baccigalupi, C. and Perrotta, F. *"Weak lensing in generalized gravity theories"*, Phys. Rev. D **70**, *023515 (2004).*

[57] Brans, C. and Dicke, R. H., *"Mach's principle and a relativistic theory of gravitation"*, Phys. Rev. **124**, *925 (1961).*

[58] Sahni, V. and Starobinsky, A. A., *" The Case for a positive cosmological Lambda term"*, International J. Mod. Phys. D **9**, *373 (2000).*

[59] Peebles, P. J. E. and Ratra, B., *" The Cosmological constant and dark energy"*, Rev. Mod. Phys. **75**, *599 (2003).*

[60] Wetterich, C., *"Cosmology And The Fate Of Dilatation Symmetry"*, Nucl. Phys. B **302**, *668 (1988).*

[61] Ratra, B. and Peebles, P. J. E., *"Cosmological Consequences Of A Rolling Homogeneous Scalar Field"*, Phys. Rev. D **37**, *3406 (1988).*

[62] Coble, K., Dodelson, S. and Frieman, J. A., *"Dynamical Lambda models of structure formation"*, Phys. Rev. D **55**, *1851 (1997)*

[63] Ferreira, P. G., and Joyce, M., *"Cosmology with a primordial scaling field"*, Phys. Rev. D **58**, *023503 (1998).*

[64] Masiero, A., Pietroni, M. and Rosati, F., *"SUSY QCD and quintessence"*, Phys. Rev. D **61**, *023504 (2000).*

[65] Brax, P. and Martin, J., *"The Robustness of quintessence"*, Phys. Rev. D **61**, *103502 (2000).*

[66] Liddle, A. R. and Scherrer, R. J., *"A Classification of scalar field potentials with cosmological scaling solutions"*, Phys. Rev. D **59**, *023509 (1999).*

[67] Steinhardt, P. J., Wang, L., and Zlatev, I., *"Cosmological tracking solutions"*, Phys. Rev. D **59**, *123504 (1999).*

[68] Doran, M., Lilley, M., Schwindt, J. and Wetterich, C., *"Quintessence and the separation of CMB peaks"*, Astrophys. J. **559**, *501 (2001).*

[69] Corasaniti, P. S. and Copeland, E. J., *"Constraining the quintessence equation of state with SnIa data and CMB peaks"*, Phys. Rev. D **65**, *043004 (2002).*

[70] Balbi, A., *et al.* , *"Constraints on flat cosmologies with tracking quintessence from cosmic microwave background observations"*, Astrophys. J. Lett. **547**, *L89 (2001).*

[71] Baccigalupi, C., *et al.* , *"What's behind acoustic peaks in the cosmic microwave background anisotropies"*, Phys. Rev. D **65**, *063520 (2002).*

[72] Caldwell, R. R., Doran, *et al.* , *"Early quintessence in light of WMAP"*, Astrophys. J. Lett. **591**, *L75 (2003).*

[73] Melchiorri, A., Mersini, L., Odman, C. J. and Trodden, M., *"The State of the dark energy equation of state"*, Phys. Rev. D **68**, *043509 (2003).*

[74] Wang, Y. and Tegmark, M., *"New dark energy constraints from supernovae, microwave background and galaxy clustering"*, Phys. Rev. Lett. **92**, *241302 (2004).*

[75] Carroll, S. M., *"Quintessence and the rest of the world"*, Phys. Rev. Lett. **81**, *3067 (1998).*

[76] Sahni, V. and Habib, S., *"Does inflationary particle production suggest Omega(m) less than 1? "*, Phys. Rev. Lett. **81**, *1766 (1998).*

[77] Chiba, T., *"Quintessence, the gravitational constant, and gravity"*, Phys. Rev. D **60**, *083508 (1999).*

[78] Uzan, J. P., *"Cosmological scaling solutions of nonminimally coupled scalar fields"*, Phys. Rev. D **59**, *123510 (1999).*

[79] Bartolo, N. and Pietroni, M., *"Scalar tensor gravity and quintessence"*, Phys. Rev. D **61**, *023518 (2000).*

[80] Perrotta, F., Baccigalupi, C. and Matarrese, S., *"Extended quintessence"*, Phys. Rev. D **61**, *023507 (2000).*

[81] Faraoni, V., *"Inflation and quintessence with nonminimal coupling"*, Phys. Rev. D **62**, *023504 (2000).*

[82] Baccigalupi, C., Matarrese, S. and Perrotta, F., *"Tracking extended quintessence"*, Phys. Rev. D **62**, *123510 (2000).*

[83] Esposito-Farese, G. and Polarski, D., *"Scalar tensor gravity in an accelerating universe"*, Phys. Rev. D **63**, *063504 (2001).*

[84] Riazuelo, A. and Uzan, J. P. *"Cosmological observations in scalar - tensor quintessence"*, Phys. Rev. D **66**, *023525 (2002).*

[85] *Torres, D. F., "Cosmological observations in scalar - tensor quintessence", Phys. Rev. D* **66**, *043522 (2002).*

[86] *Mukhanov V., Feldmann H. and Brandenberger R., "Theory of cosmological perturbations", Phys. Rep.* **215**, *203 (1992).*

[87] *Will, C. M., "The Confrontation between general relativity and experiment", Living Rev. Relativity* **4**, *4 (2001).*

[88] *Bertotti, B., Iess, L., and Tortora, P., "A test of general relativity using radio links with the Cassini spacecraft", Nature* **425**, *374 (2003).*

[89] *Perrotta, F. and Baccigalupi, C., "Early time perturbations behavior in scalar field cosmologies", Phys. Rev. D* **59**, *123508 (1999).*

[90] *Perrotta, F., Matarrese, S., Pietroni, M. and Schimd, C., "Nonlinear perturbations in scalar tensor cosmologies", Phys. Rev. D* **69**, *084004 (2004).*

[91] *Linder, E. V., "Probing gravitation, dark energy, and acceleration", Phys. Rev. D* **70**, *023511 (2004).*

[92] *Matarrese, S., Baccigalupi, C. and Perrotta, F. "Approaching lambda without fine - tuning", Phys. Rev. D* **70**, *061301 (2004).*

[93] *Pettorino, V., Baccigalupi, C., and Perrotta, F., "Scaling solutions in scalar-tensor cosmologies", JCAP* **0512** *003 (2005).*

[94] *Liddle, A.R., and Lyth D.H., "Cosmological inflation and large-scale structure", Cambridge University Press, Cambridge (2000).*

[95] *Kodama, H. and Sasaki, M., "Cosmological Perturbation theory", Prog. Theor. Phys. Suppl. 78, 1 (1984).*

[96] *Amendola, L., "Coupled quintessence", Phys. Rev. D* **62**, *043511 (2000).*

[97] *Amendola, L., Quercellini, C., Tocchini-Valentini, D. and Pasqui, A., "Constraints on the interaction and selfinteraction of dark energy from cosmic microwave background", Astrophys. J. Lett.* **583**, *L53 (2003).*

[98] Matarrese, S., Pietroni, M. and Schimd, C., *"Nonlinear gravitational clustering in scalar field cosmologies"*, J. Cosm. Astroparticle Phys. **08**, *005 (2003).*

[99] Amendola, L., *"Linear and non-linear perturbations in dark energy models"*, Phys. Rev. D **69** *103524 (2004).*

[100] Armendariz-Picon, C., Mukhanov, V. and Steinhardt, P. J., *"Essentials of k essence"*, Phys. Rev. D **63**, *103510 (2001).*

[101] Caldwell, R. R., *"A phantom menace? Cosmological consequences of a dark energy component with super-negative equation of state"*, Phys. Lett. B **545**, *23 (2002).*

[102] Malquarti, M., Copeland E. J. and Liddle, A. R., *"K-essence and the coincidence problem"*, Phys. Rev. D **68**, *023512 (2003).*

[103] Fujii, Y. and Maeda, K., *"The Scalar-Tensor Theory of Gravitation"*, Cambridge University Press *(2003).*

[104] Hwang, J., *"Cosmological perturbations in generalised gravity theories: formulation"*, Class. Quantum Grav. **7**, *1613 (1990)*

[105] Hwang, J., *"Perturbations of the Robertson-Walker space - Multicomponent sources and generalized gravity"*, Astrophys. J. **375**, *443 (1991).*

[106] Lue, A., Scoccimarro, R. and Starkman, G. D., *"Probing Newton's constant on vast scales: DGP gravity, cosmic acceleration and large scale structure"*, Phys. Rev. D **69**, *124015 (2004).*

[107] Acquaviva, V. and Baccigalupi, C. *"Dark energy records in lensed cosmic microwave background"*, astro-ph/0507644.

[108] Seljak U., and Zaldarriaga M., *"A line-of-sight integration approach to cosmic microwave background anisotropies"*, Astrophys. J. **469**, *437 (1996).*

[109] Perrotta, F. and Baccigalupi C., *"Early time perturbations behavior in scalar field cosmologies"*, Phys. Rev. D **59**, *123508 (1999).*

[110] Chevallier M. and Polarski D., *"Accelerating universes with scaling dark matter"*, Int. J. Mod. Phys. D **10**, 213 (2001).

[111] Linder E.V., *"Exploring the expansion history of the Universe"*, Phys. Rev. Lett. **90**, 091301 (2003).

[112] Zaldarriaga, M. and Seljak, U., *"Gravitational lensing effect on Cosmic Microwave Background polarization"*, Phys. Rev. D **58**, 023003 (1998).

[113] Ma, C. P., Caldwell, R. R., Bode, P. and Wang, L., *"The mass power spectrum in quintessence cosmological models"*, Astrophys. J. Lett. **521**, L1 (1999).

[114] Bartelmann M., Perrotta F. and Baccigalupi C., *"Halo concentrations and weak-lensing number counts in dark energy cosmologies"*, Astron. Astrophys. **396**, 21 (2002).

[115] Gold, B. *"Limits of dark energy measurements from CMB lensing-ISW-galaxy count correlations"*, Phys. Rev. D **71**, 063522 (2005)

[116] Hirata, C. and Seljak, U., *"Reconstruction of lensing from the cosmic microwave background polarization"*, Phys. Rev. D **68**, 083002 (2003).

[117] Smith, S., Challinor, A., and Rocha, G., *"What can be learned from the lensed cosmic microwave background b-mode polarization power spectrum?"*, Phys. Rev. D **73**, 023517 (2005).

[118] Lewis A., *"Lensed CMB simulation and parameter estimation"*, Phys. Rev. D **71**, 083008 (2005).

[119] Smith, K. M., Hu, W., and Kaplinghat, M., *"Weak lensing of the CMB: Sampling errors on B-modes"*, Phys. Rev. D **70**, 043002 (2004).

[120] Oxley, P. et al. 2004, *"The EBEX experiment"*, Earth Observing Sustem IX. Edited by William L. Barnes and James J. Butler, Proceedings of the SPIE, 5543, 320.

[121] http://bolo.berkeley.edu/polarbear/.

[122] Kaplinghat, M., Knox, L. and Song, Y., *"Determining neutrino mass from the CMB alone"*, Phys. Rev. Lett. **91**, *241301 (2003).*

[123] Smith, K. M., Hu, W. and Kaplinghat, M., *"Cosmological information from lensed CMB Power Spectra"*, astro-ph/0607315.

[124] Hu, W., Huterer, D. and Smith, K. M., *"Supernovæ, Lensed CMB and Dark Energy"*, astro-ph/0607316.

[125] Tegmark, M., *"CMB mapping experiments: A Designer's guide"*, Phys. Rev. D **56**, *4514 (1997).*

[126] Giovi, F., Baccigalupi, C., and Perrotta, F., *"Cosmic microwave background constraints on dark energy dynamics: Beyond the power spectrum analysis"*, Phys. Rev. D **71**, *103009 (2005).*

[127] Verde, L. and Spergel, D. N., *"Dark energy and cosmic microwave background bispectrum"*, Phys. Rev. D **65**, *043007 (2002).*

[128] Albert. J. et al. for the SNAP collaboration, *"Probing dark energy via weak gravitational lensing with the Supernova Acceleration Probe (SNAP)"*, astro-ph/0507460.

[129] Acquaviva, V., et al. , *"Structure formation constraints on the Jordan-Brans-Dicke theory"*, Phys. Rev. D **71**, *104025 (2005).*

[130] Will, C. M., *" Theory and Experiment in Gravitational Physics"*, Cambridge University Press (1993).

[131] Liddle, A. R., Mazumdar, A., and Barrow, J. D., *"Radiation matter transition in Jordan-Brans-Dicke theory"*, Phys. Rev. D **58**, *027302 (1998).*

[132] Chen, X. and Kamionkowski, M., *"Cosmic microwave background temperature and polarization anisotropy in Brans-Dicke cosmology"*, Phys. Rev. D **60**, *104036 (1999).*

[133] Nagata, R., Chiba, T., and Sugiyama, N., *"WMAP constraints on scalar-tensor cosmology and the variation of the gravitational constant"*, Phys. Rev. D **69**, *083512 (2004).*

[134] Damour, T, and Pichon, B., *"Big bang nucleosynthesis and tensor-scalar gravity"*, Phys. Rev. D **59**, 123502 (1999).

[135] Weinberg, S., *"General Relativity and Cosmology"*, Wiley, (1972).

[136] Clifton, T., Mota, D. F., and Barrow, J. D., *"Inhomogeneous gravity"*, MNRAS **358**, 601 (2005).

[137] Nariai, H., *"On the Brans solution in the scalar-tensor theory of gravitation"*, Prog. Theor. Phys. **42**, 544 (1969).

[138] Mather, J. C. et al. , *"Calibrator design for the COBE infrared absolute spectrophotometer (FIRAS)"*, Astrophys. J. **512**, 511 (1999).

[139] Grainge, K. et al., *"The CMB power spectrum out to l=1400 measures by the VSA"*, MNRAS **341**, L23 (2003);
Dickinson, C., et al., *"High sensitivity measurements of the CMB power spectrum with the extended Very Small Array"*, MNRAS **353**, 752 (2004).

[140] Pearson, T. J., et al. , *"The Anisotropy of the microwave background to l=3500: Mosaic observations with the Cosmic Background Imager"*, Astrophys. J. **591**, 556 (2003);
Readhead, A. C. S., et al. , *"Extended mosaic observations with the Cosmic Background Imager"*, Astrophys. J. **609**, 498 (2004).

[141] Kuo, C. L. et al. , *"High resolution observations of the CMB power spectrum with ACBAR"*, Astrophys. J. **600**, 32 (2004).

[142] Kogut A. et al. , *"First-year Wilkinson Microwave Anisotropy Probe (WMAP) observations: temperature-polarization correlation"*, Astrophys. J. Suppl. Ser. **148**, 161 (2003);
Verde, L., et al. , *"First-year Wilkinson Microwave Anisotropy Probe (WMAP) observations: Parameter Estimation methodology"*, Astrophys. J. Supp. **148**, 195 (2003);
Hinshaw G. et al. , *"First-year Wilkinson Microwave Anisotropy Probe (WMAP) observations: the angular power spectrum"*, Astrophys. J. Suppl. **148**, 135 (2003).

[143] Percival W.J. et al. , *"The 2DF Galaxy Redshift Survey: the power spectrum and the matter content of the Universe"*, Mon. Not. R. Astron. Soc. **327**, 1297 (2001).

[144] Bridle, S. L., et al. , *"Analytic marginalization over CMB calibration and beam uncertainty"*, Mon. Not. Roy. Astr. Soc. **335**, 1193 (2002).

[145] Gaztanaga, E., et al. , *"Bounds on the possible evolution of the gravitational constant from cosmological type Ia supernovæ"*, Phys. Rev. D **65**, 023506 (2002).

[146] Boisseau, B., Esposito-Farése, G., Polarski, D. and Starobinsky, A. A., *"Reconstruction of a scalar tensor theory of gravity in an accelerating universe"*, Phys. Rev. Lett. **85**, 2236-2239 (2000).

[147] Lewis, A. and Bridle, S., *"Cosmological parameters from CMB and other data: A Monte Carlo approach"*, Phys. Rev. D**66**, 103511 (2002).

[148] Jeffreys, H., Theory of Probability, 3rd ed, Oxford University Press (1961).

[149] Leach, S. M. and Liddle, A. R., *"Constraining slow-roll inflation with WMAP and 2dF"*, Phys. Rev. D **68**, 123508 (2003).

[150] Kosowsky, A., Milosavljevic, K., and Jimenez, R., *"Efficient cosmological parameter estimation from microwave background anisotropies"*, Phys. Rev. D **66**, 063007 (2002); Jimenez, R., Verde, L., Peiris, H., and Kosowsky, A., *"Fast cosmological parameter estimation from microwave background temperature and polarization power spectra"*, Phys. Rev. D **70**, 023005 (2004).

[151] Hu, W., and Dodelson, S. *"Cosmic microwave background anisotropies"*, Ann. Rev. Astron. Astrophys. **40**, 171 (2002).

[152] Madsen, M. S., *"Scalar fields in curved spacetimes"*, Class. Quantum Grav. **5**, 627 (1988).

[153] Hu, W., Scott, D., Sugiyama, N. and White, M. J., *"The Effect Of Physical Assumptions On The Calculation Of Microwave Background Anisotropies"*, Phys. Rev. D **52**, 5498 (1995).

[154] Dvali, G. R., Gabadadze, G. and Porrati, M., *"4D gravity on a brane in 5D Minkowski space"*, Phys. Lett. B **485**, *208 (2000)*.

[155] Carloni, S., Dunsby P. K. S., Capozziello, S., and Troisi, A., *"Cosmological dynamics of R^n gravity"*, Class. Quant. Grav. **22**, *4839 (2005)*.

[156] Huffenberger, K. M., and Seljak, U., *"Prospects for ACT: simulations, power spectrum, and non-Gaussian analysis"*, New Astron. **10**, *491 (2005)*; *http://www.hep.upenn.edu/ angelica/act/act.html*.

[157] Peacock, J. A., and Dodds, S. J., *"Nonlinear evolution of cosmological power spectra"*, Mon. Not. Roy. Astron. Soc. **280**, *L19 (1996)*.

[158] Van Waerbeke, L. et al. , *"Cosmic Shear Statistics and Cosmology"*, Astron. Astrophys. **374**, *757 (2001)*.

[159] Smith, R. E. et al. , *"Stable clustering, the halo model and nonlinear cosmological power spectra"*, MNRAS **341**, *1311 (2003)*.

[160] Peacock, J. A. and Smith, R. E., *"Halo occupation numbers and galaxy bias"*, MNRAS **318**, *1144 (2000)*.

[161] Seljak, U., *"Analytic model for galaxy and dark matter clustering"*, MNRAS **318**, *203 (2000)*.

[162] Ma, C., and Fry, J. N., *"Deriving the nonlinear cosmological power spectrum and bispectrum from analytic dark matter halo profiles and mass functions"*, Astrophys. J. **543**, *503 (2000)*.

[163] McDonald, P., Trac, H., and Contaldi, C., *"Dependence of the non-linear mass power spectrum on the equation of state of dark energy"*, MNRAS **366**, *547 (2006)*.

[164] Linder, E. V. and White, M., *"Going Nonlinear with Dark Energy Cosmologies"*, Phys. Rev. D **72**, *061304 (2005)*.

[165] *http://lambda.gsfc.nasa.gov/*.